ORNL/TM-2016/59
CRADA/NFE-12-03876

Ionic Liquids as Multi- Functional Lubricant Additives to Enhance Engine Efficiency

Jun Qu, Huimin Luo, Todd J. Toops, Brian H. West, Peter J. Blau, Sheng Dai

Oak Ridge National Laboratory

Brian L. Papke, Bassem Kheireddin, Hong Gao

Shell Global Solutions (U.S.)

OAK RIDGE NATIONAL LABORATORY
MANAGED BY UT-BATTELLE FOR THE US DEPARTMENT OF ENERGY

ORNL/TM-2016/59
CRADA/NFE-12-03876

Materials Science and Technology Division

CRADA Final Report

IONIC LIQUIDS AS MULTI- FUNCTIONAL LUBRICANT ADDITIVES TO ENHANCE ENGINE EFFICIENCY

Jun Qu, Huimin Luo, Todd J. Toops, Brian H. West, Peter J. Blau, Sheng Dai
Oak Ridge National Laboratory

Brian L. Papke, Bassem Kheireddin, Hong Gao
Shell Global Solutions (U.S.)

March 2016

Prepared by
OAK RIDGE NATIONAL LABORATORY
Oak Ridge, Tennessee 37831-6283
managed by
UT-BATTELLE, LLC
for the
US DEPARTMENT OF ENERGY
under contract DE-AC05-00OR22725

Approved for Public Release

CRADA TITLE: Ionic Liquids as Multi-Functional Lubricant Additives to Enhance Engine Efficiency (NFE-12-03876)

Project Start Date: July 23, 2012
Project End Date: December 31, 2015

Contractor: Oak Ridge National Laboratory (ORNL)
Participant: Shell Global Solutions (U.S.)

CRADA Technical Team:

ORNL PIs: Jun Qu (lead-PI), Huimin Luo, Todd J. Toops, Brian H. West, Peter J. Blau (retired), and Sheng Dai
Shell PIs: Brian L. Papke (retired), Hong Gao, Bassem Kheireddin, and Cheng Chen (left)

Other Key Technical Contributors:

ORNL: William C. Barnhill, Harry M. Meyer III, Donovan N. Leonard, Cheng Ma, Miaofang Chi, Jonathan Poplawsky, D. William Brookshear, Alexander Landauer, Wei Guo. D. W. Coffey
Shell: Matthew Richard, Stephen Mercer

ACKNOWLEDGEMENT

This research was sponsored by the Vehicle Technologies Office, Office of Energy Efficiency and Renewable Energy, US Department of Energy (DOE). Electron microscopy characterization was performed at ORNL's Center for Nanophase Materials Sciences, sponsored by the Scientific User Facilities Division, Office of DOE-BES. The authors thank Dr. J. Dyck from Cytec Industries Inc. for providing ionic liquid cation feedstocks.

TABLE OF CONTENTS

ABSTRACT

This ORNL-Shell CRADA developed and investigated ionic liquids (ILs) as multi-functional additives for next-generation low-viscosity engine oils. Several groups of oil-miscible ILs were successfully designed and synthesized with high thermal stability, non-corrosiveness, excellent wettability, and most importantly effective anti-scuffing/anti-wear and friction reduction characteristics. Synergistic effects between the common anti-wear additive zinc dialkyldithiophosphate (ZDDP) and a particular group of ILs were discovered with > 30% friction reduction and 70% wear reduction compared with using ZDDP or IL alone. The IL+ZDDP tribofilm distinguishes itself from the IL or ZDDP tribofilms with substantially higher contents of metal phosphates but less metal oxides and sulfur compounds. Notably, it was revealed that the actual concentrations of functional elements on the droplet surface of the oil containing IL+ZDDP are one order magnitude higher than their nominal values. Such significantly increased concentrations of anti-wear agents are presumably expected for the oil-solid interface and believed to be responsible for the superior lubricating performance. A prototype SAE 0W-16 engine oil using a synergistic IL+ZDDP pair as the anti-wear additive has been formulated based on the compatibility between the IL and other additives. Sequence VIE full-scale engine dynamometer tests demonstrated fuel economy improvement (FEI) for this prototype oil and revealed the individual contributions from the lower oil viscosity and reduced boundary friction. The impact of IL and IL+ZDDP on exhaust emission catalyst was investigated using an accelerated small engine aging test and results were benchmarked against ZDDP.

OBJECTIVES

To develop and demonstrate oil-soluble ionic liquids (ILs) as engine oil additives to substantially improve the mechanical efficiency of IC engines. Potential advantages and disadvantages of this new category of additives will be explored with a combination of systematic lab experiments, modeling, engine dynamometer tests, and field tests.

BENEFITS TO THE DOE FUNDING OFFICE'S MISSION

This CRADA was sponsored by the DOE Vehicle Technologies Office (VTO) Fuels and Lubricants Technologies Program. The mission of VTO is to develop more energy efficient and environmentally friendly highway transportation technologies that enable America to use less petroleum. One goal of the Fuels and Lubricants Technologies Program is to improve the engine fuel efficiency via lubricant advances. This CRADA successfully developed a series of oil-miscible ionic liquids (ILs) and made a breakthrough type discovery of synergism between a group of ILs and the conventional ZDDP. A prototype SAE 0W-16 engine oil using a synergistic pair of IL+ZDDP has been developed and demonstrated improved fuel economy in industrial standard full-size engine dynamometer tests. In addition to developing new ionic lubricants, the fundamental understanding gained here provides a solid scientific base for future R&D of fuel-efficient lubricants. This work directly supports the program office's goal.

LIST OF INVENTION DISCLOSURES, PUBLICATIONS AND PRESENTATIONS

Special Recognitions and Awards

1. ***R&D 100 Award*** (Team lead), jointly among ORNL, GM, Shell, and Lubrizol, Ionic liquid anti-wear additives for fuel-efficient engine lubricants, R&D Magazine, 2014.
2. ***U.S. DOE Vehicle Technologies Office R&D Award***, for research achievements in ionic liquid lubricants and additives, 2014.
3. "*ORNL, Shell develop a less friction/wear hybrid lubricant additive*," *World Industrial Reporter*, Sept. 2, 2015.
4. "*Reduce wear with synergistic lubricant pair*," *Materials Views*, July 28, 2015.
5. "*Low-friction engine oil*," R&D Magazine, August 19, 2014.

Patent Applications and Invention Disclosures

1. J. Qu, H. Luo, "Ionic liquids containing symmetric quaternary phosphonium cations and phosphorus-containing anions, and their use as lubricant additives," U.S. Patent Application 14/184,754, Feb. 20, 2014.
2. J. Qu, W.C. Barnhill, H. Luo, B. Kheireddin, H. Gao, B.L. Papke, "Lubricant Formulations Containing Phosphonium-Organophosphate Ionic Liquids," ORNL Invention Disclosure #201503587, Aug. 24, 2015. (Elected for patent filing)
3. J. Qu, H. Luo, "Ionic Liquids Containing Protic or Symmetric Aprotic Ammonium Cations and Phosphinate Anions as Lubricant Additives," ORNL Invention Disclosure #201503529, May 14, 2015. (Elected for patent filing)

Journal Papers

1. J. Qu, W.C. Barnhill, H. Luo, H.M. Meyer, D.N. Leonard, A.K. Landauer, B. Kheireddin, H. Gao, B.L. Papke, S. Dai, "Synergistic effects between phosphonium-alkylphosphate ionic liquids and ZDDP as lubricant additives," *Advanced Materials* 27 (2015) 4767-4774.
2. W.C. Barnhill, H. Gao, B. Kheireddin, B.L. Papke, H. Luo, B.H. West, J. Qu, "Tribological bench and engine dynamometer tests of a low viscosity SAE 0W-16 engine oil using a combination of ionic liquid and ZDDP as anti-wear additives," *Frontiers in Mechanical Engineering* 1 (2015) 12, DOI: 10.3389/fmech.2015.00012.
3. W.C. Barnhill, J. Qu, H. Luo, H.M. Meyer III, C. Ma, M. Chi, B.L. Papke, "Phosphonium-organophosphate ionic liquids as lubricant additives: effects of cation structure on physicochemical and tribological characteristics," *ACS Applied Materials & Interfaces* 6 (2014) 22585-22593.
4. A.K. Landauer, W.C. Barnhill, J. Qu, "Mechanical properties of tribofilms formed by ionic liquids (ILs), ZDDP, and IL+ZDDP combinations using nanoindentation at room and elevated temperatures," *Wear* (2016) 10.1016/j.wear.2016.03.003 (in press).

5. W.C. Barnhill, H. Luo, H.M. Meyer, C. Ma, M. Chi, B.L. Papke, J. Qu, "Tertiary and quaternary ammonium-phosphate ionic liquids as lubricant additives," *Tribology Letters* (submitted).

Invited Talks

1. J. Qu, "Oil-miscible ionic liquids as multi-functional additives for low-viscosity engine lubricants," *20th International Colloquium Tribology*, Stuttgart, Germany, Jan. 12-14, 2016.
2. J. Qu, "Low-Viscosity Lubricants Using Ionic Liquids as Base Stocks or Additives," Symposium on Molecular Chemistry and Lubricant Rheology, *STLE 70th Annual Meeting,* Dallas, May 17-21, 2015.
3. J. Qu, "Oil-miscible ionic liquids as lubricant additives" in Panel Discussion: Ionic Liquids for Lubrication, *STLE 69th Annual Meeting*, Orlando, FL, May 18-22, 2014.
4. J. Qu, "Ionic liquids as next generation anti-wear additives: molecular design to engine dynamometer testing," *38th Automotive/Petroleum Industry Forum (Detroit Advisory Panel)*, Dearborn, April 16, 2014.
5. J. Qu, "Ionic liquid-additized engine oil for improved fuel efficiency," *SAE 2014 High Efficiency IC Engine Symposium*, Detroit, April 6-7, 2014.
6. J. Qu, "Oil-miscible ionic liquids as lubricant additives" in Panel Discussion: Ionic Liquids for Lubrication, *STLE 69th Annual Meeting*, Orlando, May 18-22, 2014.

Conference Proceedings, Presentations and Posters

1. J. Qu, W.C. Barnhill, H. Luo, H.M. Meyer, D.N. Leonard, A.K. Landauer, B. Kheireddin, H. Gao, B.L. Papke, S. Dai, "A Synergistic Hybrid Anti-Wear Additive by Combining a Phosphonium-Alkylphosphate Ionic Liquid and a ZDDP," *2015 STLE Tribology Frontiers Conference, Denver*, October 25-27, 2015.
2. W.C. Barnhill, J. Qu, H. Luo, B.H. West, B.L. Papke, H. Gao, B. Kheireddin. "Compatibility of a Phosphonium-Organophosphate Ionic Liquid with Common Engine Oil Additives with Tribological Bench and Engine Tests." *70th Annual Society of Tribologists and Lubrication Engineers Meeting*. Dallas, TX, May 17-21, 2015.
3. C. Xie, T.J. Toops, M.J. Lance, J. Qu, "Impact of Lubricant Oil Additives on the Performance of Three Way Catalysts," *8th International Conference on Environmental Catalysis (ICEC)*, Asheville, TN, August 24-27, 2014.
4. J. Qu, "Oil-soluble ionic liquids as next-generation lubricant anti-wear additives," *248th ACS National Meeting*, San Francisco, August 10-14, 2014.
5. J. Qu, B.L. Papke, W.C. Barnhill, B. Kheireddin, H. Luo, C. Chen, P.J. Blau, B.H. West, M. Richard, S. Mercer, S. Dai, "Ionic liquids as ashless oil additives: correlations between molecular structures and oil-solubility and lubricating characteristics," *STLE 69th Annual Meeting*, Orlando, May 18-22, 2014.
6. J. Qu, B.L. Papke, H. Luo, C. Chen, H. Gao, P.J. Blau, B.H. West, "Oil-Miscible Phosphonium- and Ammonium-Phosphate Ionic Liquids as Potential Ashless Anti-Wear Lubricant Additives," *STLE 68th Annual Meeting*, Detroit, MI, May 5-10, 2013.

TECHNICAL DISCUSSION OF WORK PERFORMED BY ALL PARTIES

CHAPTER 1. Introduction

Reducing friction and wear is a persistent issue facing many industries, consumers and societies around the world. The US automotive industry in particular faces increasing governmental regulation [1] and consumer demand [2] to improve the effectiveness of lubricants. Incremental improvements in lubricants can not only reduce financial losses associated with component failure, but can also conserve material, energy and the environment. Frictional energy dissipation in internal combustion (IC) engines may cost the US nearly 1.3 billion barrels of oil annually [3] with engine bearing irreversibilities costing 10% to 15% of total engine energy production [3,4]. Power production in IC engines depends on reciprocating, sliding surface interactions that continually vary the lubrication regime between boundary lubrication (BL), mixed lubrication (ML), elastohydrodynamic lubrication (EHL) and hydrodynamic lubrication (HL). This range of lubrication behavior presents a twofold problem when minimizing energy dissipation at the most important piston ring cylinder liner interface: 1) higher viscosity engine oil can better counter the tendency for lubricant films to become deleteriously thinner as sliding speed decreases and temperature rises (*i.e.* in ML or BL) near the top ring reversal region of a stroke, but 2) most of a piston stroke has little to no asperity contact (*i.e.* in EHL or HL); therefore, a lower viscosity lubricant would be preferable to reduce parasitic friction, but posts a challenge for wear protection. Novel lubricant additive formulations that allow lower viscosity engine oils while retaining anti-wear (AW) benefits are a logical path for researchers to follow in order to resolve these issues.

Since the seminal work in 2001 [5], exploration of ionic liquids (ILs) [6] as lubricants and lubricant additives has proliferated. These room temperature molten salts generally possess low volatility and flammability and have high decomposition temperatures—ideal lubricant properties. Initial work involved ILs with imidazolium cations and fluorine-containing anions [7-10], but IL research in lubrication since has diversified [11-14]. Although most earlier studies focused on the feasibility of using ILs as base or neat lubricants, a few tried polar base oil stocks to overcome ILs' inherent insolubility in common non-polar oils [15-17] while others tested oil-IL emulsions or very low concentrations of ILs in non-polar base oil [18-23]. ILs with quaternary alkylphosphonium cations and various anions have been investigated for beneficial tribological properties by several groups [24-29]. Fully oil-miscible alkylphosphonium-organophosphate ILs were recently developed in our chemistry lab [32-35] and found to effectively decrease friction and wear in BL and ML, as confirmed later by other research groups [36, 37]. This family of ILs was shown to be non-corrosive and have decomposition temperatures above hydrocarbon base oils and common AW additives, such as zinc dialkyldithiophosphate (ZDDP) [38]. Additionally, ammonium-based ILs caught our interest because they have already found widespread applications in many industries and are produced economically in quantities on the order of tons per year as solvents, gas capture agents, phase-transfer catalysts, coating materials, surfactants,

metal extracting agents and anti-microbial agents. [39, 40] Within the realm of lubrication, a related class of salts of alkylated ammonium phosphates has been used as corrosion inhibitors and ashless anti-wear additives for years. [41, 42] Some ammonium-based ILs have been examined as neat lubricants or additives more recently. [18, 43-48] Other recent work has revealed the merits of protic ILs. [49-54]

In this CRADA, we developed and investigated several families of oil-miscible ILs as engine oil additives specifically as AW and friction-reducing agents. These ILs were first tested in base oil as a screening measure to rank each IL's lubricating performance and to gain fundamental understanding of the anti-wear and friction reduction mechanisms. Remarkable synergy was discovered between the group of alkylphosphonium-organophosphate ILs and ZDDP that was then explored in details. A prototype SAE 0W-16 engine oil using a synergistic IL+ZDDP pair as the anti-wear additive has been formulated based on the compatibility between the IL and other additives. Sequence VIE full-scale engine dynamometer tests demonstrated fuel economy improvement (FEI) for this prototype oil and revealed the individual contributions from the lower oil viscosity and reduced boundary friction. The impact of IL and IL+ZDDP on exhaust emission catalyst was investigated using an accelerated small engine aging test and results were benchmarked against ZDDP.

CHAPTER 2. Phosphonium-Organophosphate Ionic Liquids as Lubricant Additives: Effects of Cation Structure on Physicochemical and Tribological Characteristics

2.1 Experimental and Materials

2.1.1 Synthesis

Five quaternary phosphonium-organophosphate ionic liquids with different cation structures but the same anion structure were investigated in this study. They are tetraoctylphosphonium bis (2-ethylhexyl) phosphate ([P_{8888}][DEHP]), [P_{66614}][DEHP], tributyltetradecylphosphonium bis (2-ethylhexyl) phosphate ([P_{44414}][DEHP]), tributyloctylphosphonium bis (2-ethylhexyl)phosphate ([P_{4448}][DEHP]), and tetrabutylphosphonium bis (2-ethylhexyl) phosphate ([P_{4444}][DEHP]). The ionic structures of these ILs are shown in Fig. 2.1 and their physical properties are listed in Table 2.1.

The synthesis of [P_{66614}][DEHP] had been reported in our earlier work [32] and [P_{4444}][DEHP] was kindly provided by Cytec Industries Inc., Niagara Falls, ON, Canada. The purity of [P_{66614}][DEHP] and [P_{4444}][DEHP] was determined using titration at Cytec to be 98% and 97%, respectively.

[P_{8888}][DEHP]

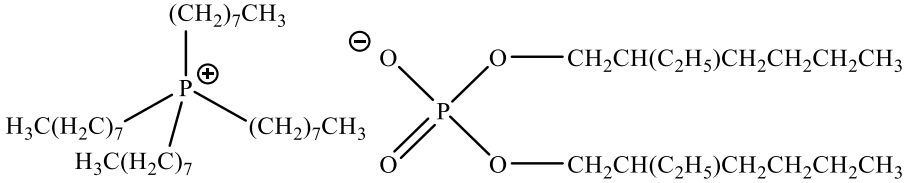

[P_{66614}][DEHP]

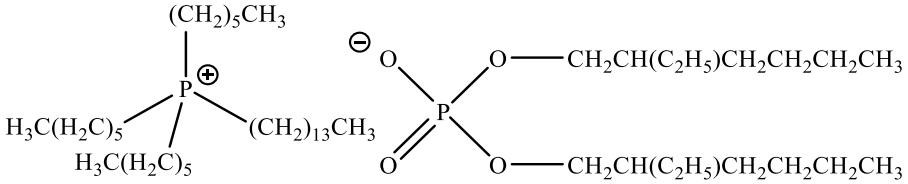

[P_{44414}][DEHP]

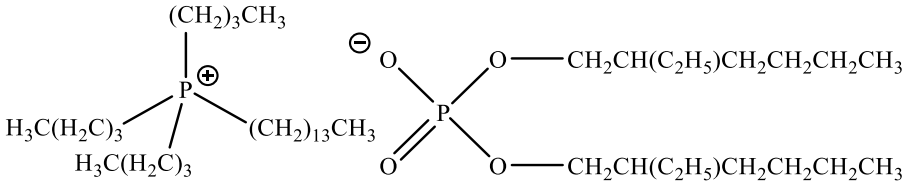

[P_{4448}][DEHP]

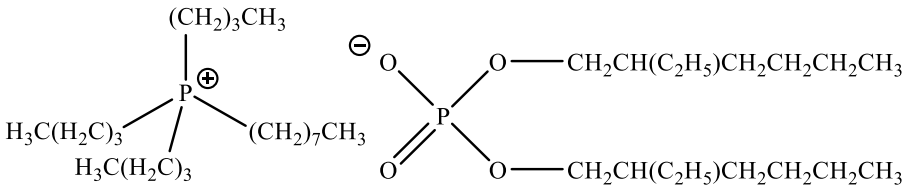

[P_{4444}][DEHP]

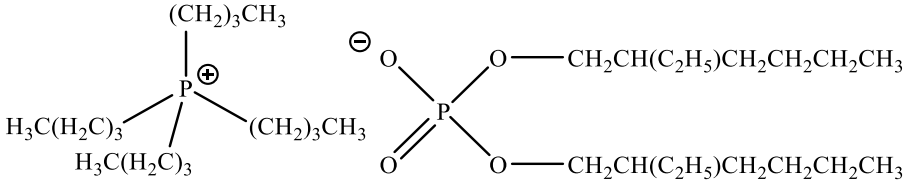

Figure 2.1. Molecular structures of selected phosphonium-organophosphate ILs [73].

Table 2.1. Molecular weight, oil-solubility, density, and viscosity of selected ILs.

Ionic Liquid	Molecular Weight	Density (g/cm^3)	Viscosity of neat IL (cP)			Viscosity Index	Solubility in base oil oil (wt.%)
			23°C	40°C	100°C		
[P_{8888}][DEHP]	805.26	0.86	>1500[†]	611.8	68.2	188	>50
[P_{66614}][DEHP]	805.26	0.91	951.0	390.4	45.0	173	>50
[P_{44414}][DEHP]	721.10	0.88	711.4	252.8	25.2	128	~1
[P_{4448}][DEHP]	636.94	0.89	788.6	282.9	30.5	147	<1
[P_{4444}][DEHP]	580.83	0.94	940.7	320.1	30.9	134	<1

[†]*Above the upper limit of the measurement range.*

[P_{8888}][DEHP], [P_{44414}][DEHP], and [P_{4448}][DEHP] were newly synthesized and characterized at ORNL and the detailed procedures are described as following. Proton nuclear magnetic resonance (NMR) analysis was carried out using a Bruker MSL-400 at 400 MHz. Spectra were obtained in $CDCl_3$ with reference to TMS (0 ppm) for ^1H.

[P_{8888}] [DEHP]: Tetraoctylphosphonium bromide ([P_{8888}]Br, 40.58 g, 72.0 mmol) and bis(2-ethylhexyl)phosphoric acid (HDEHP, 23.2 g, 72.0 mmol) were mixed in 90 mL of deionized water (D.I. H_2O, 18.2 MΩ-cm) and 100 mL of hexanes. To this stirred suspension was added a solution of sodium hydroxide (NaOH, 2.88 g, 72.0 mmol) in 75 mL of D.I. H_2O drop wise at room temperature. The white suspension became clear after the addition of NaOH was completed. The mixture continued to be stirred at room temperature overnight.The upper organic phase was separated and washed with D.I. H_2O four times to ensure removal of NaBr. Solvents

were distilled off by rotary evaporator and the product was dried at 70 ^{O}C under vacuum for 4 h to yield [P_{8888}]][DEHP] as a viscous liquid (57.0 g, 70.8 mmol, yield: 93.8%). The water content of [P_{8888}]][DEHP] was 0.1%. Proton nuclear magnetic resonance (^{1}H NMR, $CDCl_3$, ppm): 0.85-0.87 (m, 24H, 8CH_3), 1.27-1.36 (m, 56H, 28CH_2), 1.44 (m, 2H, 2CH), 1.67 (m, 8H, 4CH_2), 3.31 (m, 8H, 4NCH_2), 3.80 (m, 4H, 2OCH_2); ^{13}C NMR ($CDCl_3$, ppm): 10.81 (2CH_3), 13.96 (4CH_3), 14.02 (2CH_3), 22.02 (4CH_2), 22.52 (4CH_2), 23.04 (2CH_2), 23.09 (4CH_2), 26.28 (4CH_2), 28.92 (2CH_2), 29.06 (4CH_2), 29.87 (4CH_2), 31.64 (4CH_2), 40.09 (2CH), 58.84 (4NCH_2), 67.82 (2OCH_2).

[P_{44414}] [DEHP]: Tributyltetradecylphosphonium chloride ([P_{44414}]Cl, 36.47 g, ~49% in aqueous solution, 41.1 mmol) and bis(2-ethylhexyl)phosphoric acid (HDEHP, 13.26 g, 41.1 mmol) were mixed in 58 mL of hexanes. To this stirred mixture was added a solution of sodium hydroxide (NaOH, 1.64 g, 41.1 mmol) in 45 mL of D.I. H_2O (18.2 MΩ-cm) drop wise at room temperature. The mixture continued to be stirred at room temperature overnight. The upper organic phase was separated and washed with D.I. H_2O four times to ensure removal of NaCl. Solvents were distilled off by rotary evaporator and the product was dried at 70 ^{O}C under vacuum for 4 h to yield [P_{44414}]][DEHP] as a viscous liquid (29.1 g, 40.4 mmol, yield: 98.3%). The water content of [P_{44414}]][DEHP] was 0.3%. ^{1}H NMR ($CDCl_3$, ppm): 0.85-0.90 (m, 24H, CH_3), 1.24-1.31 (m, 36H, CH_2), 1.50-1.55 (m, 18H CH_2 & CH), 2.45 (m, 8H, PCH_2), 3.72 (m, 4H, OCH_2); ^{13}C NMR ($CDCl_3$, ppm): 10.94 (CH_3), 13.48 (CH_3), 14.09 (CH_3), 18.44 (CH_3), 18.91 (CH_3), 21.91 (CH_2), 22.61 (CH_2), 23.13 (CH_2), 23.31 (CH_2), 23.88 (CH), 29.04 (CH_2), 29.27 (CH_2), 29.56 (CH_2), 30.11 (CH_2), 31.63 (CH_2), 40.45 (CH_2), 67.30 (2CH_2)

[P_{4448}] [DEHP]: Tributyloctylphosphonium chloride ([P_{4448}]Cl, 10.96 g, 31.3 mmol) and bis(2-ethylhexyl)phosphoric acid (HDEHP, 10.08 g, 31.3 mmol) were mixed in 40 mL of hexanes. To this stirred mixture was added a solution of sodium hydroxide (NaOH, 1.25 g, 31.3 mmol) in 30 mL of D.I. H_2O (18.2 MΩ-cm) drop wise at room temperature. The mixture continued to be stirred at room temperature overnight. The upper organic phase was separated and washed with D.I. H_2O four times to ensure removal of NaCl. Solvents were distilled off by rotary evaporator and the product was dried at 70 ^{O}C under vacuum for 4 h to yield [P_{4448}]][DEHP] as a viscous liquid (17.68 g, 27.8 mmol, yield: 88.8%). The water content of [P_{4448}]][DEHP] was 0.3%. ^{1}H NMR ($CDCl_3$, ppm): 0.85-1.00 (m, 24H, CH_3), 1.28-1.40 (m, 24H, CH_2), 1.49-1.54 (m, 18H CH_2 & CH), 2.42 (m, 8H, PCH_2), 3.74 (m, 4H, OCH_2); ^{13}C NMR ($CDCl_3$, ppm): 10.90 (CH_3), 13.44 (CH_3), 14.05 (CH_3), 18.40 (CH_3), 18.67 (CH_3), 21.65 (CH_2), 22.50 (CH_2), 23.09 (CH_2), 23.27 (CH_2), 23.85 (CH), 28.91 (CH_2), 29.01 (CH_2), 30.06 (CH_2), 31.62 (CH_2), 40.40 (CH_2), 67.39 (2CH_2)

A low viscosity (4 cSt at 100 ^{o}C) base oil was provided by Shell Global Solutions (TX, US) and used as the base stock in this research.

All ILs in this work contain phosphorous. International Lubricants Standardization and Approval Committee (ILSAC) GF-5 specifications limit phosphorous content in engine oils to

800 ppm. Guided by this restriction, the five ILs were blended with base oil to the maximum allowable phosphorous content resulting in treat rates of 0.75-1.04 wt.%, as shown in Table 2.2.

Table 2.2. IL treat rates in the base oil and viscosities of the oil-IL blends [73].

Lubricant	Target IL Conc. (wt.%)	P Conc. (wt.%)	Viscosity of base oil-IL blend (cP)		
			23°C	40°C	100°C
base oil	0	0	29.92	15.11	3.28
base oil + $[P_{8888}][DEHP]$	1.04	0.08	29.97	15.08	3.25
base oil + $[P_{66614}][DEHP]$	1.04	0.08	30.02	15.04	3.26
base oil + $[P_{44414}][DEHP]$	0.93	0.08	30.13	15.14	3.27
base oil + $[P_{4448}][DEHP]$	0.82	0.08	*Not measured*		
base oil + $[P_{4444}][DEHP]$	0.75	0.08	30.04	15.06	3.27

2.1.2 Characterization

Each IL's oil solubility was determined by incrementally decreasing combinations of IL and base oil from a 1:1 ratio until solubility was reached. The solute and solvent were mixed and vigorously shaken for one minute. The samples were then placed in a centrifuge for three minutes at 13,000 rpm. The oil-IL blends were examined under bright lighting for evidence of separation or cloudiness right after centrifuge and 24-hr after.

Thermogravimetric analysis (TGA) was performed on the ILs in air (allowing oxidation) using a TA Instruments (DE, USA) TGA-2950 at a 10° C per minute heating rate.

Viscosities of the neat ILs and oil-IL blends at 23, 40, and 100 ^{o}C were measured using a Petrolab (OK, USA) MINIVIS II viscometer (falling ball technique). At least four measurements were conducted for each fluid to ensure a standard deviation less than 1%.

2.1.3 Corrosion and tribological testing and analysis

Open-air corrosion testing was performed by placing a drop of each candidate IL directly onto a 25.4x25.4 mm^2 CL35 cast iron surface in an ambient environment for 7 days. Evaporation was not a concern due to ILs' low volatility. Electrochemical corrosion tests were carried out on the two oil-miscible ILs, $[P_{8888}][[DEHP]$ and $[P_{66614}][DEHP]$ at room temperature, using the potentiodynamic polarization technique with a three-electrode electrochemical cell. A disk of cast iron with 1 cm^2 exposed area was used as the working electrode, which was immersed in the electrolyte for 15 min before starting the experiment. 20 ml of the IL to be tested served as the electrolyte. A Pt wire was used as the counter electrode, and Ag/AgCl (4M KCl internal

solution) was the reference electrode. The sample was polarized at potentials from -1.0 to +1.50 V versus open circuit potential at a scanning rate of 0.166 mV/s under aerated conditions. All electrochemical tests were conducted in the ambient environment using a potentiostat model CHI 700C (CH Instruments, Inc., Austin, TX, USA).

Tribological wear and friction testing was performed on a Phoenix Tribology Ltd. (Hampshire, England) Plint TE77 reciprocating sliding tribometer. A ball-on-flat geometry was chosen using an AISI 52100 steel ball against a CL35 (Metal Samples Company, AL, USA) grey cast iron flat. The cast iron flats were first polished using 600 grit silicon carbide grinding paper producing a lay perpendicular to the sliding direction. All interacting surfaces were cleaned with isopropyl alcohol and air dried before testing. The Plint TE77 obtains friction data *in situ* by taking tangential force measurements using a piezoelectric load cell. All lubricant blends were well-shaken before use. Testing for all specimens was carried out at 100 ºC under a normal load of 100 N for a total sliding distance of 1000 m. The ball reciprocated at 10 Hz with a stroke of 10 mm against the flat. At least three replicate tests were performed for each IL-oil blend and the base oil to assess repeatability. After tribological testing, balls and flats were cleaned with acetone and then isopropyl alcohol. Wear volumes were measured using a Veeco (now Bruker, TX, USA) Wyko NT9100 white light interferometer.

A Hitachi S-4800 (Tokyo, Japan) scanning electron microscope (SEM) equipped with an EDAX SDD energy-dispersive spectroscopy (EDS) system was used to analyze the worn surface from the top. Cross-sectional composition and nanostructure was examined using a Hitachi HF-3300 transmission electron microscope (TEM) (300kV, 1.3 Å resolution) bundled with a Bruker solid-state EDS detector. TEM samples were prepared using a Hitachi NB5000 focused ion beam (FIB) system with a gallium ion source to extract a thin cross-section of the tribofilm of interest. A carbon film and then a tungsten layer were deposited onto the wear scar before the FIB process to protect the tribofilm. A Thermo Scientific (MA, USA) K-Alpha x-ray photoelectron spectrometer (XPS) was used for chemical analysis of the selected tribofilm. The x-rays used were monochromatic Al-kα photons, and photo emitted electrons were analyzed with a hemispherical energy analyzer. Surface compositions were calculated by measuring peak areas of the primary core levels for all elements present and normalizing the peak areas using tabulated sensitivity factors. Composition-depth profiles were obtained under 1 kV ion beam energy at high a current setting.

2.2 Results and Discussion

2.2.1 Physical and Chemical Properties

2.2.1.1 Oil Solubility

Due to the identical anion structure among the five ILs, changes in oil solubility are governed solely by the cation structures. We hypothesized that more carbon atoms in the alkyl groups on the cation would improve the oil solubility by: (1) diluting the charge density thus decreasing ion coordination, and (2) increasing intermolecular London dispersion forces between lipophilic moieties of the cations with the base oil molecules. ILs with long alkyl chain cations may possess interesting physicochemical properties [29], and the effects of the anion chemistry and alkyl structure and chain length on the IL's oil solubility had been discussed elsewhere.[33-35, 37]

Table 2.1 and Fig. 2.2a show the oil solubility for each candidate IL. $[P_{66614}][DEHP]$ and $[P_{8888}][DEHP]$ are mutually miscible (>50 wt.%) in the base oil cSt base oil. The remaining ILs have marked lower oil solubility: $[P_{44414}][DEHP]$, $[P_{4448}][DEHP]$, and $[P_{4444}][DEHP]$ showing solubility limits of ~1, <1, and <1 wt.%, respectively. Similar solubility was observed for the five ILs in a poly-alpha-olefin (PAO) 4 cSt base oil. The prevailing trend from this data strongly supports our hypothesis of longer alkyl chains improving oil solubility. The abrupt drop in oil solubility due to shorter alkyl chains either on the cation (from $[P_{66614}]$ to $[P_{44414}]$) or on the anion (from [DEHP] to dibutyl phosphate as observed in our previous study [34]) implies that six carbons could be the critical minimum alkyl chain length for phosphonium-organophosphate ILs to achieve high oil miscibility. Table 2.2 lists the treat rates of ILs in the base oil cSt base oil and the viscosities of the oil-IL blends. Evidently, the addition of ILs at such treat rates resulted in little change in viscosity.

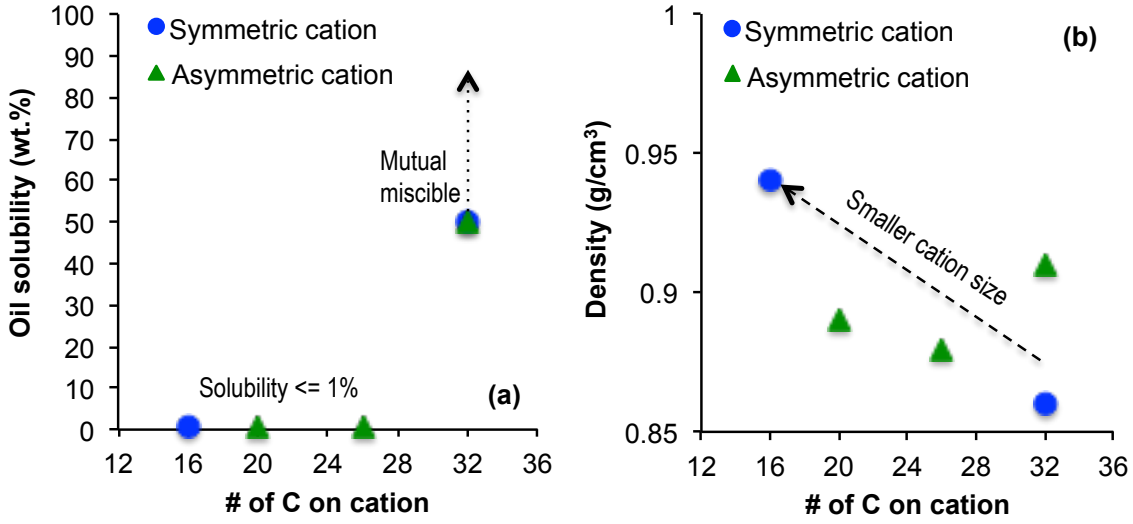

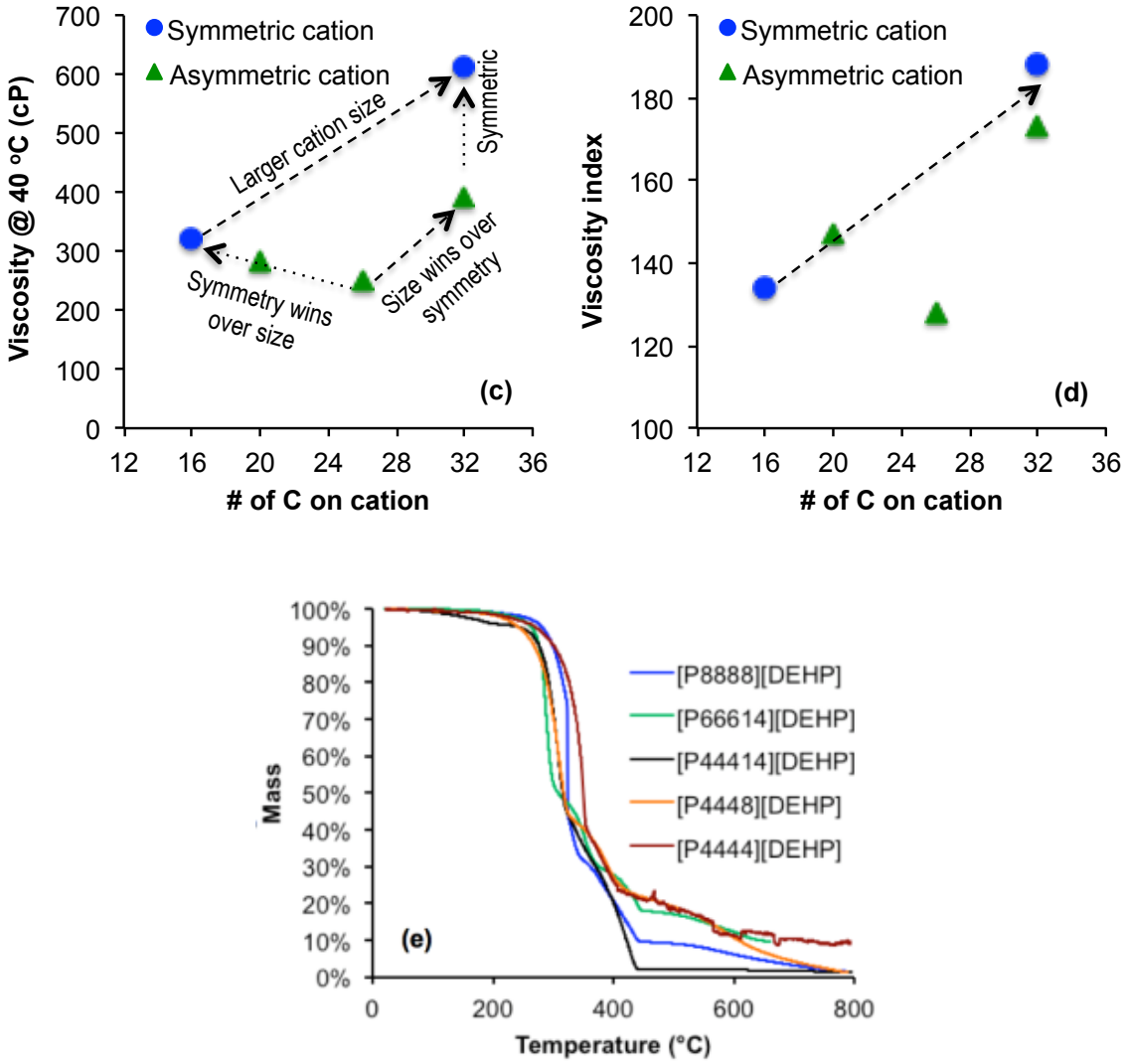

Figure 2.3. Effects of the cation structure on ILs' (a) oil-solubility, (b) density, (c) viscosity, (d) viscosity index, and (e) thermogravimetric behavior.

2.2.1.2 Density, viscosity and thermal stability

Densities (ρ), viscosities, and viscosity indices of the five ILs are compared in Table 2.1 and Figs. 2.2(b-d). The ILs' densities are moderately affected by changes in cationic alkyl groups. As illustrated in Fig. 2.2b, closer packing and thus higher density seems to be achieved by reducing the size of the hydrocarbon chains.

The cationic alkyl groups' effect on viscosity (η) seems twofold: (1) more carbons per chain increase interionic interaction, (2) and higher symmetry causes closer packing and thus more interaction, as shown in Fig. 2.2c. Both effects cause increased resistance to shear flow and higher viscosity. For example, η ([P_{66614}][DEHP]) > η ([P_{44414}][DEHP]), η ([P_{8888}][DEHP]) > η ([P_{4444}][DEHP]), and η([P_{8888}][DEHP]) > η([P_{66614}][DEHP]). For [P_{44414}][DEHP]

vs. $[P_{4448}][DEHP]$, the former has a slightly larger cation but the latter has a slightly higher symmetry, and, as a result of the competition between these two effects, the viscosities of these two ILs turn out to be similar. Evidently for $[P_{44414}][DEHP]$ vs. $[P_{4444}][DEHP]$, the effect of cation symmetry was more significant.

The viscosity index (VI) is a measure of the variation in viscosity over an arbitrary temperature range. Reference temperatures of 40 and 100 ºC are typically used in the automotive industry. Higher viscosity indices indicate more stable lubrication performance over this temperature range. Contrary to viscosity, the viscosity index generally seems to relate to IL mass but is little affected by the cation symmetry, as shown in Fig. 2.2d. For instance, $[P_{8888}][DEHP]$ and $[P_{66614}][DEHP]$ both have identical mass and the highest mass of the five ILs but have different cation symmetry. These two ILs also possess higher viscosity indices than the other three ILs. Except that of $[P_{44414}][DEHP]$, the VIs of the remaining four ILs appeared to be proportional to their respective masses.

Figure 2.2e compares the TGA curves and the on-site decomposition temperatures of all five ILs fall within a range of 300 to 350 ºC. The two ILs with symmetric cations ($[P_{4444}][DEHP]$ and $[P_{8888}][DEHP]$) showed slightly higher thermal stability than the rest three.

2.2.1.3 Corrosion behavior

No evidence of pitting or other hints of corrosion were present on any of the cast iron surfaces that were exposed to the five ILs in open-air tests. Figure 2.3 shows the potentiodynamic polarization curves obtained for cast iron in neat $[P_{8888}][[DEHP]$ and $[P_{66614}][DEHP]$. Both showed classic active-passive behavior with strong passivation at a current density in the order of 10^{-4} A/cm^2. No corrosion damage or morphology change was observed on either of the iron surfaces electrochemically tested in the two ILs.

2.2.2 Friction and Wear Results

Because of the questionable oil solubility of $[P_{44414}][DEHP]$, $[P_{4448}][DEHP]$, and $[P_{4444}][DEHP]$ at the target concentrations (see Table 2.2), only $[P_{8888}][DEHP]$ and $[P_{66614}][DEHP]$, mutually miscible in the base oil base oil, were selected for tribological testing and analysis.

Each friction trace in Fig. 2.4 represents the average of three repeated tests. The baseline oil, base oil, exhibited a rapidly increasing friction coefficient during the initial 25 meters of sliding—an indication of scuffing.[55, 56] Neither base oil + 1.04% $[P_{8888}][DEHP]$ nor base oil + 1.04% $[P_{66614}][DEHP]$ had such a rapid friction increase in the beginning of the tests. And, each blend reduced the average steady-state friction coefficient by ~10% compared to base oil.

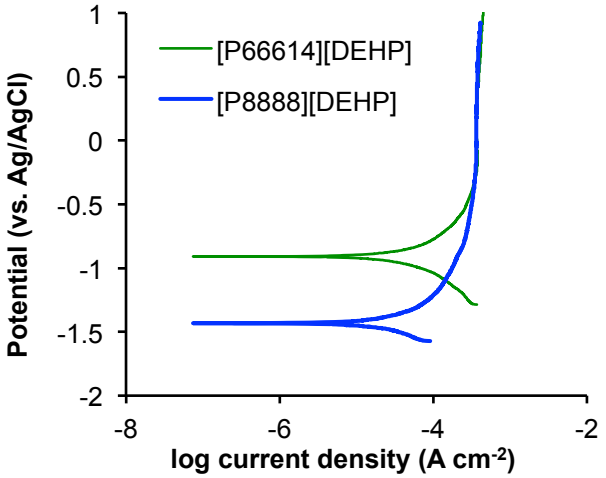

Figure 2.3. Potentiodynamic polarization curves of cast iron in the two oil-miscible ILs showing strong passivation [73].

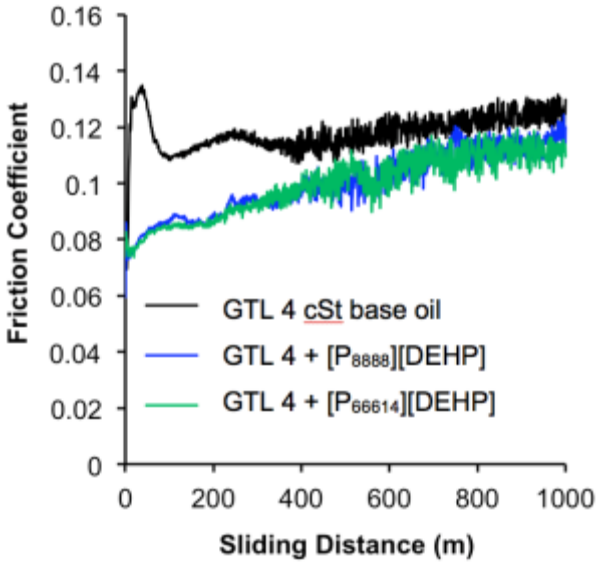

Figure 2.4. Friction coefficient traces of the base oil without and with IL additives [73].

Addition of either $[P_{8888}][DEHP]$ or $[P_{66614}][DEHP]$ at the 1.04 wt.% treat rate into the base oil significantly reduced the wear for the cast iron flat and steel ball (Table 2.3). Wear results here are an average of three replicates for each lubricant. Wear on the reciprocating steel ball specimens was consistently two orders of magnitude smaller than that on the cast iron flats. Two out of three repeats for base oil without additive revealed scuffing and associated high wear, leading to a high standard deviation between tests. It is interesting to note the moderately better

performance of base oil + 1.04 wt.% [P_{8888}][DEHP] than that of base oil + 1.04 wt.% [P_{66614}][DEHP] (Table 2.3). Phosphates have been used for years in lubricants and are known to be facilitators of protective tribofilm formation. Additionally, anti-wear characteristics of ILs are thought to be more sensitive to changes in the anion. [P_{8888}][DEHP] and [P_{66614}][DEHP] share the identical organophosphate anion and have the same molecular weight, and differ only in their distribution of alkyl groups about the central phosphorus atom in their cations. Thus the difference in wear performance may be attributed to the symmetry of the quaternary phosphonium cation. We hypothesize that the symmetric structured cation might allow better mobility for [P_{8888}][DEHP] in the base oil to reach and interact with the surface asperities upon collisions to be more readily available in forming the protective tribofilm. Such hypothesis warrants further investigation.

Table 2.3. Summary of wear results in the base oil without and without IL additives [73].

Lubricant	Flat wear volume (mm^3)	Ball wear volume (mm^3)	Total wear volume (mm^3)
base oil cSt base oil	$1.12^{\pm 0.61}$	$0.51^{\pm 0.25}\times 10^{-2}$	$1.17^{\pm 0.61}$
base oil + [P_{8888}][DEHP]	$0.10^{\pm 0.05}$	$0.10^{\pm 0.02}\times 10^{-2}$	$0.10^{\pm 0.05}$
base oil + [P_{66614}][DEHP]	$0.18^{\pm 0.05}$	$0.09^{\pm 0.02}\times 10^{-2}$	$0.18^{\pm 0.05}$

2.2.3 Wear scar examination and tribofilm Analysis

All wear scars were first examined using SEM for morphology imaging and using EDS for element detection. More comprehensive three-dimensional characterization [57] was then conducted on the tribofilm on the cast iron surface lubricated by base oil + 1.04 wt.% [P_{8888}][DEHP]. Aided by FIB, cross-sectional examination was carried out using TEM for film thickness measurement, using electron diffraction for phase identification, and using EDS for elemental mapping. XPS was used to analyze the tribofilm composition and ion sputtering allowed layer-by-layer analysis for revealing the composition variation of the tribofilm from top to bottom.

2.2.3.1 Top surface SEM morphology examination and EDS element analysis

Representative SEM micrographs of the worn flat surface for each lubricant along with the corresponding EDS spectra are shown in Fig. 2.5. The baseline lubricant (base oil) caused adhesive wear and plastic deformation as demonstrated by the deep grooves formed along the entire width and length of the scar. base oil + 1.04% [P_{66614}][DEHP] generated a smoother wear

track with some shallower grooves. base oil + 1.04% [P_{8888}][DEHP] produced even less surface damage with the smoothest worn surface with fewest grooves in a more random pattern. The level of surface damage correlates well with the wear results described above.

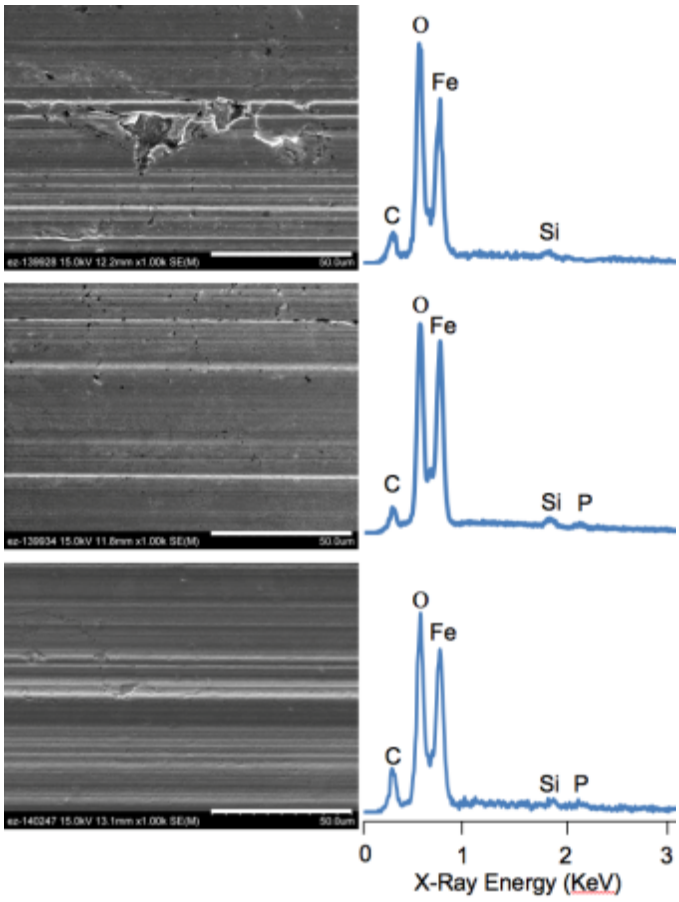

Figure 2.5. SEM micrographs and EDS spectra. From top to bottom, wear scars lubricated by base oil cSt base oil, base oil + [P_{8888}][DEHP], and base oil + [P_{66614}][DEHP]. SEM micron bar: 50 μm [73].

In addition to the carbon, iron, and silicon peaks, EDS spectra in Fig. 2.5 show prominent oxygen signal on the cast iron worn surfaces suggesting metal oxidation during the wear process. The wear tracks produced with the two oil-IL blends contain phosphorous as shown by the small peaks just above 2 keV — indicative of IL-induced tribofilms on the worn surfaces.

2.2.3.2 Cross-sectional TEM nanostructure examination and EDS elemental mapping

Tribofilms formed by asymmetric-cation IL [P_{66614}][DEHP] (blended in PAO 4 cSt base oil) on cast iron surfaces were previously examined.[32, 58] In this study, the tribofilm examination was focused on the new symmetric-cation IL [P_{8888}][DEHP] due to its superior wear protection (Table 2.3). Aided by FIB milling, cross-sectional TEM micrographs, EDS element

mapping, and electron diffraction pattern of the tribofilm on the cast iron flat lubricated by base oil + $[P_{8888}]$[DEHP] were obtained (Fig. 2.6). This tribofilm appears to be single layered with a thickness varying from 10 to 200 nm. The diffraction pattern implies an amorphous matrix populated with nanocrystalline inclusions. The size of these inclusions is determined to be 1-10 nm by high magnification TEM imaging. EDS elemental maps show relatively uniform distribution of oxygen, iron and phosphorous and discrete areas containing carbon (excluding the carbon signals across the top that are from FIB processing) throughout the thickness of the tribofilm. This tribofilm appears similar compared to that of the single-layer tribofilm from $[P_{66614}]$[DEHP] reported in [32], differing from the two-layer tribofilm observed in [33]. Table 2.4 compares the tribofilm characteristics (based on cross-sectional TEM/EDS examination) between this work on $[P_{8888}]$[DEHP] and our previous studies on $[P_{66614}]$[DEHP]. Although mixed with different base oils, at different treat rates, against different sliders, and under different test conditions, the tribofilms formed on cast iron surfaces by these two ILs seem to have similar nanostructure and chemical composition. The only notable distinction is the double-layer structure (with a discrete oxide interlayer) observed in Ref. 33, which might be attributed to the combined higher load (240 N) and elevated temperature (100 ^{o}C) compared to Ref. 32 (160 N and 23 ^{o}C) and this work (100 N and 100 ^{o}C). Under the higher thermomechanical stresses in Ref. 33, more significant oxidation may occur on surface asperities in collision to form pads of oxides during wear-in before sufficient IL ions decomposed to become available to form the IL tribofilm on top of the oxide layer.

Table 2.4. Comparison of tribofilms formed by $[P_{8888}]$[DEHP] and $[P_{66614}]$[DEHP] observed in three studies [73].

IL	Reciprocating sliding test (10 Hz oscillation with 10 mm stroke)			Tribofilm (cross-sectional TEM/EDS)		
	Base oil, IL treat rate	Substrate (slider)	L, T, SD*	Major elements	Thickness (nm)	Structure
$[P_{8888}]$[DEHP] (this study)	base oil cSt, 1.04 wt%	Cast iron (52100 steel ball)	100 N, 100 ^{o}C, 1000 m	Fe, O, P, C	10-200	Single layer
$[P_{66614}]$[DEHP] (Ref. 32)	PAO 4 cSt, 5.0 wt%	Cast iron (Mo-coated piston ring)	160 N, 23 ^{o}C, 1000 m	Fe, O, P, C	120-180	Single layer
$[P_{66614}]$[DEHP] (Ref. 33)	PAO 4 cSt, 1.0 wt%	Cast iron (Mo-coated piston ring)	240 N, 100 ^{o}C, 4320 m	Fe, O, P, C	60-220	Double-layer

**L – normal load, T – lubricant bulk temperature, SD – sliding distance*

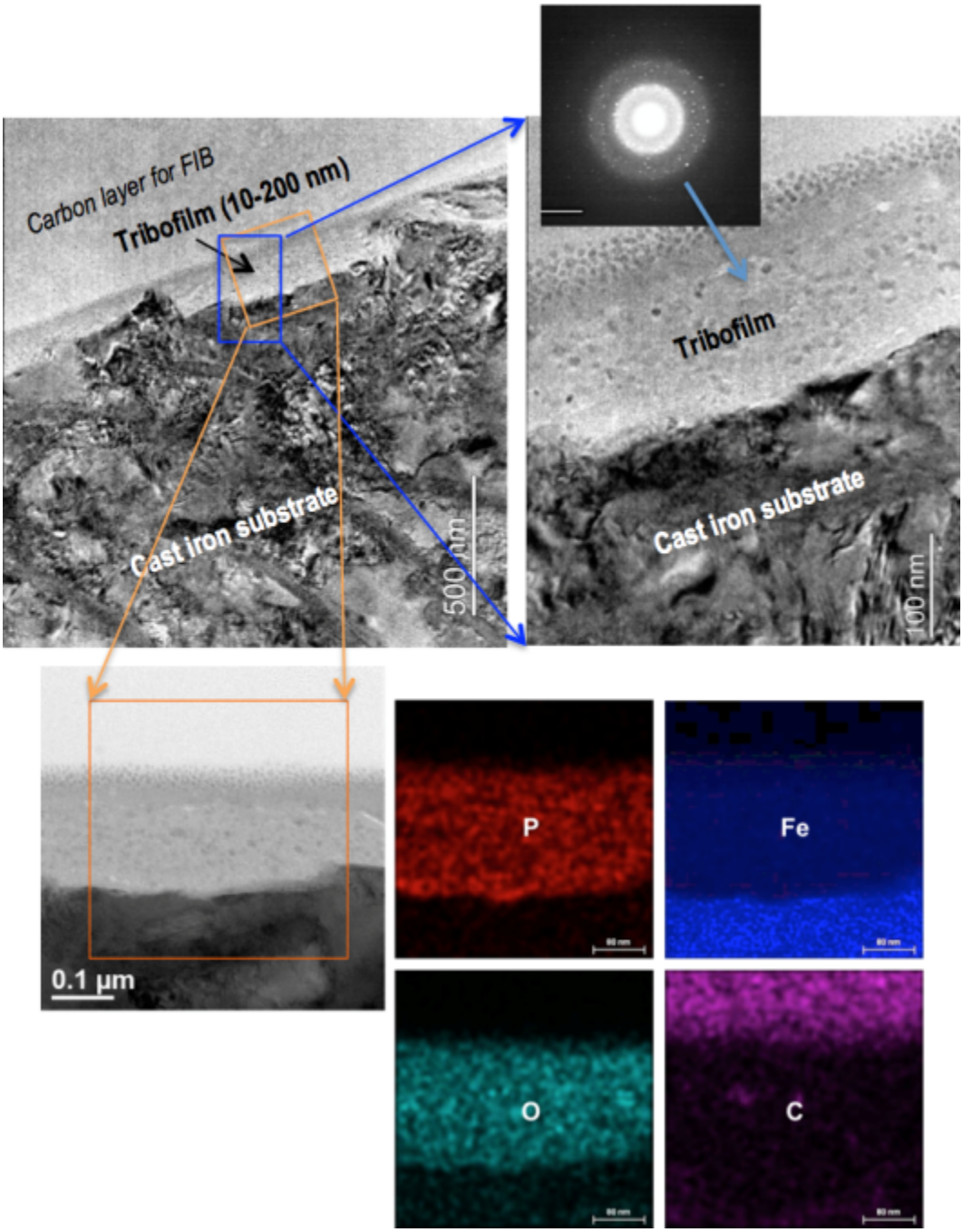

Figure 2.6. Cross-sectional TEM micrographs and electron diffraction pattern (top) and EDS elemental maps (bottom) of the tribofilm on the cast iron surface lubricated by base oil + $[P_{8888}][DEHP]$ [73].

2.2.3.3 Layer-by-layer XPS chemical analysis

XPS core level spectra of key elements of the worn cast iron surface lubricated by base oil + $[P_{8888}][DEHP]$ are shown in Fig. 2.7. The red spectra represent binding energies for the

initial 2-3 nm of the surface including the top of the tribofilm and any lubricant residue (even though all wear scars were carefully cleaned by solvents after wear testing). The green spectra were produced after 60 s of ion sputtering of the tribofilm to eliminate the surface contaminants.

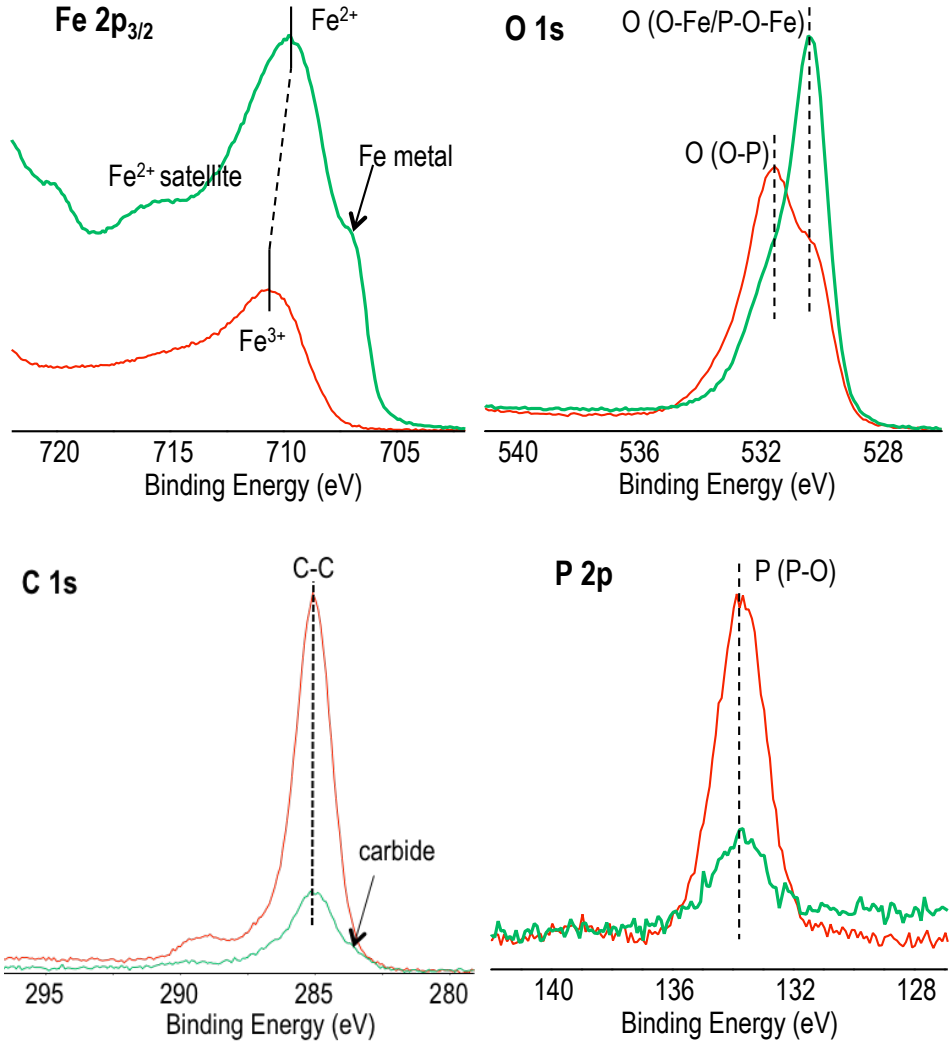

Figure 2.7. XPS core level spectra of key elements for the tribofilm on the cast iron surface lubricated by base oil + $[P_{8888}][DEHP]$ [73].

As compared in the core level spectra, iron on the top surface of the tribofilm is primarily in the Fe^{3+} oxidation state (710.5 eV binding energy, BE) while Fe^{2+} (709.7 eV BE) becomes the major peak after 60 sec sputtering. The ferric iron on the top surface is likely manifested as iron(III) oxide that developed during storage (several weeks) before XPS analysis. The phosphorus 2p spectra show a dominating P-O bond (133.7 eV BE) suggesting phosphates. The O 1s shows two distinct features: a peak at ~531.5 eV BE is assigned to O-P bonding (excluding P-O-Fe) and

another at 530.3 eV is attributed to O-Fe/P-O-Fe bonds. The higher amount of O-P detected on the top surface is possibly introduced by the IL residue, and the stronger O-Fe/P-O-Fe signal after 60 s of ion sputtering suggests most O atoms are bonded with iron phosphates and oxides. The same C 1s spectra (both before and after 60 sec of sputtering) show a dominant peak at 285.0 eV BE assigned to C-C bonding. This indicates that the carbon content in the tribofilm might be from residue hydrocarbon chains on the partially decomposed organophosphate anions. The metallic Fe and carbide peaks after 60-sec ion sputtering may be introduced by two sources: (1) iron substrate exposed by ion sputtering and (2) iron wear debris within the tribofilm. Based on binding energy analyses, the tribofilm formed by $[P_{8888}][DEHP]$, similar to that by $[P_{66614}][DEHP]$, is believed to be a composite of iron phosphates (or polyphosphates) and iron oxides.

The deconvoluted composition-depth profile (from 60 to 1790 sec of ion sputtering) is shown in Fig. 2.8a. As revealed in the cross-sectional TEM/EDS images in Fig. 2.6, the thickness of the tribofilm varies (10-200 nm in a 2 μm-long TEM sample), and Fe, O, and P have relatively uniform distributions in the tribofilm from the top surface to the interface with the substrate. Therefore, the rising signals of metallic iron and carbide and dropping signals of tribofilm elements along the sputtering time are largely a consequence of substrate exposure from material removal during ion sputtering. Assuming minimal metallic iron and carbide is embedded in the tribofilm (both less than 1 at% on the surface survey scan), we removed these two substrate signals, re-normalized other elements, and re-plotted the profile in Fig. 2.8b. This mitigates the bias from the increasingly exposed substrate and better reflects the composition change through the thickness of the tribofilm. The ratios of O(O-P):P and O(O-Fe/P-O-Fe):Fe(ion) are relatively constant throughout the film thickness, though the oxygen contents are somewhat higher than expected. Results indicate two possibilities: (1) phosphates gradually decrease while iron oxides increase inside the tribofilm from the top surface to the interface with the substrate, and (2) preferential sputtering removes phosphates faster than oxides.

The carefully designed group of five ILs with identical phosphate anions but different phosphonium cations allowed a systematic study of the effects of cation alkyl chain length and symmetry on critical physicochemical and tribological properties, which provide fundamental insights for future cation design in developing the promising phosphonium-phosphate ILs as lubricant additives. A new U.S. patent application [58] has recently been filed for the phosphonium-organophosphate ILs containing symmetric cations. Results suggest oil-soluble phosphonium-phosphate ILs as potentially candidate lubricant additives in friction and wear control, which may help allow the use of lower viscosity engine and industrial oils to improve machinery efficiency and durability.

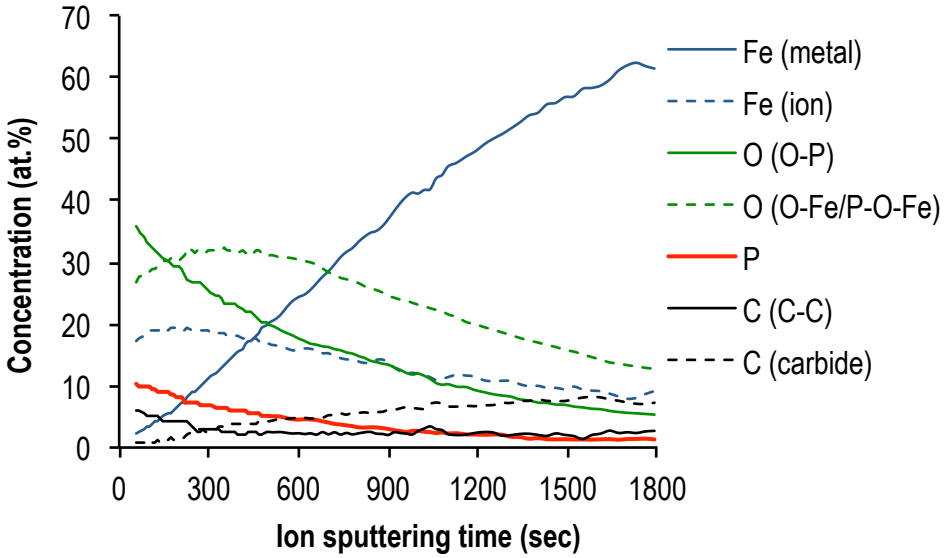

(a) Raw signals

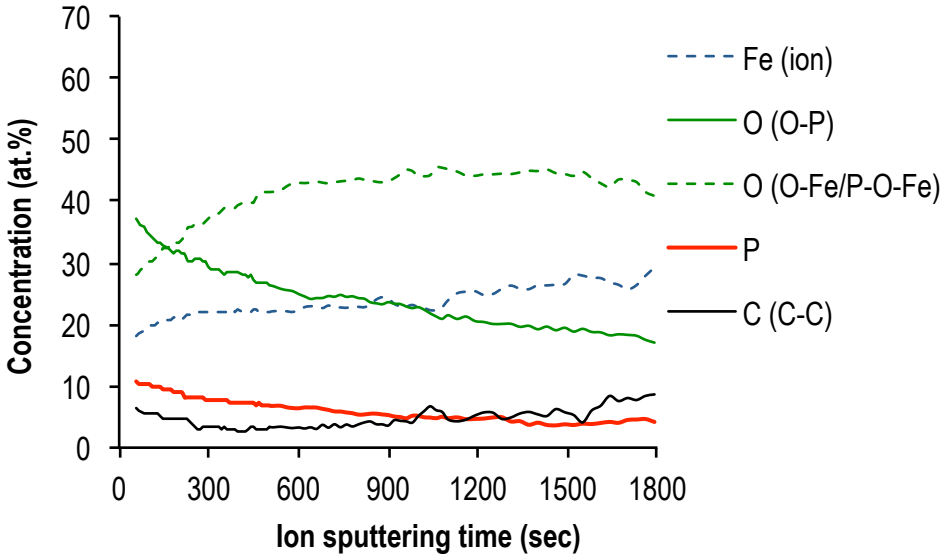

(b) Re-normalized after removing Fe (metal) and C (carbide) from the exposed substrate

Figure 2.8. XPS composition-depth profile of the tribofilm on the cast iron surface lubricated by base oil + $[P_{8888}][DEHP]$ [73].

CHAPTER 3. Tertiary and Quaternary Ammonium-Phosphate Ionic Liquids as Lubricant Additives

3.1. Experimental details and materials

Nine tertiary (protic) and quaternary (aprotic) ammonium cation ILs with organophosphate anions were synthesized in this study whose structures are located in Figure 3.1. The five aprotic ILs include tetraethylammonium bis(2-ethylhexyl) phosphate ($[N_{2222}][DEHP]$), tetrabutylammonium bis(2-ethylhexyl) phosphate ($[N_{4444}][DEHP]$), tetrahexylammonium bis(2-ethylhexyl) phosphate ($[N_{6666}][DEHP]$), tetraoctylammonium bis(2-ethylhexyl) phosphate ($[N_{8888}][DEHP]$), and trioctylmethylammonium bis(2-ethylhexyl) phosphate ($[N_{8881}][DEHP]$). The four protic ILs are triethylammonium bis(2-ethylhexyl) phosphate ($[N_{222}H][DEHP]$), tributylammonium bis(2-ethylhexyl) phosphate ($[N_{444}H][DEHP]$), trihexylammonium bis(2-ethylhexyl) phosphate ($[N_{666}H][DEHP]$), and trioctylammonium bis(2-ethylhexyl) phosphate ($[N_{888}H][DEHP]$). The synthesis of each IL is described below.

[Nnnnn][DEHP]

n = 2, 4, 6, 8

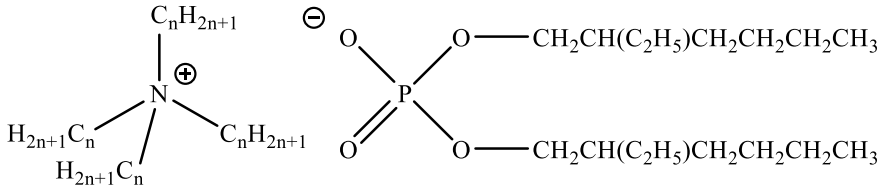

[N_{8881}][DEHP]

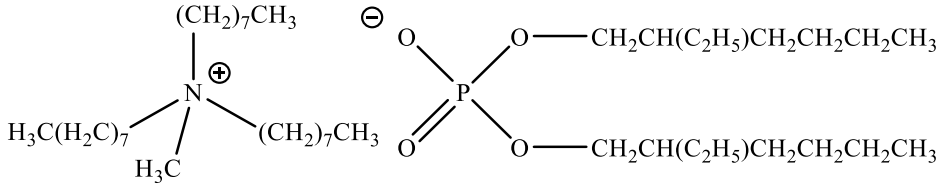

[NnnnH][DEHP]

n = 2, 4, 6, 8

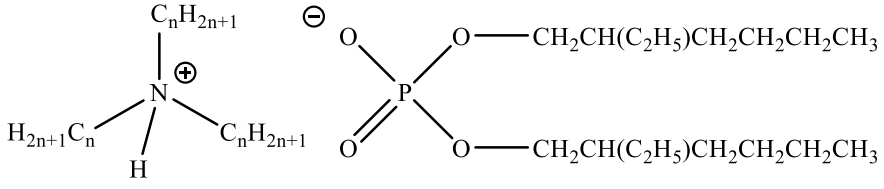

Figure 3.1. Molecular structures of the nine candidate ILs.

Viscosities of selected ILs were measured with a Petrolab MINIVIS II falling ball viscometer (OK, US). Three measurements were taken at each data point (23, 40 or 100 degrees

Celsius) to ensure a standard deviation below 1%. $[N_{888}H][DEHP]$ was selected for thermogravimetric analysis (TGA) to determine decomposition temperature in both air and nitrogen environments. A TA Instruments (DE, USA) TGA-2950 was used for TGA at a 10° C/min heating rate.

A low viscosity (4 cSt at 100 ^{o}C) based oil and an experimentally formulated (EF) engine oil without anti-wear (AW) additive were provided by Shell Global Solutions (TX, US) and served as the base lubricants in this study.

IL solubility in the base oil was determined by combining an IL with base oil starting at 1:1 ratio and shaking vigorously by hand for one minute. These shaken samples were then placed into a centrifuge at 13,000 rpm for 10 minutes. Any observed separation or cloudiness under bright lighting indicated insolubility. If separation or cloudiness was evident, the ratio was incrementally decreased until solubility was reached.

Ambient air corrosion tests were completed by placing a drop of each IL directly onto a 25.4 × 25.4 mm^2 CL35 cast iron surface and left for 49 days. The ILs' low volatility prevented evaporation from being a concern. Electrochemical corrosion experiments were performed on $[N_{888}H][DEHP]$ at room temperature using the potentiodynamic polarization technique with a three-electrode electrochemical cell. A cast iron disk (1 cm^2 exposed area) served as the working electrode, which was immersed in the electrolyte ($[N_{888}H][DEHP]$) for 15 min prior to testing. A Pt wire was the counter electrode, and Ag/AgCl (4M KCl solution) was the reference electrode. The sample was polarized at potentials from -1.0 to +1.50 V versus open circuit potential at a scanning rate of 0.166 mV/s in aerated conditions. The electrochemical test was conducted using a CHI 700C device (CH Instruments, Inc., Austin, TX, USA).

A Plint TE77 (Phoenix Tribology Ltd., UK) tribometer was used to evaluate the lubricant performance in boundary lubrication. This device produced a reciprocating sliding motion using a 10 mm AISI 52100 steel ball against a CL35 cast iron flat (Metal Samples Company, AL) submerged in candidate lubricants. Cast iron specimens were polished with 600-grade silicon carbide abrasive paper producing a lay perpendicular to the sliding direction. Interacting surfaces were cleaned with isopropyl alcohol and air dried before submersion in lubricant. Each test was performed at 100ºC under a 100 N load with an oscillation frequency of 10 Hz and a 10 mm stroke. Three replicate experiments were performed for each lubricant to determine repeatability. Balls and flats were cleaned in acetone and then isopropanol after testing. A Veeco (now Bruker, TX) Wyko NT9100 optical interferometer was used for measuring wear volumes.

A Hitachi S-4800 (Tokyo, Japan) scanning electron microscope (SEM) was used to study the worn surface. Cross-sectional makeup and nanostructure was examined with a Hitachi HF-3300 transmission electron microscope (TEM) (300kV, 1.3 Å resolution) equipped with a Bruker solid-state EDS detector. The TEM specimen was prepared using a Hitachi NB5000 focused ion beam (FIB) machine with a gallium ion source to extract a thin cross-section of the tribofilm. A

carbon film and then a tungsten layer were deposited onto the wear scar before the FIB process to preserve the tribofilm. A Thermo Scientific (MA, USA) K-Alpha x-ray photoelectron spectrometer (XPS) was applied to assess the chemical makeup of the selected tribofilm. The x-rays were monochromatic Al-kα photons. Photo emitted electrons were analyzed with a hemispherical energy analyzer. Surface compositions were calculated by computing peak areas of the primary core levels for all elements present and normalizing using tabulated sensitivity factors. Composition-depth profiles were obtained by Ar ion sputtering under 1 kV ion beam energy at high current.

3.2 Results

3.2.1 Solubility and Physical Properties

Oil solubility results of the set of ammonium-organophosphate ILs are listed in Table 3.1. Since each IL has the same anion, difference in solubility is solely due to the cation structure. Each aprotic IL ([Nnnnn][DEHP] and [N_{8881}][DEHP]) consistently showed less than 1 wt.% solubility in the base oil for n=2, 4, 6, or 8. In contrast, protic ILs ([NnnnH][DEHP]) displayed a trend of increasing solubility from <1 wt.% for n = 2 to >10 wt.% for n=8. Increasing solubility with larger alkyl moieties can be explained by a corresponding increase in dispersion forces coupled with a dilution of charge within the ion pair. The protic IL series' improved solubility is most likely a result of hydrogen bonding between the cation and anion to form a quasi-neutral molecule that is more compatible with the non-polar neutral base oil. Such hydrogen bonding is not present in the aprotic ILs. The maximum treat rate of each IL was calculated based on the upper limit of the phosphorous content (800 ppm, regulated by International Lubricants Standardization and Approval Committee GF-5 specifications) as shown in Table 3.1.

Table 3.1 IL molecular weight, oil solubility, target concentration and dynamic viscosity.

Ionic liquid	Molecular weight	Solubility in base oil (wt%)	Solubility in EF w/o AW (wt%)	IL max treat rate in oil (wt%)	Viscosity (cSt)	
					40 ^{o}C	100 ^{o}C
[N_{2222}][DEHP]	452	<1	<1	1.17		
[N_{4444}][DEHP]	568	<1	<1	1.46	667	32.7
[N_{6666}][DEHP]	676	<1	<1	1.75		
[N_{8888}][DEHP]	792	<1	<1	2.04	1292	93.1
[N_{8881}][DEHP]	694	>3, <5	>3, <5	1.78		
[N_{222}H][DEHP]	427	<1	<1	1.09		
[N_{444}H][DEHP]	511	>5	>2, <5	1.31		
[N_{666}H][DEHP]	595	>5	>2, <5	1.53		
[N_{888}H][DEHP]	676	>10	>10	1.74	178	13.7

TGA results for the protic IL series are shown in Figure 3.2. ILs in this series with fewer carbons per alkyl chain show lower onset decomposition temperatures than their larger-alkyl counterparts.

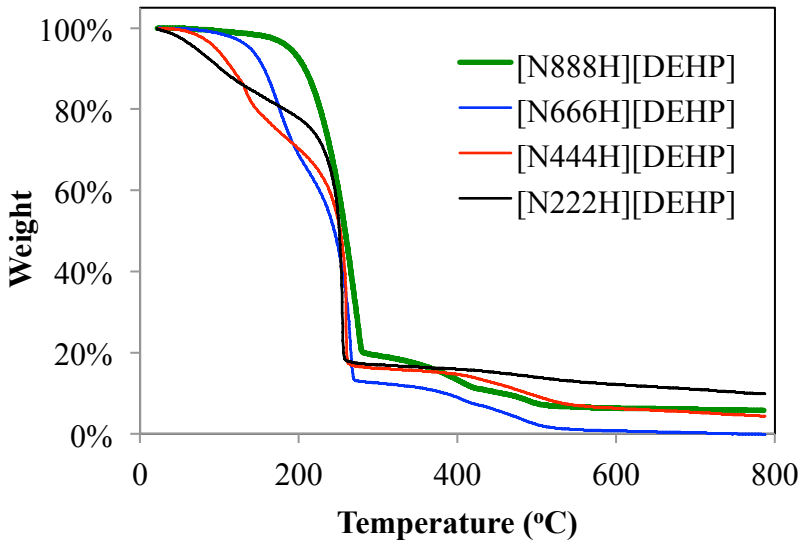

Figure 3.2 Thermal decomposition curves of protic ILs in N_2.

3.2.2 Corrosion Behavior

In open air corrosion tests the cast iron surface showed some pits for aprotic ILs ([Nnnnn][DEHP] where N=2,4,6,8) by day 14, but the corrosion features had no propagation between days 14 and 49. This implies that corrosion is likely caused by the impurities in the ILs, such as residue of Cl^- or Br^- from the feedstocks, instead of the ILs themselves.

On the other hand, the protic ILs ([N_{nnn}H][DEHP] n=2,4,6,8) showed no signs of corrosion in the open air tests. [N_{888}H][DEHP] was then chosen for electrochemical measurement. Figure 3.3 shows the potentiodynamic polarization curve that clearly shows active-passive behavior with strong passivation at a current density on the order of 10^{-4}A/cm. No morphology change on the cast iron surface was evident after testing.

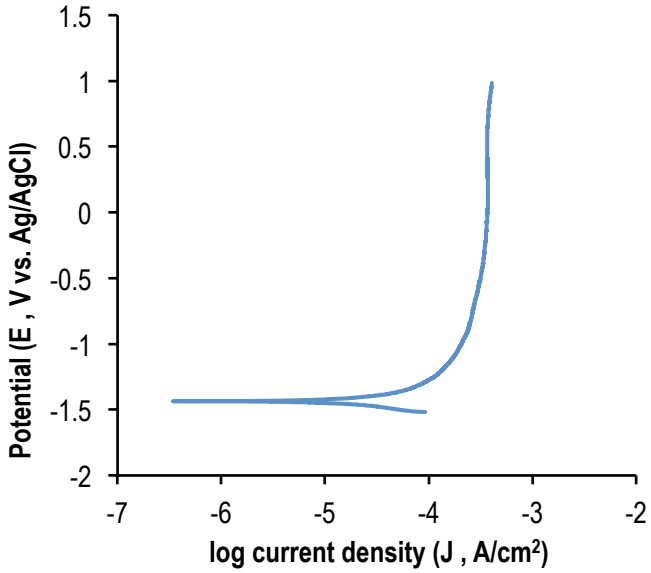

Figure 3.3 Potentiodynamic polarization curve for $[N_{888}H][DEHP]$ on cast iron showing strong passivation.

3.2.3 Tribological Results

3.2.3.1 ILs in Base Oil

Three ILs were chosen for tribological testing as additives in the base oil: $[N_{8888}][DEHP]$, $[N_{8881}][DEHP]$ and $[N_{888}H][DEHP]$ with treat rates of 2.04, 1.78, and 1.74 wt%, respectively. Although $[N_{8888}][DEHP]$ and $[N_{8881}][DEHP]$ have true oil solubility less than 1 wt% upon centrifuging, they are able to suspend in the oils at the above described treat rates for a short period (hours). The oils containing the two aprotic ILs were shaken well prior to tribo-testing. Friction and wear results for each of these ILs in base oil are shown in Figure 3.4. During the initial 25 m of sliding, the friction coefficient for the base oil rose sharply indicating a more severe break-in compared to the IL-containing lubricants. The base oil's average friction coefficient dropped after break-in but remained elevated throughout the tests compared to IL-containing oils. All three ILs demonstrated friction-reducing capability when blended with the base oil. Each lubricant in this series generated similar friction traces with only slight differences in steady-state friction (~4%) with the $[N_{888}H][DEHP]$ blend slightly outperforming the others.

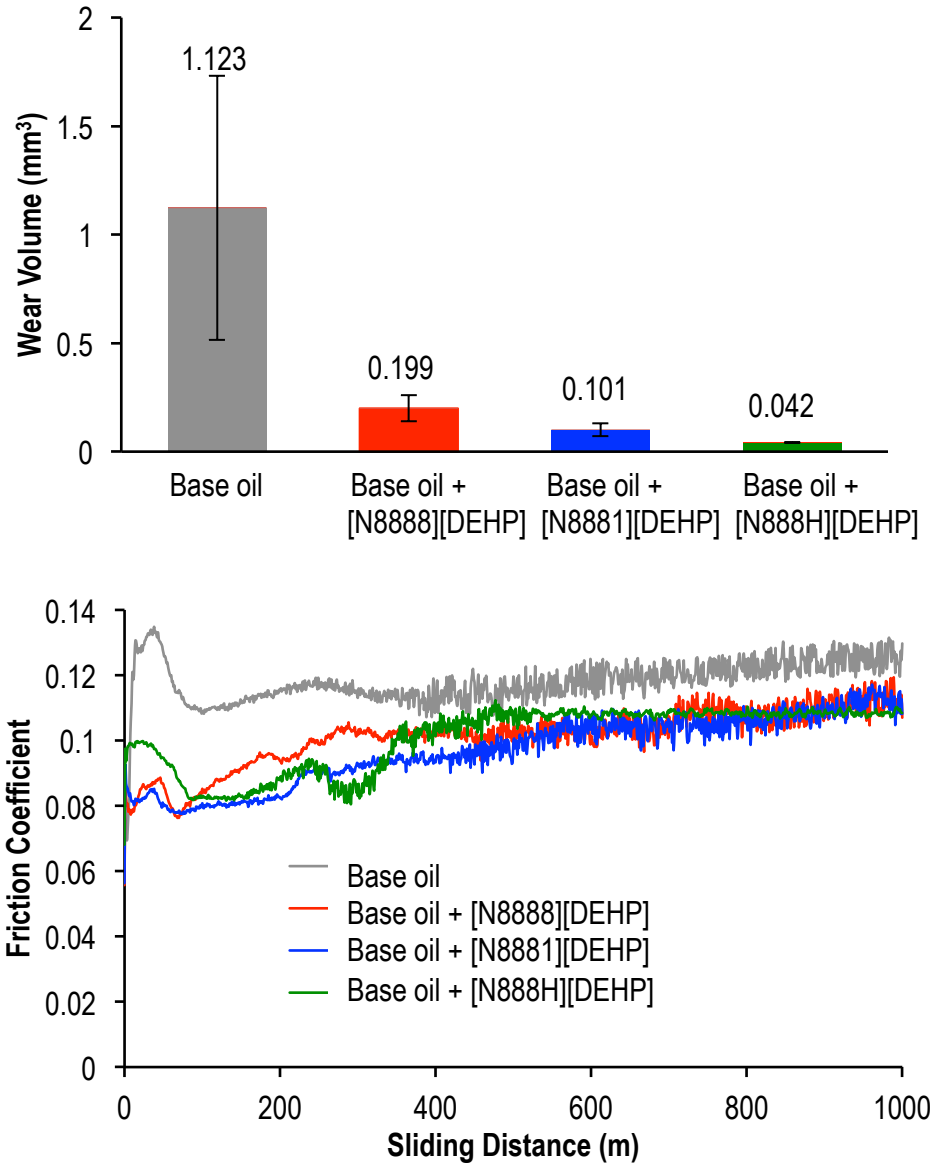

Figure 3.4 Wear (top) and friction (bottom) results for the base oil + IL tests. Each wear data point and friction trace represents an average of three repeated tests. Ball wear volume is shown but is too small to be visible atop the flat wear volume bars.

In addition to friction reduction, each IL induced a significant reduction in wear compared to the base oil (by 82% to 96%) with the protic [N_{888}H][DEHP] generating the least amount of wear. The neat base oil experienced elevated wear associated with scuffing for two out of three tests producing a large error bar. Steel ball wear was consistently two orders of magnitude smaller than that of the softer cast iron flats in all tests.

3.2.3.2 ILs in Experimentally Formulated Engine Oil

The same three ILs were added to the experimentally formulated engine oil without AW for further tribological evaluation. Results for this series are shown in Figure 3.5. Among the two aprotic ILs, $[N_{8888}][DEHP]$ slightly reduced the friction while $[N_{8881}][DEHP]$ had little impact. The protic $[N_{888}H][DEHP]$-additized EF oil showed the lowest steady-state friction coefficient by a larger margin compared with the EF oil without AW or with either aprotic IL.

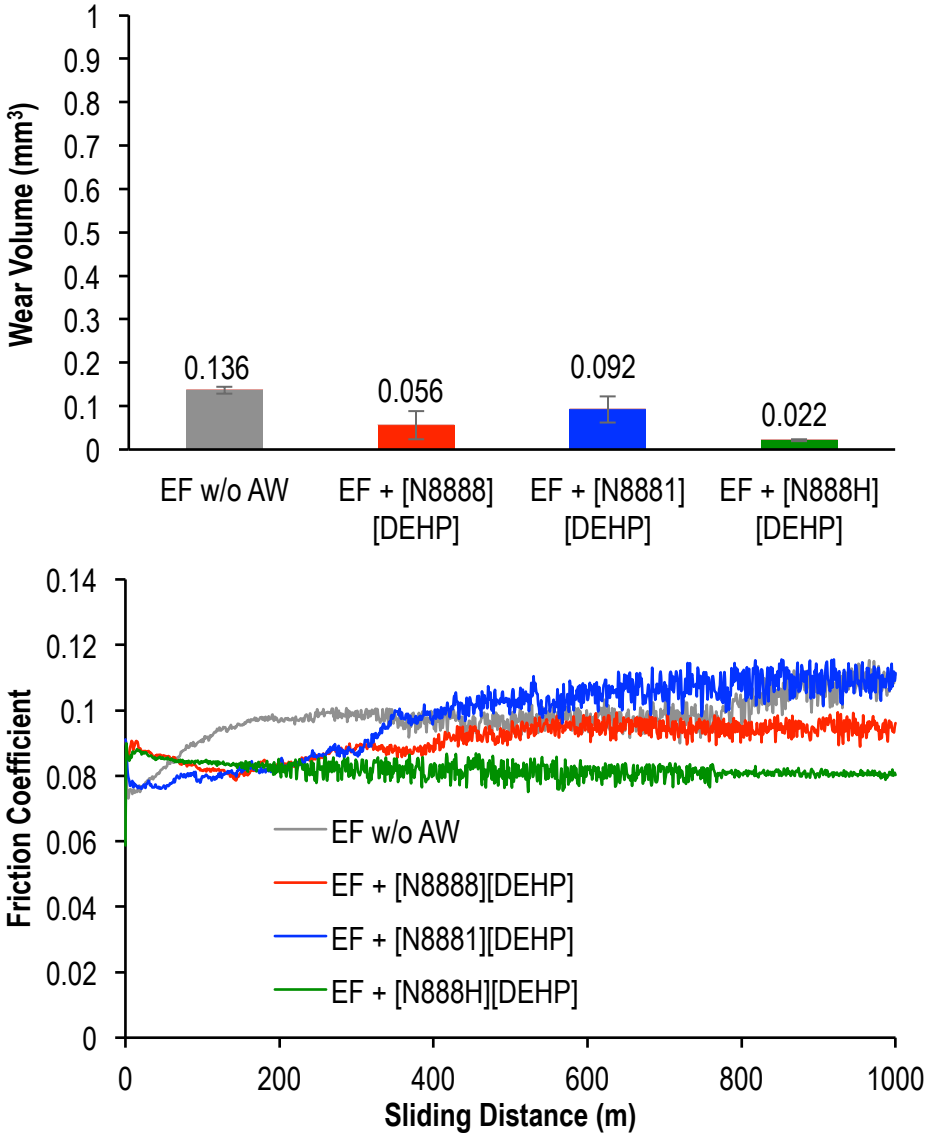

Figure 3.5 Wear (top) and friction (bottom) results for the experimental formulation (EF) + IL tests. Each wear data point and friction trace represents an average of three repeated tests. Ball wear volume is shown but is too small to be completely visible atop the flat wear volume bars.

In terms of wear, each IL provided benefit compared to the EF oil without AW. The protic IL, [N_{888}H][DEHP], again demonstrated better wear protection than the two aprotic ILs.

3.2.4 Surface Analysis

3.2.4.1 Scanning Electron Microscopy

Owing to its superior friction- and wear-reducing properties, the wear scar generated on a cast iron flat by base oil + 1.74% [N_{888}H][DEHP] was chosen for more detailed surface analysis beginning with SEM top surface morphology examination. Figure 3.6 shows two SEM micrographs for wear scars generated by both the neat base oil without and with 1.74% [N_{888}H][DEHP]. The base oil produced a wear scar with many tightly spaced longitudinal grooves. The higher magnification micrograph shows indications of abrasive and adhesive wear. In contrast, the scar generated by the IL-containing oil is much narrower and shallower. Grooving is sparser with interspersed darker patches that appear relatively smooth.

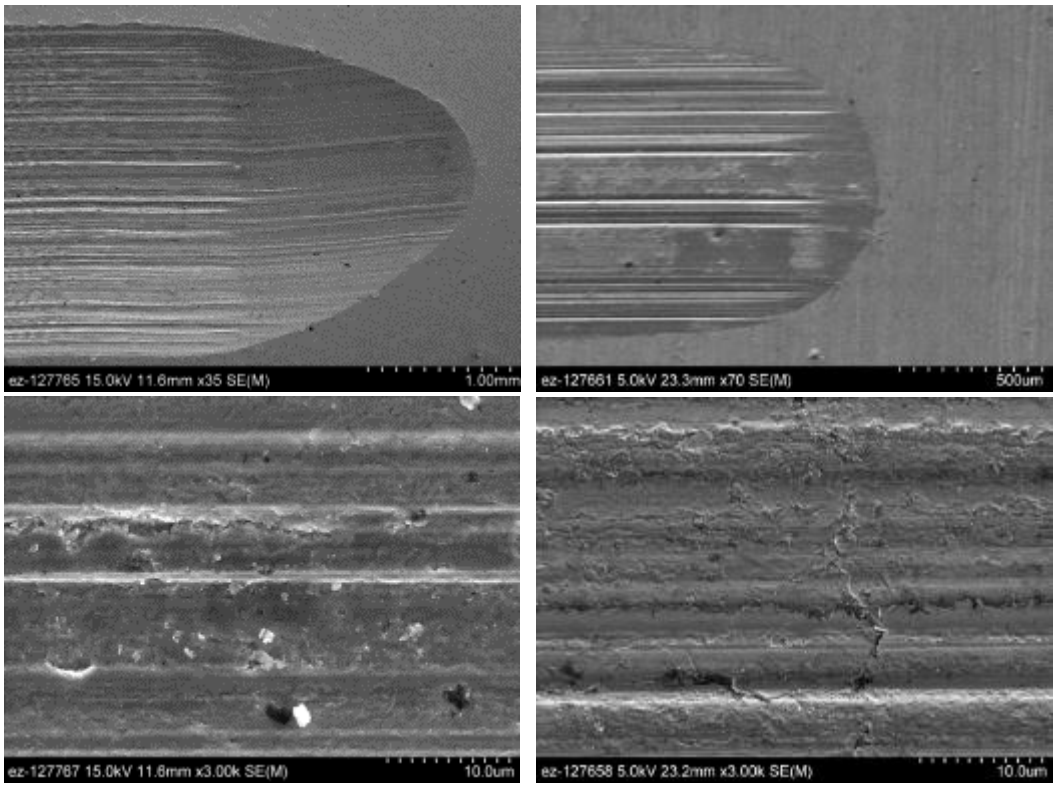

Figure 3.6 SEM micrographs of wear scars lubricated by the base oil (left) and base oil + 1.74% [N_{888}H][DEHP] (right).

3.2.4.2 Transmission Electron Microscopy

Assisted by FIB milling, cross-sectional TEM imaging, EDS elemental mapping and electron diffraction were completed from the wear scar produced by the base oil containing 1.74% [N_{888}H][DEHP] (Figure 3.7). TEM micrographs reveal the presence of a protective tribofilm up to approximately 350 nm thick. EDS results appear to show a double-layer film with by P, O, and Fe rich in the top layer, suggesting a mixture of iorn phosphates and oxides and an interlayer likely predominantly consisting of iron oxides. It should be noted that this double-layer structure is not necessarily representative of the entire tribofilm as lower magnification micrographs in previous work [33] of a phosphonium-organophosphate IL clearly show transitions between single- and double-layer films around valleys in the substrate. N is indicated sparsely throughout both layers of the film. Excluding the C signals from the uppermost layer (a protective film for FIB processing) and from the substrate, C appears to be present in relatively small amounts in the tribofilm, suggesting low contents of organic compounds. Within each layer, P, Fe and O are dispersed rather uniformly. Electron diffraction indicates that the film is amorphous and populated with many small (<10 nm) nanocrystals.

3.2.4.3 XPS Core Level Spectra

XPS core level spectra of the worn cast iron flat lubricated with base oil + 1.74% [N_{888}H][DEHP] is shown in Figure 3.8. The spectra were recorded after 60 s of ion sputtering of the surface. The C 1s spectrum shows dominating C-C bonding peak (285 eV). Organic carbon is present within the film likely originating from undecomposed IL constituents. The P 2p spectrum suggests the presence of phosphates, commonly observed tribochemical components, due to the strong P-O binding energy peak (133.7 eV), but this does not preclude other iron-phosphorous compounds. Additionally, a small amount of P-metal bonds are revealed. Fe core level spectrum suggests a mixture of ferrous, ferric and metallic iron. The presence of metallic iron along with the carbide peak in C 1s spectrum are a result of substrate exposure (tribofilm removed by ion sputtering) and unreacted wear debris inclusion in the tribofilm. O 1s core level spectrum confirms the presence of oxides and phosphates.

3.2.4.4 Comparison between phosphonium-phosphate and ammonium-phosphate ILs

The tribological performance of phosphonium-phosphate (e.g., [P_{8888}][DEHP] and [P_{66614}][DEHP]) and ammonium-phosphate ILs (e.g., [N_{888}H][DEHP]) and their compatibility when used together with ZDDP have been compared side-by-side, and results are presented and discussed in next chapter.

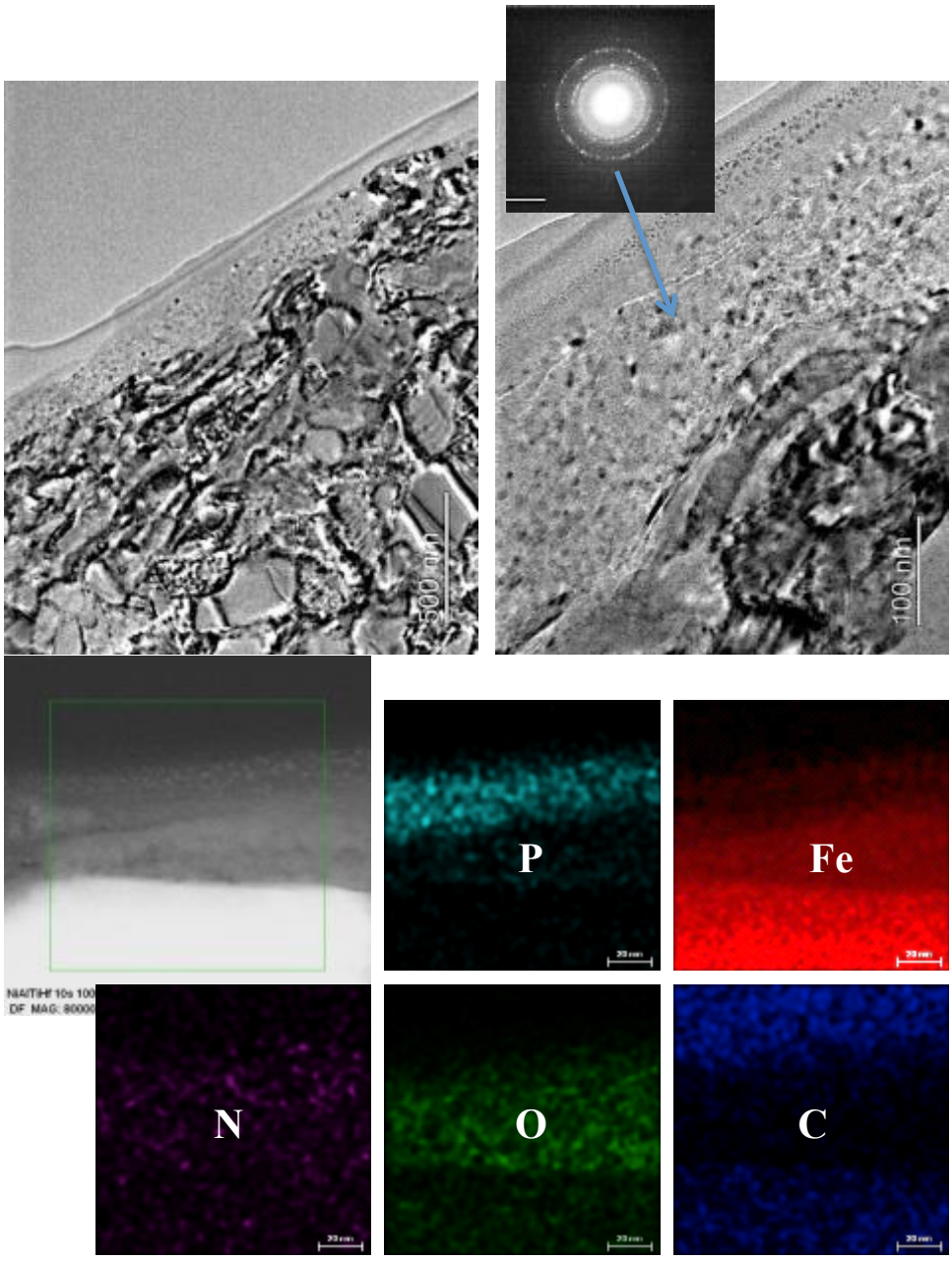

Figure 3.7 Cross-sectional TEM micrographs, EDS elemental mapping and electron diffraction of tribofilm on the cast iron flat lubricated by base oil + 1.74% [N_{888}H][DEHP].

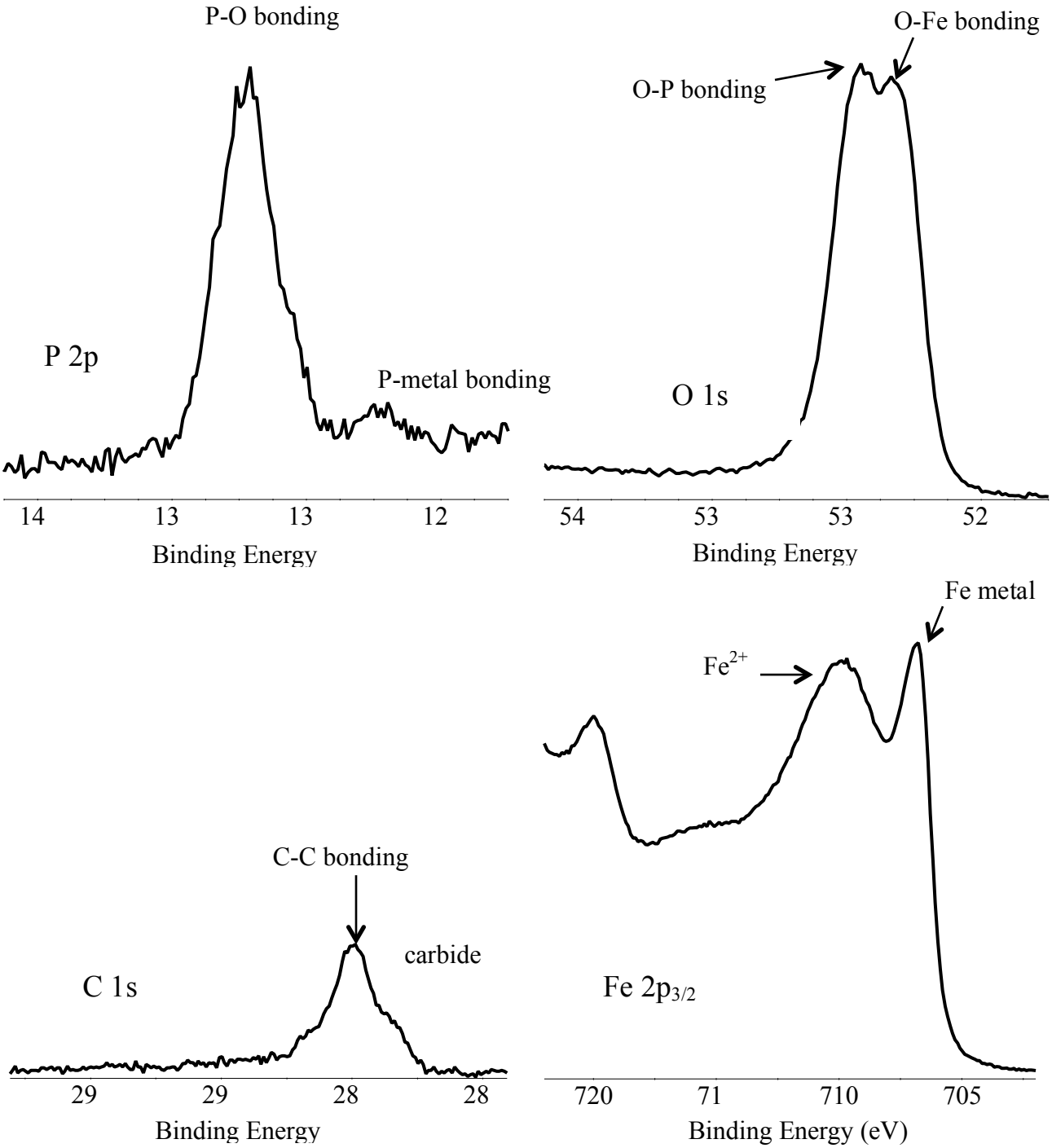

Figure 3.8 XPS core level spectra of the tribofilm on the cast iron flat lubricated by base oil + 1.74% [N_{888}H][DEHP]. Signals collected after 60 s of ion sputtering.

CHAPTER 4. Synergistic Effects Between Ionic Liquids and ZDDP as Lubricant Additives

4.1 Experimental section

The base oil cSt base oil was provided by Shell Global Solutions (US). Its density is 0.82 g/cc and viscosity is 18.5 and 4.0 cSt at 40 and 100 ^{o}C, respectively. The four ILs studied here were synthesized in our chemical labs using processes reported by Sun et al. [59] Detailed synthesis for the specific four ILs have been reported previously: [P_{66614}][DEHP], [P_{66614}][BTMPP], [P_{8888}][DEHP], and [N_{888}H][DEHP]. The phosphonium cation feedstocks were kindly provided by Cytec Industries, and the other starting materials were purchased from Sigma-Aldrich. All four ILs are mutually miscible in the base oil base oil. This particular ZDDP was supplied by Lubrizol and is a blend of a secondary ZDDP with 5-10% mineral oil and has a solubility of 1-2 wt% in the base oil base oil. Viscosities were measured using a Petrolab MINIVIS II viscometer based on the falling-sphere technique.

The International Lubricants Standardization and Approval Committee (ILSAC) GF-5/6 specifications limit the phosphorous content up to 0.08 wt% in automotive engine oils. Therefore, in this study, the ZDDP, ILs, and ZDDP+IL combinations were blended into the base oil base oil at the same phosphorous level of 0.08 wt%. As a result, the treat rates (wt%) are 0.8% for ZDDP, 1.0-1.74% for ILs, and half amount of each for ZDDP+IL combinations. In any combination, the ZDDP and IL contribute equal amount of phosphorus. The change in oil viscosity when adding ZDDP and/or IL was minimal due to the low treat rates.

Tribological tests were conducted on a Phoenix-Tribology Plint TE77 reciprocating sliding tribometer using an AISI 52100 steel ball against a CL35 grey cast iron flat (polished using 600 grit SiC grinding paper). The reason we used steel rubbing against grey cast iron is to mimic the common materials interface of the piston ring (steel) against cylinder liner (grey cast iron) in an actual engine. At a controlled oil temperature of 100 ºC, tests were carried out under a 100 N normal load at a 10 Hz oscillation with a 10 mm stroke for 1000 m sliding. At least three replicate tests were performed for each lubricant. Friction force was captured *in situ* by measuring the tangential force using a piezoelectric load cell. After testing, all specimens were cleaned with acetone and then isopropyl alcohol. Wear volumes were quantified using a Wyko NT9100 white light interferometer.

Cross-sectional examination of the tribofilms was carried out using a Hitachi HF-3300 TEM (300kV) bundled with a Bruker solid-state EDS detector. TEM samples were prepared using a Hitachi NB5000 focused ion beam (FIB) system with a gallium ion source to extract a thin cross-section of the surface area of interest. A protective carbon film and then a tungsten layer were deposited onto the wear scar before the FIB process. A Thermo Scientific K-Alpha XPS was used to analyze the chemical compositions of tribofilms and the oil+additive blends. The x-rays used were monochromatic Al-kα photons, and photo emitted electrons were analyzed

with a hemispherical energy analyzer. Compositions were calculated by measuring peak areas of the primary core levels for all elements present and normalizing the peak areas using tabulated sensitivity factors. Composition-depth profiles of tribofilms were obtained by 1 kV Ar-ion sputtering. XPS core level spectra were acquired after 30 s of ion sputtering to eliminate any surface contaminants. The base oil base oil, ZDDP, ILs used in this study, and oil-+additive blends all have such low vapor pressures that they can survive in the XPS vacuum chamber long enough to be analyzed. By pressing clean Al foil over 2 mm clear holes in the XPS sample holder, small wells were formed that could hold a single drop of liquid. The liquid drop was visually monitored during pump-down in the load-lock of the XPS system to confirm stability. The liquid was then passed into the chamber and positioned normally for XPS characterization. No special data acquisition routine was required to obtain wide energy range survey spectra (0-1350 eV, 1 eV steps, pass energy 200 eV) or narrow energy range core level spectra (0-20 eV range, 0.1 eV steps, 50 eV pass energy). FT-IR spectra were measured using a Perkin Elmer FT-IR spectrometer (Frontier LR 64912C) equipped with Universal ATR Sampling Accessory.

Nanoindentation was conducted on selected tribofilms using a TI-950 TriboIndenter I (Hysitron, Minneapolis, MN). The system was calibrated using a 100-indent area function routine on fused-quartz. Indentation was carried out under load control with a diamond Berkovich tip. The load function was trapezoidal with a peak load of 1200 μN and a hold period of 10 sec. More than 50 indents were collected for each tribofilm. Indents were examined under microscope and 'bad' indents (e.g., located at surface defects) were excluded from the data analysis.

4.2 Results and Discussion

While our previous results on using ILs alone as oil additives are promising, here we report interesting new observations of unique synergistic effects between phosphonium-alkylphosphate ILs and a conventional anti-wear additive zinc dialkyldithiophosphate (ZDDP). [60] This study also provides fundamental insights of the roles of cations and anions in the synergism, change in the tribofilm's composition and mechanical properties when both the IL and ZDDP present in the lubricant, and possible chemical interactions between IL and ZDDP molecules. Such a discovery straddles the range between organic chemistry, surface science, and mechanical engineering, and is important for both scientific understanding and technology implementation.

The molecular structure of the IL, tetraoctylphosphonium bis(2-ethylhexyl)phosphate ([P_{8888}][DEHP]) is illustrated in Fig. 4.1a. We had previously reported tribological characteristics of [P_{8888}][DEHP] when used alone as an oil additive [73]. Here, a test lubricant was prepared using a base oil (4 cSt at 100 ^{o}C) with addition of 0.4 wt% ZDDP and 0.52 wt% [P_{8888}][DEHP] (1:1 molecular ratio for ZDDP:IL), and was benchmarked against two oils containing either the

ZDDP (0.8 wt%) or the IL (1.04 wt%) alone. All contain the same phosphorus content of 0.08 wt%. The addition of the ZDDP and/or IL induced little change to the oil viscosity. Figure 4.1a compares the friction and wear results for the three lubricants evaluated using a reciprocating sliding tribo-test with a steel ball against a cast iron flat. Each friction coefficient trace or wear volume represents the mean of three repeat tests. Results clearly show that using ZDDP+IL reduced the steady-state friction coefficient by ~30% and the wear volume by >70% compared to that using the ZDDP or IL alone. Such a synergistic effect raises several fundamental questions: Q1: Is this unique to phosphonium-alkylphosphate ILs? Q2: Between the cation or anion, which plays the critical role? Q3: Does the ZDDP+IL combination affect the tribofilm nanostructure or composition? And most importantly, Q4: What is the underlying mechanism?

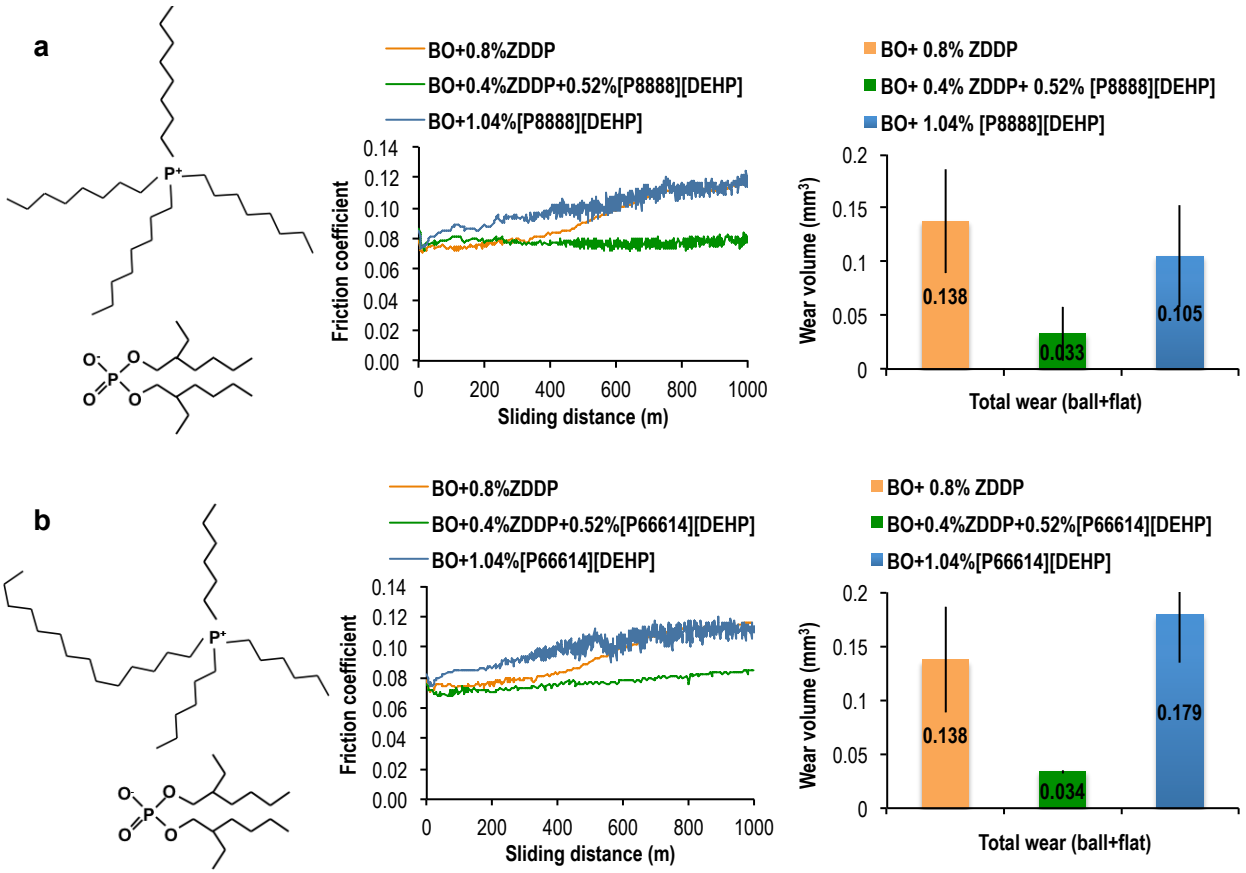

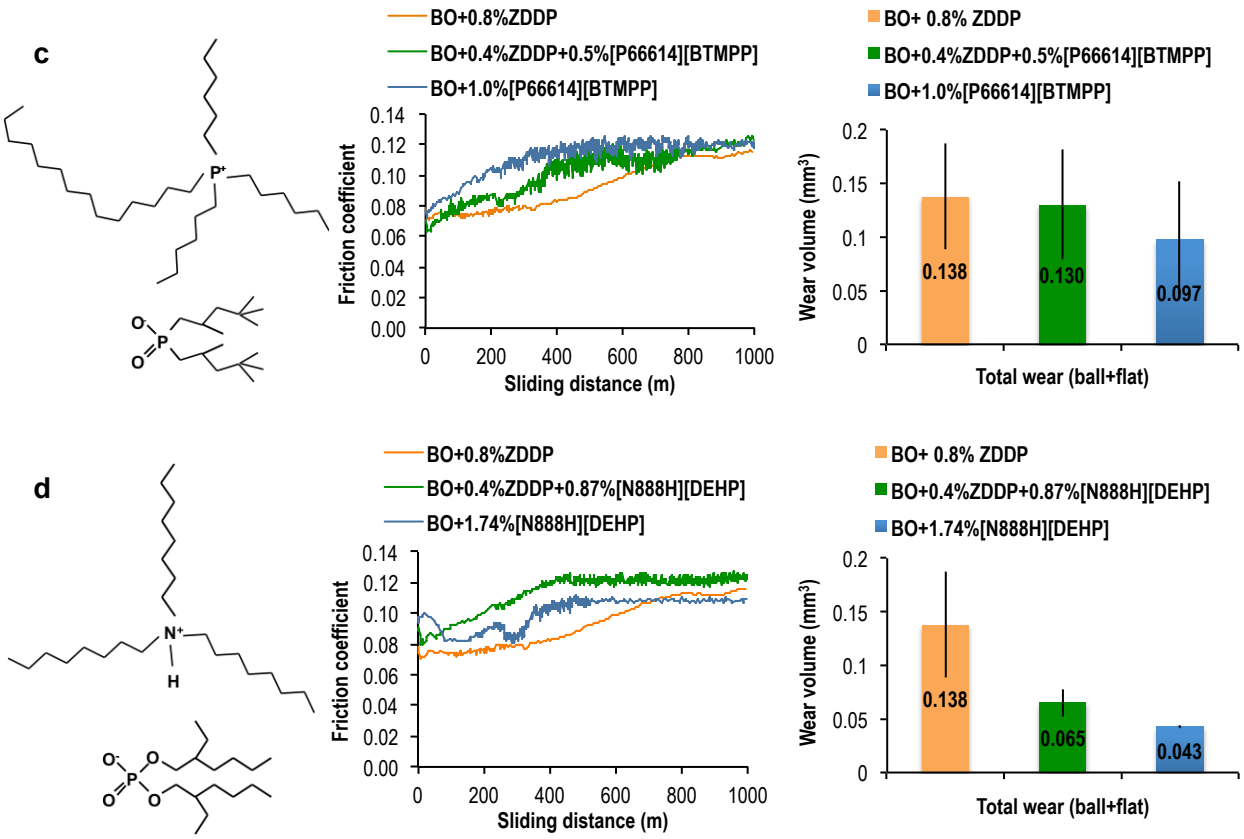

Figure 4.1. Molecular structures of four ILs from three groups and tribological results when using them alone and together with ZDDP as lubricant additives. Phosphonium-alkylphosphate: (a) $[P_{8888}][DEHP]$ and (b) $[P_{66614}][DEHP]$, phosphonium-alkylphosphinate: (c) $[P_{66614}][BTMPP]$, and ammonium-alkylphosphate: (d) $[N_{888}H][DEHP]$. Results clearly show synergistically reduced friction and wear when combining $[P_{8888}][DEHP]$ or $[P_{66614}][DEHP]$ with ZDDP, compared with using the IL or ZDDP alone. In contrast, no such synergism with ZDDP for either $[P_{66614}][BTMPP]$ or $[N_{888}H][DEHP]$, even though the former has the identical cation as $[P_{66614}][DEHP]$ and the latter shares the same anion with $[P_{8888}][DEHP]$ and $[P_{66614}][DEHP]$. [*Note: The relative low wear for using $[N_{888}H][DEHP]$ alone is attributed to the 2x anion concentration compared to other three ILs. The large deviations of wear volumes are primarily caused by the naturally inhomogeneous microstructure of the grey cast iron samples.*] [74]

To answer the first two questions, three additional ILs were selected: trihexyltetradecylphosphonium bis(2-ethylhexyl)phosphate ($[P_{66614}][DEHP]$), trihexyltetradecylphosphonium bis(2,4,4-trimethylpentyl)alkylphosphinate ($[P_{66614}][BTMPP]$), and trioctylammonium di(2-ethylhexyl)phosphate ($[N_{888}H][DEHP]$). As illustrated in Figs. 4.1(b-d), $[P_{66614}][DEHP]$ shares the identical cation with $[P_{66614}][BTMPP]$ and a matching anion with $[N_{888}H][DEHP]$. All three ILs are mutually miscible with the base oil base oil and possess anti-wear functionality when used as oil additives. Here six test lubricants were prepared using each of the three ILs alone and together with the ZDDP, all having the same phosphorus content

of 0.08 wt% . Tribological results are summarized in Fig. 4.1(b-d). $[P_{66614}][DEHP]$, from the same phosphonium-alkylphosphate group as $[P_{8888}][DEHP]$, showed similar synergistic friction and wear reductions when used together with ZDDP. In contrast, neither $[P_{66614}][BTMPP]$ nor $[N_{888}H][DEHP]$ had such synergistic effects with ZDDP, even though these two ILs share either the same cation or the same anion with $[P_{66614}][DEHP]$. Results indicate that the synergy with ZDDP is unique for phosphonium-alkylphosphate ILs and both the cation and anion are critical.

To understand the impact on the tribofilm (Q3), transmission electron microscopy (TEM), energy-dispersive X-ray spectroscopy (EDS), and X-ray photoelectron spectroscopy (XPS) were used to characterize the worn cast iron surfaces. Figure 4.2a shows the cross-sectional TEM image and EDS elemental maps, aided by focused-ion beam (FIB), of a tribofilm generated in base oil+ZDDP+$[P_{8888}][DEHP]$. The tribofilm is 10-200 nm thick in the imaging area, appears to be amorphous, and is rich in Fe, Zn, O, and P with little S. The XPS chemical analysis results in Fig. 4.2b indicate that the tribofilm composition is quite different from that produced by ZDDP or $[P_{8888}][DEHP]$ alone. For oxygen 1s, the O−P bond (531.5 eV BE) of phosphates is more intense than the O−M bond (530.3 eV BE) of metal oxides. Sulfur is primarily in the metal sulfide state, similar to that in a ZDDP tribofilm, but the concentration is much lower. As summarized in Fig. 4.2c, the ZDDP+$[P_{8888}][DEHP]$ tribofilm distinguishes itself with (1) elevated Zn compounds (considering only half amount of Zn in base oil+ZDDP+$[P_{8888}][DEHP]$ compared to that in base oil+ZDDP), (2) suppressed S content (considering more S supply than Zn), and (3) increased content of phosphates but less oxides. Zinc and iron phosphates seem to be the dominant compounds. For comparison, similar XPS analysis was applied to the tribofilms generated in the two non-synergistic lubricants base oil+ZDDP+$[P_{66614}][BTMPP]$ and base oil+ZDDP+$[N_{888}H][DEHP]$, and their composition-depth profiles and elemental contents are shown in Fig. 4.2c. In either case, the tribofilm contains little Zn or S with an oxide-phosphate ratio similar to that produced by the ZDDP or IL alone. Results imply a correlation between the content of metal phosphates in the tribofilm and wear protection.

a

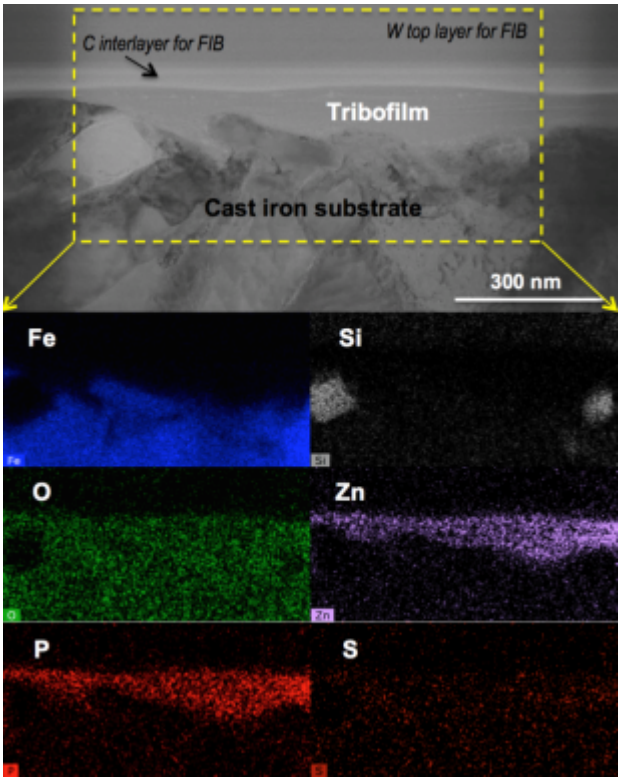

b

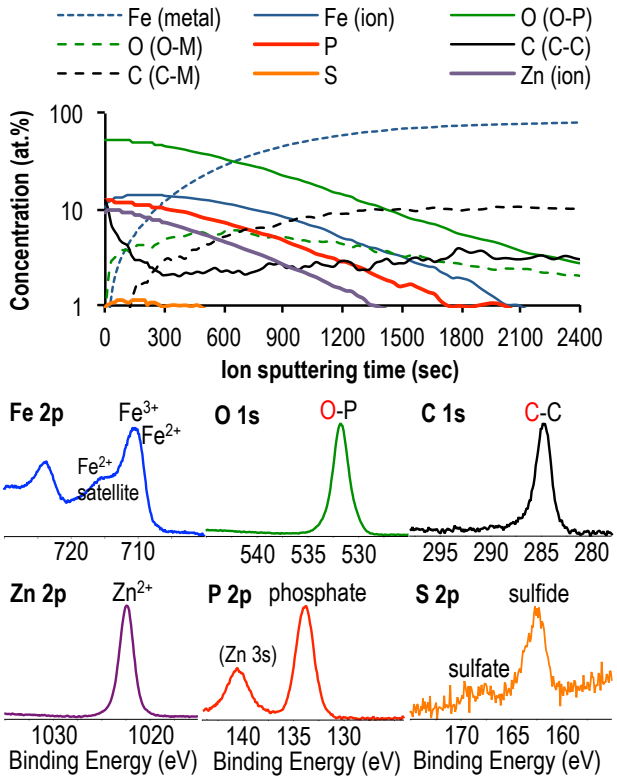

c

Element in tribofilm (at%)	C	Fe^0	$Fe^{2+/3+}$	O (O-M)	O (O-P)	P	S	Zn
base oil+0.8%ZDDP	6.7	0.7	13.3	11.1	42.8	10.3	8.4	6.5
base oil+1.04%[P_{8888}][DEHP]	7.0	1.2	16.3	25.1	39.3	11.1	0	0
base oil+0.4%ZDDP+0.52%[P_{8888}][DEHP] as shown in (a) and (b)	7.0	1.2	12.8	**2.9**	**52.8**	**12.2**	**1.1**	**10.0**
base oil+1.0%[P_{66614}][BTMPP]	17.4	3.6	24.2	31.3	20.7	2.8	0	0
base oil+0.4%ZDDP+0.5%[P_{66614}][BTMPP]	8.0	14.7	21.7	39.3	12.8	1.3	1.7	0.4
base oil+1.74%[$N_{888}H$][DEHP]	14.2	15.9	10.8	22.2	28.9	8.0	0	0
base oil+0.4%ZDDP+0.87%[$N_{888}H$][DEHP]	12.3	5.7	22.7	12.8	36.5	7.1	1.7	1.2

d

by nanoindentation	Hardness (GPa)	Reduced modulus (GPa)	P/S^2 ($nm^2/\mu N$)
base oil+0.8%ZDDP	$5.1^{\pm 1.4}$	$124^{\pm 27}$	**$0.27^{\pm 0.10}$**
base oil+1.04%[P_{8888}][DEHP]	$7.8^{\pm 1.6}$	$163^{\pm 20}$	**$0.24^{\pm 0.07}$**
base oil+0.4%ZDDP+0.52%[P_{8888}][DEHP]	$6.5^{\pm 2.9}$	$171^{\pm 42}$	**$0.17^{\pm 0.05}$**

Figure 4.2. Characterization of tribofilms on cast iron flats lubricated by oils containing ILs, ZDDP, or combinations of them. (a) Cross-sectional TEM image and EDS elemental maps (aided by FIB) of the

tribofilm formed in base oil+0.4%ZDDP+0.52%[P_{8888}][DEHP]; (b) XPS composition-depth profile (aided by Ar-ion sputtering) and core-level spectra of the same tribofilm shown in (a); (c) Tribofilm compositions by XPS survey scan after 30 s sputtering; and (d) Nanoindentation measured mechanical properties of selected tribofilms. Compared to those produced by ZDDP or IL alone, the tribofilm by ZDDP+[P_{8888}][DEHP] contains substantially increased zinc and iron phosphates and much reduced metal oxides and sulfides and possesses a high modulus and a lower ratio of hardness to stiffness squared (P/S^2), while the tribofilms by ZDDP+[P_{66614}][BTMPP] and ZDDP+[$N_{888}H$][DEHP] see significant reductions in both zinc and sulfur compounds. [*Note: O-P: phosphates, O-M: metal oxides, C-M: carbides. Note that, in the composition-depth profile, the rising signals of metallic iron and carbide and fading signals of tribofilm elements along with the sputtering time reflect a combination of the sputtering-induced substrate exposure and the composition change throughout the film thickness.*] [74]

By comparing the XPS composition-depth profiles, we may roughly rank the maximum thicknesses of the tribofilms (proportional to the sputtering time): ZDDP > [$N_{888}H$][DEHP] > ZDDP+[$N_{888}H$][DEHP] > [P_{66614}][BTMPP] > ZDDP+[P_{8888}][DEHP] > [P_{8888}][DEHP] > ZDDP+[P_{66614}][BTMPP]. It seems no direct correlation between the tribofilm thickness and wear protection performance. (It is difficult to calculate the exact film thickness using ion sputtering time due to the lack of precise material removal rate.)

On the other hand, the mechanical properties (by nanoindentation) of selected tribofilms showed good connections with the friction and wear behavior. The hardness, reduced modulus, and the ratio of hardness to stiffness squared (P/S^2) of tribofilms formed in base oil+ZDDP, base oil+[P_{8888}][DEHP], and base oil+ZDDP+[P_{8888}][DEHP] are summarized in Fig. 4.2d. While the hardness values showed no connection to the tribological behavior, a higher modulus seems loosely correlated to a better performance. Interestingly, the P/S^2 ratio of the ZDDP+IL tribofilm is 0.17 $nm^2/\mu N$, much lower than that of the ZDDP (0.27 $nm^2/\mu N$) or IL (0.24 $nm^2/\mu N$) tribofilm. The P/S^2 ratio appears to be inversely proportional to the wear protection, which is in an opposite trend as reported for bulk materials in the literature [61]. For a bulk material, a higher P/S^2 ratio is associated with a higher resistance to plastic deformation and thus lower wear. In contrast, a tribofilm is in-situ formed, sacrificial, and self-healing, and therefore a lower P/S^2 ratio would lead to lower friction (easier to shear) and lower wear (more compliant to absorb more energy upon surface asperity collisions to reduce the damage to the substrate that the tribofilm protects).

Furthermore, XPS analysis of untested lubricant droplets provided interesting insights for understanding the mechanism of synergy (Q4). The atomic concentrations (excluding hydrogen) of lubricants of interest are listed in Fig. 4.3a. For the oil containing either ZDDP or [P_{8888}][DEHP] alone, the measured concentrations of the signature elements (O, Zn, S, and P) are slightly (<2X) higher than the nominal values assuming a homogeneous dispersion. This is not surprising due to the surfactant nature of ZDDP and [P_{8888}][DEHP]. For base oil+[P_{8888}][DEHP], the measured surface O:P atomic ratio of 2.4:1 is somewhat higher than the nominal 2:1 for

[P_{8888}][DEHP], probably because the alkylphosphate anion is a stronger surfactant than the phosphonium cation.

a

Element concentration on oil surface (at%) (ratio of measured/nominal)	**O**	**Zn**	**S**	**P**
base oil+0.8%ZDDP (nominal)	*0.0731*	*0.0183*	*0.0731*	*0.0365*
base oil+0.8%ZDDP (measured)	0.125 (1.7x)	0.035 (1.9x)	0.11 (1.5x)	0.06 (1.6x)
base oil+1.04%[P_{8888}][DEHP] (nominal)	*0.0728*	*0*	*0*	*0.0364*
base oil+1.04%[P_{8888}][DEHP] (measured)	0.143 (2.0x)	0	0	0.06 (1.6x)
base oil+0.4%ZDDP+0.52%[P_{8888}][DEHP] (nominal)	*0.0730*	*0.0091*	*0.0365*	*0.0365*
base oil+0.4%ZDDP+0.52%[P_{8888}][DEHP] (measured)	**4.40 (60x)**	**0.68 (74x)**	**1.19 (33x)**	**1.19 (33x)**
base oil+0.4%ZDDP+0.52%[P_{66614}][DEHP] (nominal)	*0.0730*	*0.0091*	*0.0365*	*0.0365*
base oil+0.4%ZDDP+0.52%[P_{66614}][DEHP] (measured)	**2.89 (40x)**	**0.55 (60x)**	**1.09 (30x)**	**1.11 (30x)**
base oil+0.4%ZDDP+0.5%[P_{66614}][BTMPP] (nominal)	*0.0548*	*0.0091*	*0.0360*	*0.0365*
base oil+0.4%ZDDP+0.5%[P_{66614}][BTMPP] (measured)	0.20 (3.7x)	0.05 (5.5x)	0.10 (2.8x)	0.09 (2.5x)
base oil+0.4%ZDDP+0.87%[$N_{888}H$][DEHP] (nominal)	*0.1215*	*0.0061*	*0.0244*	*0.0365*
base oil+0.4%ZDDP+0.87%[$N_{888}H$][DEHP] (measured)	0.24 (2.0x)	0.03 (4.9x)	0.04 (1.6x)	0.05 (1.4x)

b

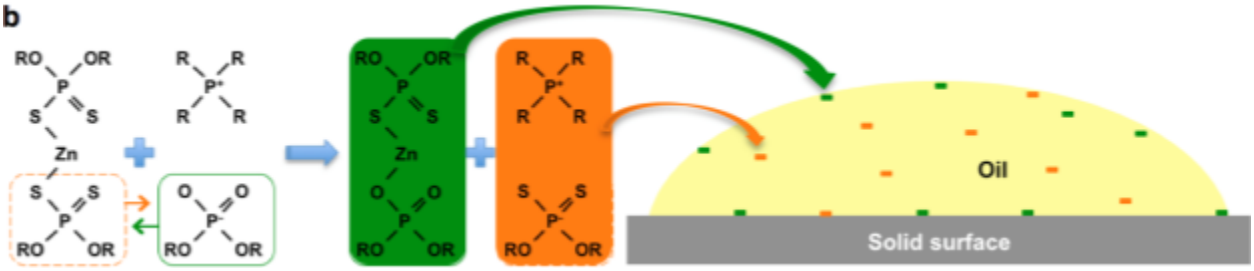

Figure 4.3. XPS chemical analysis of lubricants and hypothetic reactions between ILs and ZDDP. (a) XPS-detected element concentrations on the fluid surface of oils containing ILs, ZDDP, or combinations of them. When adding [P_{8888}][DEHP] or [P_{66614}][DEHP] together with ZDDP into the base oil, the measured concentrations of O, Zn, S, and P on the oil surface are 30-70x higher than their nominal values. This is believed to be responsible for the superior tribological performance and distinct tribofilm composition. (b) Based on chemical hardness principle, anion exchange is hypothesized between the IL and ZDDP to produce possibly a new compound ZOTP, whose atomic ratio of O:Zn:S:P matches well with that detected on the oil surface. [*Note: XPS is very surface sensitive, and all collected singles reflect the chemical contents in the top 3-5 nm of the fluid surface (interface with vacuum).*] [74]

A remarkable observation was made on base oil+ZDDP+[P_{8888}][DEHP]: assuming a homogeneous dispersion, the concentrations of O, Zn, S, and P should be 0.0730, 0.0091, 0.0365, and 0.0365 at%, respectively; however, the XPS-measured concentrations on the oil surface were 4.40, 0.68, 1.19, 1.19 at%, which are 60x, 74x, 33x, and 33x higher than the nominal values (Fig. 4.3a). Considered as an interface phenomenon (oil-vacuum interface, in the XPS chamber), such significantly increased concentrations of key elements are also expected to occur at the interface between the oil and metal surfaces being lubricated, though direct measurement of these elements' concentrations at the oil-metal interface is difficult. As a result, the increased supply of anti-wear agents at the bearing interface would make the tribofilm formation more effective, leading to a superior wear protection as observed in tribological testing. The increased content of phosphates in the tribofilm could also be attributed to the greater concentration of alkylphosphate anions at the interface.

In addition to the much increased concentrations of active elements at the oil droplet surface, the measured atomic ratio of O:Zn:S:P (3.7:0.57:1:1) was quite different from the nominal ratio of ZDDP+[P_{8888}][DEHP], 2:0.25:1:1. This implies that a new compound may have been formed. The possible reactions between ZDDP and [P_{8888}][DEHP] may be explained by the chemical hardness principle [62]. Since a neutral organic is more difficult to lose electrons than a neutral metal, a neutral organic is considered as a softer base compared to a neutral metal. Thus, the phosphonium cation of [P_{8888}][DEHP] is a Lewis harder acid than the zinc cation of ZDDP. Because O^0 is stronger acid than S^0, the alkylphosphate anion of [P_{8888}][DEHP] (2 oxygen donors) is a softer Lewis base than the dithiophosphate anion of ZDDP (2 sulfur donors). Therefore, it is energetically favorable for [P_{8888}][DEHP] and ZDDP to exchange anions. Since they were mixed at 1:1 molecular ratio, ultimately each ZDDP would have one of its two dithiophosphate anions replaced with an alkylphosphate anion from [P_{8888}][DEHP], as illustrated in Fig. 4.3b. The new compounds would be zinc alkylphosphate alkyldithiophosphate (noted as ZOTP here) and phosphonium-alkyldithiophosphate. The nominal atomic ratio of O:Zn:S:P for ZOTP is 3:0.5:1:1, quite similar to the measured ratio (3.7:0.57:1:1) on the oil surface. This supports the anion exchange hypothesis and suggests ZOTP highly preferentially residing on the oil surface.

Similarly to base oil+ZDDP+[P_{66614}][DEHP], much increased contents of O, Zn, S, and P (30-60x, higher than the nominal values) were observed on the oil surface with an atomic ratio of 2.6:0.49:0.98:1 close to that of ZOTP (Fig. 4.3a).

In contrast, for base oil+ZDDP+[P_{66614}][BTMPP] and base oil+ZDDP+[$N_{888}H$][DEHP] that lack the synergism, the concentration increases of O, Zn, S, and P on the oil surfaces are 'only' 6X and 4X higher than the nominal values (Fig. 4.3a), respectively, one order of magnitude lower compared with that of the oil containing a phosphonium-alkylphosphate IL together with ZDDP. Interestingly, no N was detected on the oil surface of base oil+ZDDP+[$N_{888}H$][DEHP]. Since [P_{66614}][BTMPP]'s anion is a softer base than ZDDP's anion, anion exchange likely occurs to produce zinc alkylphosphinate dithiophosphate (noted as ZCTP),

whose nominal atomic ratio of O:Zn:S:P (2:0.5:1:1) matches well with the measured ratio of 2:0.5:1:0.9 on the oil surface. Since $[N_{888}H][DEHP]$ was mixed with ZDDP at 2:1 molecular ratio in the oil, complete anion exchange would produce zinc dialkylphosphate (noted as ZDOP here) but the hydrogen bonding between the IL's cation and anion could hinder the process. The measured atomic ratio of O:Zn:S:P on the oil surface (4.8:0.6:0.8:1) suggests a mixture of original and new compounds. Still, it is unclear why ZOTP resides on the oil surface much more preferentially than ZCTP or ZDOP.

To validate the anion exchange hypothesis, ZDDP was mixed directly with each of the four ILs (without the base oil involved). During mixing/stirring, the neat ZDDP+IL blends became warm. For example, the temperature of ZDDP+$[P_{8888}][DEHP]$ increased to 31 ^{o}C (compared to the ambient 23 ^{o}C) as monitored by a thermocouple during mixing. This is implication of chemical reactions. While ZDDP+$[N_{888}H][DEHP]$ (1:2 molecular ratio) appeared to be a clear solution, other three ZDDP+IL mixtures (at 1:1 molecular ratio) appeared cloudy initially. After long centrifuging (300 min at 13,000 rpm), the cloudy ZDDP+$[P_{8888}][DEHP]$ and ZDDP+$[P_{66614}][DEHP]$ became clear with a small amount (<5%) of white solid settled at the bottom, while ZDDP+$[P_{66614}][BTMPP]$ showed a clear liquid on top and a thick gel on the bottom. Fourier transform infrared spectroscopy (FTIR) analysis was conducted and the spectra are shown in Fig. 4.4. The spectrum of the white solid basically matches with that of ZDDP (Fig. 4.4a), suggesting the solid is precipitated short-chain ZDDPs, which are solid in an ambient environment and normally suspended by the liquid long-chain ZDDPs [63] but some settled out when the equilibrium was broken in reactions with the IL. The 811 cm^{-1} peak in the spectrum of $[P_{8888}][DEHP]$ (Fig. 4.4a) does not exist in that of HDEHP [64] or $[P_{66614}]Cl$ [65], and therefore likely reflects the stretching vibration of the non-alkyl P-O bond on [DEHP] with attraction from $[P_{8888}]$. This peak totally disappears in the spectrum of the clear liquid phase of ZDDP+$[P_{8888}][DEHP]$, indicating separation of [DEHP] from $[P_{8888}]$. The P-S stretching of ZDDP [66] generates two peaks at 653 and 748 cm^{-1}, which became two doublets at 658/668 and 753/763 cm^{-1}, respectively, in the ZDDP+$[P_{8888}][DEHP]$ mixture (Fig. 4.4a). Such change may be attributed to the proposed anion exchange: one alkyldithiophosphates now pairs with $[P_{8888}]$ (much larger than a zinc ion) leading to a weaker attraction between P-S and the cation, and thus the P-S bond becomes stronger; the P-S bond on the other alkyldithiophosphate (stilled paired with zinc) is also slightly stronger because the zinc ion is more attracted to the newly bonded [DEHP]. Identical observations can be made for ZDDP+$[P_{66614}][DEHP]$ (Fig. 4.4b).

For ZDDP+$[P_{66614}][BTMPP]$ (Fig. 4.4c), the spectrum of the clear liquid phase shows similar change in P-S stretching compared with that of ZDDP+$[P_{8888}][DEHP]$, and misses the P-O bond of [BTMPP] [65] at 1170 cm^{-1}. The gel phase has rather weak signal of P-S stretching but stronger-than-expected P-O and P=O stretching, implying possibly oxidized product(s) of alkyldithiophosphates. The spectrum of ZDDP+$[N_{888}H][DEHP]$ (Fig. 4.4d) shows stronger P-S bond and a new peak at 1206 cm^{-1} for P=O bond that is a signature for ZDOP [67]. Results

indicate that new compounds were produced in all four ZDDP+IL mixtures, supporting the anion exchange prediction.

The IL+ZDDP synergism may be attributable to the much increased concentrations of active agents (hypothetical new compounds via anion exchange) at the oil surface/interface. Such a unique phenomenon has not been seen when combining ZDDP with other conventional lubricant additives [38] , such as detergents [68] dispersants [69] , or friction modifiers [70], with either synergistic [38, 68, 70] or antagonistic [38, 69] effects reported.

Synergistic effects have been observed with ~30% friction and >70% wear reductions when using a phosphonium-alkylphosphate IL together with a conventional ZDDP as lubricant additives. The IL+ZDDP tribofilm distinguishes itself from the IL or ZDDP tribofilms with substantially higher contents of zinc and iron phosphates but much less metal oxides and sulfur compounds. Notably, it was revealed that the actual concentrations of O, Zn, S, and P on the droplet surface of the oil+IL+ZDDP blend are 30-70x higher than their nominal values. Such significantly increased concentrations of anti-wear agents are expected to also occur at oil-solid interfaces and believed to be responsible for the superior tribological performance. The ratio of hardness to stiffness squared of selected tribofilms was determined by nanoindentation and seems inversely proportional to the wear protection, which reflects the sacrificial and self-healing nature of tribofilms. While anion exchange between the IL and ZDDP to produce a new compound ZOTP is hypothesized and supported by XPS and FTIR analyses, it still remains to be investigated why the concentration of ZOTP on the oil surface is more than one order of magnitude higher than nominal. Synergy with ZDDP however was not observed with phosphonium-alkylphosphinate or ammonium-alkylphosphate ILs even though they share either the same cation or the same anion with phosphonium-alkylphosphate ILs. This implies that both the cation and anion play critical roles.

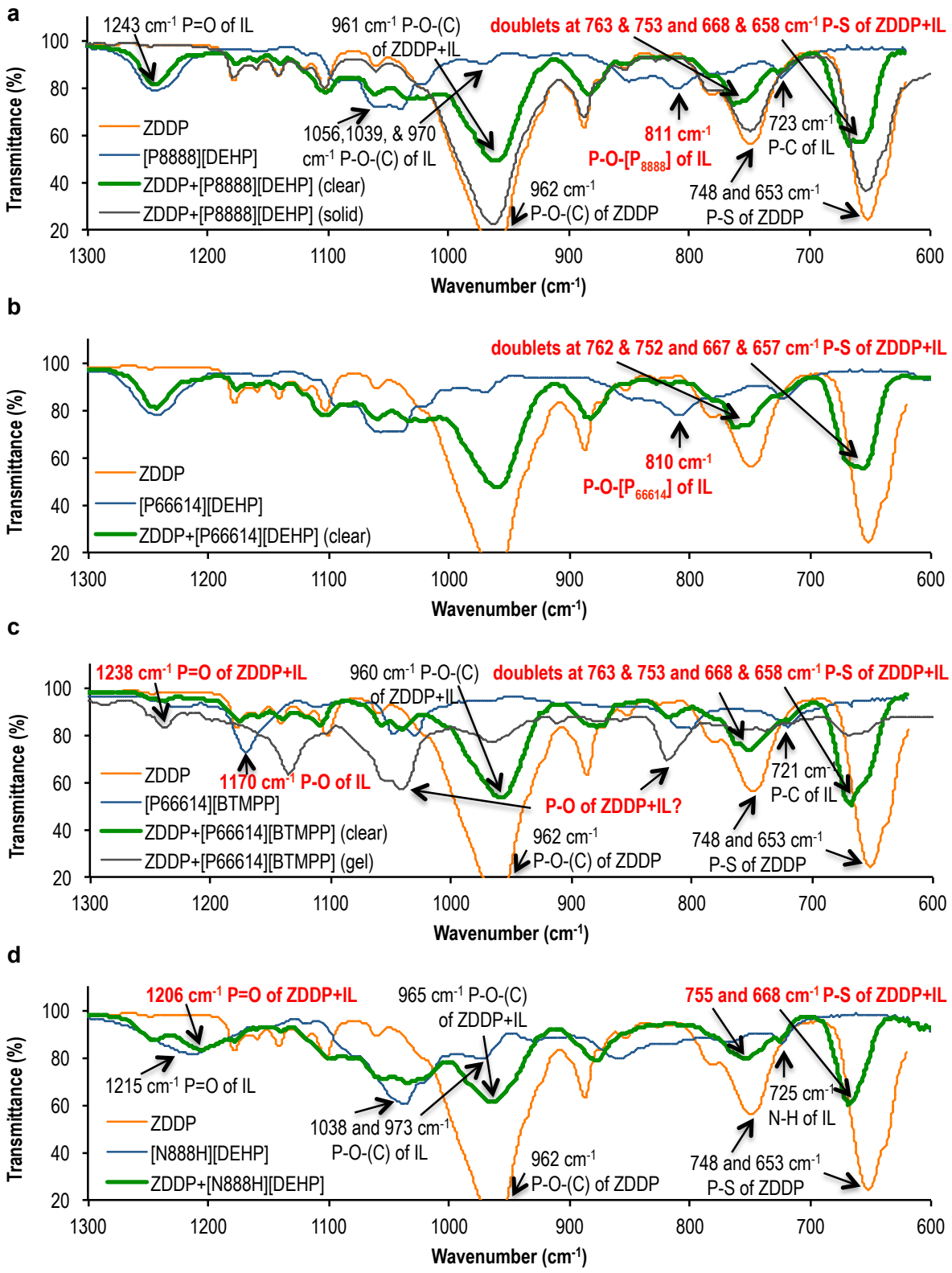

Figure 4.4. Comparison of FTIR spectra of ZDDP, ILs, and ZDDP+IL mixtures. (a) $[P_{8888}][DEHP]$, (b) $[P_{66614}][DEHP]$, (c) $[P_{66614}][BTMPP]$, and (d) $[N_{888}H][DEHP]$. Notable changes of stretching vibrational bands of P-S and P-O bonds when mixing ZDDP and ILs support the anion exchange hypothesis. [74]

CHAPTER 5. Tribological Bench and Engine Dynamometer Tests of a Low Viscosity SAE 0W-16 Engine Oil Using a Combination of Ionic Liquid and ZDDP as Anti-wear Additives

5.1 Experimental methods and materials

The IL of interest in this work, tetraoctylphosphonium bis(2-ethylhexyl) phosphate ([P_{8888}][DEHP]), was synthesized in an organic chemistry lab at ORNL with a 93.8% yield and a water content of 0.1%. Oil solubility assessment for this IL was conducted by combining it with base oil cSt base oil up to a 1:1 ratio and shaking it for one minute. The combination was then placed into a centrifuge for three minutes at 13,000 rpm. No separation was evident. A commercial secondary ZDDP was provided by Lubrizol (OH) with a zinc content of 11.0 wt.% and phosphorous content of 10.0 wt.%. Characterization and chemical structures related to both AW additives in this work are shown in Table 5.1 and Figure 5.1 respectively. The viscosities were measured using a Petrolab MINIVIS II viscometer and the standard deviation was controlled to be less than 1%.

Table 5.1. Characterization of neat anti-wear additives used. Decomposition temperature was measured in air. [75]

Anti-Wear Additive	Density (g/cm^3)	Decomposition Temp. (°C)	P Content (wt. %)	Zn Content (wt.%)	KV (cSt)	
					40 °C	100 °C
Secondary ZDDP	1.20	189	10	11	407.6	13.5
[P8888][DEHP]	0.86	290	7.7	0	711.4	79.3

[P_{8888}][DEHP]

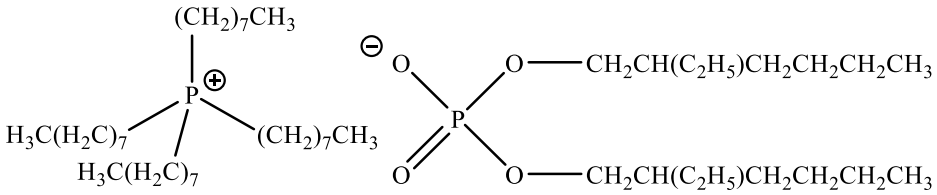

ZDDP

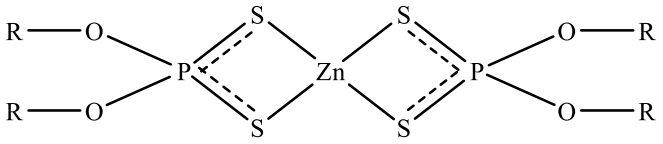

Figure 5.1. Structures of tetraoctylphosphonium bis(2-ethylhexyl) phosphate and zinc dialkyldithiophosphate. [75]

The experimental engine oil formulation (EF) in this work is a blend of base oil cSt and 8 cSt base oils with a package of additive components provided and blended by Shell Global Solutions (TX) that includes detergent, dispersant, viscosity modifier (VM), anti-oxidant (AO), friction modifier (FM), pour-point depressant (PPD), anti-foam (AF) and AW additives that are detailed in Table 5.2. The EF is a result of a systematic study of compatibility between the IL and each additive in the package (to be reported in a separate publication). Three lubricants were tested: EF w/o AW, EF + 0.8 wt% ZDDP, and EF + 0.52 wt% IL + 0.4 wt% ZDDP. Lubricants were blended to adhere to International Lubricants Standardization and Approval Committee (ILSAC) GF-5/6 specifications such that phosphorus concentrations do not exceed 800 ppm. The measured phosphorus contents in EF + 0.8 wt% ZDDP, and EF + 0.52 wt% IL + 0.4 wt% ZDDP are 723 and 705 ppm, respectively. It should be noted that EF + 0.52% $[P_{8888}][DEHP]$ + 0.4% ZDDP was blended so each AW additive contributes roughly equal phosphorus concentration. The high temperature-high shear (HTHS) viscosity was measured using a tapered bearing simulator (Tannas Co.) and the kinematic viscosity (KV) was measured using a CAV-2100 automatic viscometer (Cannon Instrument Co.). The cold-cranking simulator (CCS) viscosity measurement was performed using a G-109-CCS-2100 model viscometer (Cannon Instrument Co.). Table 5.3 details the density, rheological properties, and concentrations of phosphorus and zinc for each lubricant.

Table 5.2 Experimental formulation (EF) additive composition. Percentages are on a mass basis. [75]

Lubricant	**Salicylate Detergent**	**High MW Dispersant**	**VM**	**AO**	**Organic FM**	**PPD**	**AF**	**AW**	
								ZDDP	**[P8888][DEHP]**
EF w/o AW	3%	2%	2.4%	1%	0.8%	0.3%	0.03%	**0%**	**0%**
EF + ZDDP	3%	2%	2.4%	1%	0.8%	0.3%	0.03%	**0.8%**	**0%**
EF + IL + ZDDP	3%	2%	2.4%	1%	0.8%	0.3%	0.03%	**0.4%**	**0.52%**

A Plint TE77 (Phoenix Tribology Ltd.) tribometer was used to obtain *in situ* friction data and to produce wear tracks. The machine is arranged to produce an alternating sliding motion against a test material immersed in lubricant. Wear tracks were created on 25.4 mm × 25.4 mm × 3.175 mm CL35 cast iron flats (Metal Samples Company, AL) rubbing against 10 mm AISI 52100 steel balls. Cast iron test specimens were polished with 600-grade silicon carbide abrasive paper with a unidirectional lay at 90º to the sliding axis. Both steel balls and cast iron flats were cleaned with isopropanol and allowed to dry before submersion in lubricant. Each test was performed at 100ºC with a normal load of 100 N for an overall sliding distance of 1000 m. Scars were formed under fully sliding conditions with a 10 mm stroke at 10 Hz. The point-contact ensures test conditions completely within the BL regime. Two tests were executed for each lubricant. After wear testing, balls and flats were cleaned in acetone and then isopropanol. Wear measurements were taken with a Veeco (now Bruker, TX) Wyko NT9100 optical interferometer.

Table 5.3 Density, P and Zn content, viscosity indices and rheological data for each lubricant. [75]

Lubricant	Density (g/cm^3)	P Content (ppm)	Zn Content (ppm)	Viscosity Index	HTHS @150C (cP)	CCS @ -35 °C (cP)	KV (cSt)	
							40ºC	100ºC
EF w/o AW	0.84	0	0	155	2.4	5220	38.9	7.3
EF + 0.8% ZDDP	0.84	723	836	157	2.4	*NM*	38.5	7.3
EF + 0.52% IL + 0.4% ZDDP	0.84	705	392	155	2.4	*NM*	38.8	7.3

Scanning electron microscopy (SEM) and top-surface elemental analysis was completed using a Hitachi S-4800(Tokyo, Japan) scanning electron microscope with EDAX (NJ) silicon drift detector energy dispersive x-ray spectroscopy (EDS) capability. EDS was completed at a potential of 5.0 kV over a time span of one minute for each measurement.

Two sets of Stribeck curves for EF + 0.8% ZDDP, EF + 0.52% IL + 0.4% ZDDP and SAE 20W-30 reference oil without friction modifier or viscosity improver (same baseline oil as Sequence VIE standard) were produced using ball-on-disc rolling-sliding on a PCS Instruments (UK) Mini Traction Machine 2 (MTM). Both the ball and the disc were made of hardened AISI 52100 bearing steel. The ball had a diameter of 19.5 mm and hardness of 64 R_c. The disc had a hardness of 62.5 R_c. Test parameters for both test sets are given in Table 5.4 with slide-roll ratio (SRR) = $\Delta U/U_e$, and $\Delta U = U_1 - U_2$ is the sliding velocity and $U_e = (U_1 + U_2)/2$ is the mean velocity.

Arithmetic average surface roughness (R_a) was quantified for both sets of tests using the Wyko NT9100 for the balls and a Dektak XT stylus profilometer for the discs.

Table 5.4 Test parameters for both MTM Stribeck scan experiments. [75]

	MTM Method 1 (Figure 5.5)			MTM Method 2 (Figure 5.6)		
Speed (mm/s)	2500-2000	2000-200	200-20	2500-2000	2000-500	500-50
Speed Step Size (mm/s)	250	200	20	100	100	50
Number of Scans	20 over entire range per scan			5	20	10
Approx. Time per Step (s)	10			10		
Load (N)	30			30		
Temperature (ºC)	100			120		
Slide-Roll Ratio (%)	100			100		

Fuel economy improvement of the addition of IL was further assessed using FEI 1 of the impending ILSAC GF-6 Sequence VIE engine dynamometer test at Intertek Automotive Research (TX). The Sequence VIE is an update to the standard Sequence VID test (ASTM D 7589 [71]) with increased fuel economy limits and change of the test engine to a 2012 GM Malibu 3.6 L engine. This standard testing procedure compares a test lubricant's performance with that of a SAE 20W-30 baseline lubricant over six different stages of engine operation. Each lubricant was first aged over 16 hours of engine operation at 2250 rpm and 120ºC oil temperature. The first six-stage measurements (FEI 1) are then made at the conditions outlined in Table 5.5.

Table 5.5 Sequence VIE engine test fuel economy test conditions. [75]

	Stage 1	Stage 2	Stage 3	Stage 4	Stage 5	Stage 6
Torque (N•m)	105.0 ± 0.1	105.0 ± 0.1	105.0 ± 0.1	20.0 ± 0.1	20.0 ± 0.1	40.0 ± 0.1
Speed (rpm)	2000 ± 5	2000 ± 5	1500 ± 5	695 ± 5	695 ± 5	695 ± 5
Oil Gallery Temperature (ºC)	115 ± 2	65 ± 2	115 ± 2	115 ± 2	35 ± 2	115 ± 2
Nominal Power (kW)	22.0	22.0	16.5	1.5	1.5	2.9
Weight Factor	0.300	0.032	0.310	0.174	0.011	0.172
Lubrication Regime	**EHL/HL Dominant**			**More BL/ML**	**Some BL/ML**	**More BL/ML**

5.2 Results and discussion

5.2.1 Boundary lubrication wear and friction

Ball-on-flat reciprocating wear tests were performed in the BL regime to compare the wear protection performance between the IL-ZDDP combination and the ZDDP-only lubricant. As shown in Fig. 5.2a, EF + 0.52% [P_{8888}][DEHP] + 0.4% ZDDP produced the lowest wear, at roughly 90% reduction over EF w/o AW and about 9% reduction over EF + 0.8% ZDDP. Each data point represents an average of two repetitions per lubricant. Due to the hardness disparity between the balls and flats, ball wear volumes are on the order of two magnitudes less than flat wear volumes.

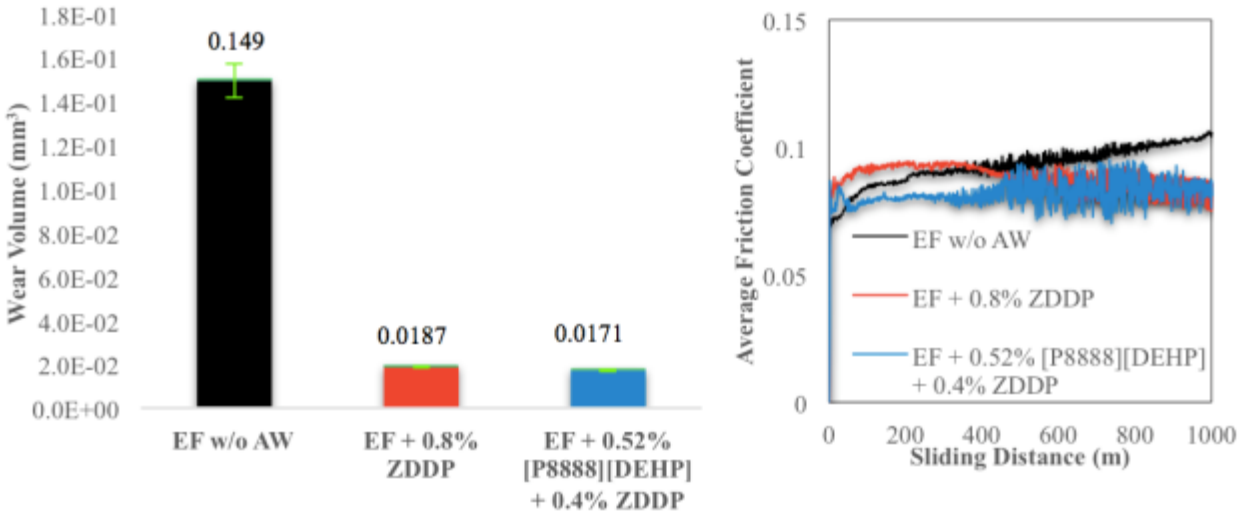

Figure 5.2 Wear summary (left: a) for reciprocating-sliding bench tests. Ball wear volume (in green on top of each bar) and error bars are included but are very small for the second and third entries. Averaged friction results for 2 repetitions per lubricant (right: b). [75]

Friction results from the reciprocating-sliding bench test are shown in Figure 5.2b and represent an averaged performance over two repetitions. The lubricant without AW had the highest steady-state friction coefficient with a final value above 0.10. EF + 0.52% [P_{8888}][DEHP] + 0.4% ZDDP produced the lowest friction coefficient for the first 500 m of sliding, after which, both lubricants containing AW showed a similar friction coefficient around 0.08.

5.2.2 Wear scar morphology examination and chemical analysis

The wear scars produced by the two lubricants containing either ZDDP only or ZDDP+IL were examined using SEM for top-surface morphology imaging and EDS for chemical analysis. Figure 5.3 consists of the SEM micrographs and EDS spectra of the surface pair lubricated with EF + 0.8% ZDDP. The steel ball shows an elliptical wear pattern with relatively evenly dispersed parallel scratch patterns. The worn surfaces appear covered by dark tribofilms with some patchy areas of exposed substrate. EDS spectra provide further evidence of the tribofilms: on a surface lubricated by a ZDDP-containing oil, both mating surfaces show the presence of zinc, phosphorus and sulfur—elements which could only have originated from ZDDP in the lubricant. Increased amounts of these elements on the cast iron flat may indicate a more substantial film with better coverage on this surface compared to that of the ball. Calcium is also present in trace amounts at the surface originating from the detergent in the EF. It has been shown that calcium phosphates form in a separate phase in ZDDP tribofilms whenever calcium-containing detergent is present in the lubricating oil with a detrimental effect on its overall anti-wear characteristic [72]. Figure 5.4 shows SEM micrographs and EDS spectra of the tribosystem lubricated with EF

+ 0.52% [P_{8888}][DEHP] + 0.4% ZDDP. The morphologies of these surfaces are visually similar to those shown in Figure 5.3. The elliptical ball wear scar is slightly smaller than the previous, and both ball scars show oblique wiping marks—artifacts of cleaning. The worn cast iron flat lubricated with EF + 0.52% [P_{8888}][DEHP] + 0.4% ZDDP EDS spectrum shows a marked reduction of zinc and sulfur on the surface and an increased ratio of phosphorous to zinc suggesting both AW constituents are participating in tribofilm growth. Again, a high iron peak on the ball is observed indicating a thinner tribofilm on the steel ball. A similar amount of calcium is present compared to that in Figure 5.3.

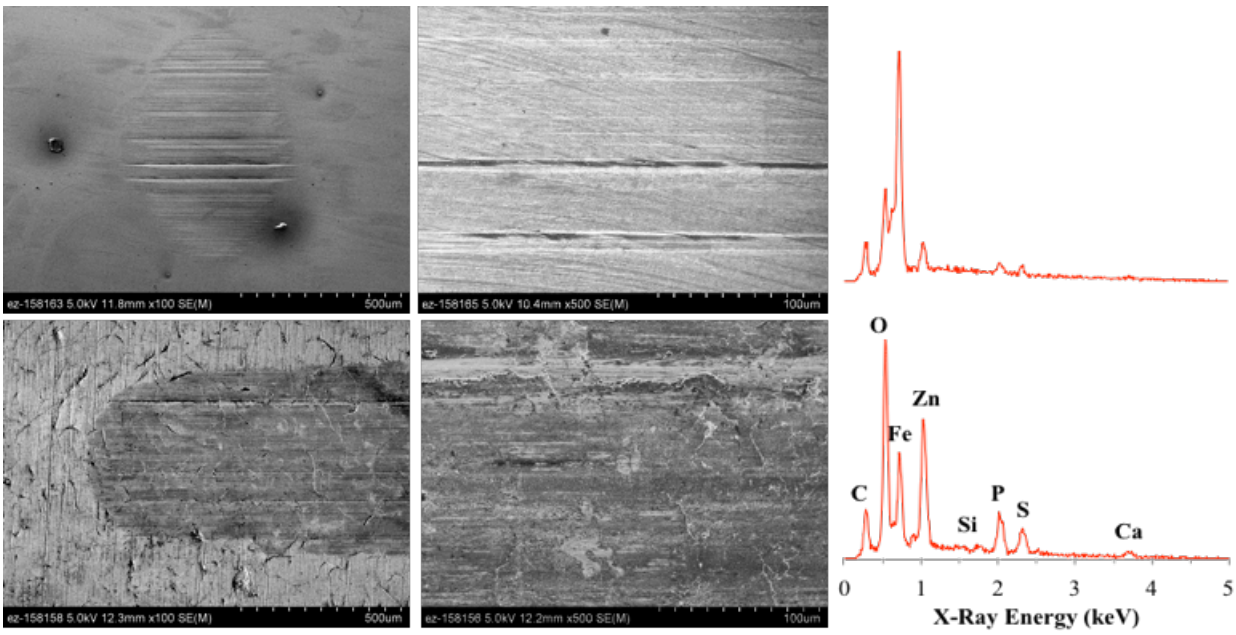

Figure 5.3 SEM micrographs of worn surfaces lubricated with EF + 0.8% ZDDP. *Top:* Steel ball surface with corresponding EDS. *Bottom:* Cast iron flat surface with corresponding EDS. [75]

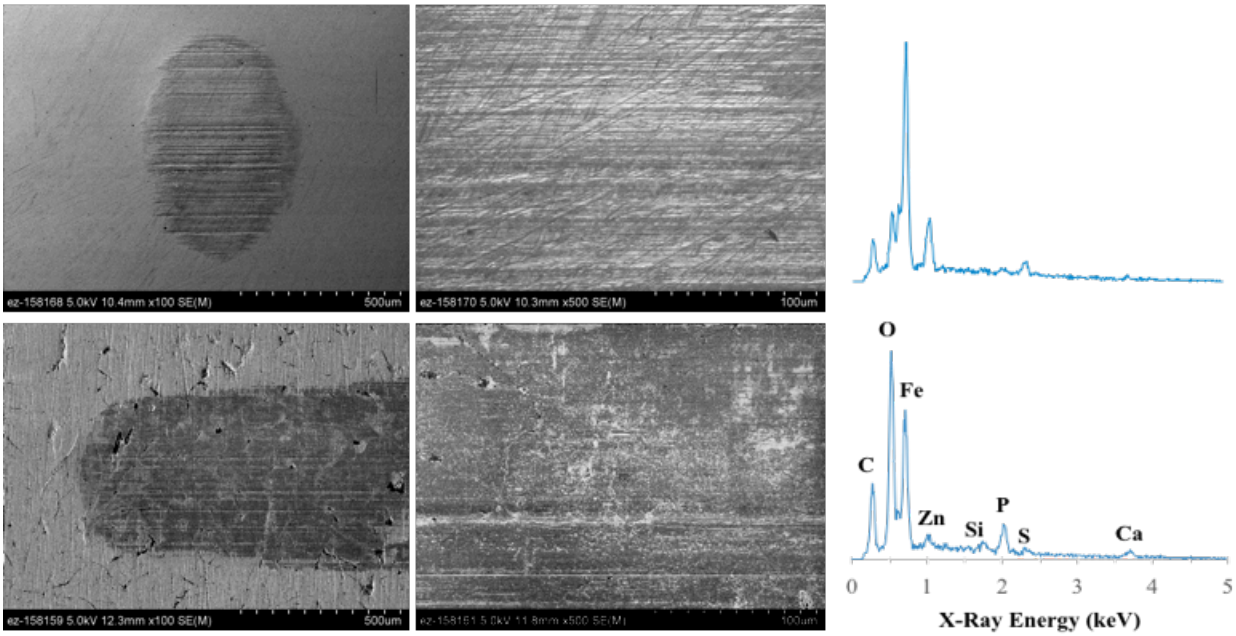

Figure 5.4 SEM micrographs of worn surfaces lubricated with EF + 0.52% [P8888][DEHP] + 0.4% ZDDP. *Top:* Steel ball surfaces with corresponding EDS. *Bottom:* Cast iron flat surface with corresponding EDS. [75]

5.2.3 Mini traction machine Stribeck curves

Having verified synergy between the IL and ZDDP in the formulated oil in boundary wear and friction, we shift attention to friction behavior in a broader survey of lubrication regimes. MTM full-range speed scans generated Stribeck curves are shown in Figure 5.5, subject the tribosystem to mostly ML with some BL and EHL at a temperature of 100ºC. The SAE 20W-30 reference oil and EF + 0.8% ZDDP display very similar behavior in terms of how friction evolves as each repetition is executed. The first scan for each produced the lowest friction and the last showed the highest. A pattern emerges for these two blends of increasing friction as the tribofilm develops with increasing number of scans though EF + 0.8% ZDDP increases within a narrower band than the 20W-30 baseline oil. An opposite trend was observed for EF + 0.52% IL + 0.4% ZDDP as it, for the most part, showed slightly decreasing friction as the tribofilm develops and the number of scans increases. As a result, the steady-state friction curve, an average of the last 3 of 20 scans, for EF + 0.52% IL + 0.4% ZDDP is substantially lower than the other two lubricants as shown in the summary chart (Fig. 5.5d). EF + 0.52% IL + 0.4% ZDDP exhibits the highest advantage over EF + 0.8% ZDDP in the ML regime, but as EHL is approached, the friction curves tend to convergence as expected for lubricants of the same viscosity grade.

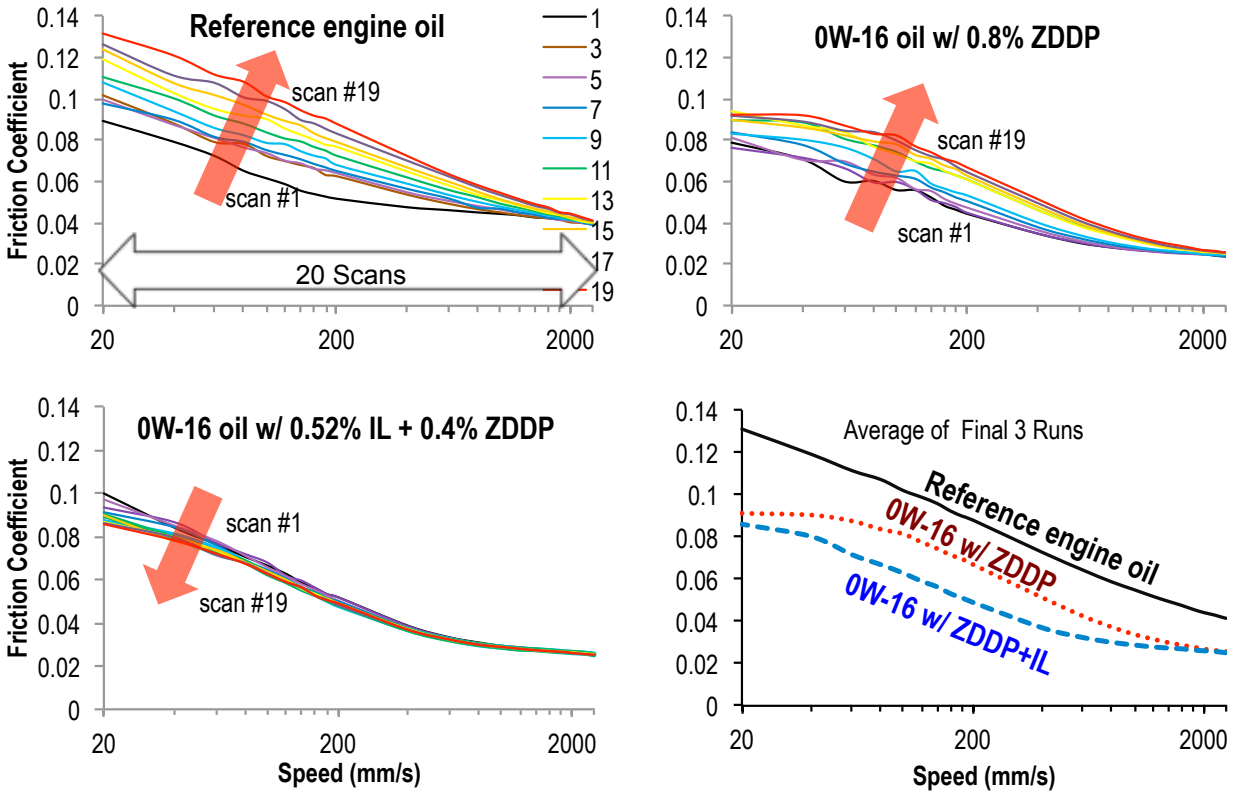

Figure 5.5 MTM representative ball-on-disk Stribeck curves for each lubricant and a summary average of the final three scans for each lubricant. 20 scans were completed for each blend, but only every odd repeat is shown for clarity. [75]

The second set of Stribeck scans was completed with the sliding speed varied over three separate ranges as opposed to one scan over a broader range as in the previous tests. As shown in Figure 5.6, a similar pattern of increased friction as the tribofilm is built is noted here in both the SAE 20W-30 baseline and EF + 0.8% ZDDP except in the third and fastest test range (EHL) in which all lubricants showed minimal variation as more repeats were completed. EF + 0.52% IL + 0.4% ZDDP again showed the lowest friction overall and a reduced friction coefficient as the tribofilm developed. For the average of final three scans, an even more distinct improvement was observed in ML as a result of the IL's presence.

Surface roughness for balls and discs produced in both MTM Stribeck scan sets is quantified in Table 5.6. Both methods show excellent correlation with the friction results in Figures 5.5 and 5.6. EF + 0.52% IL + 0.4% ZDDP produced smoother surfaces on both balls and discs in each case.

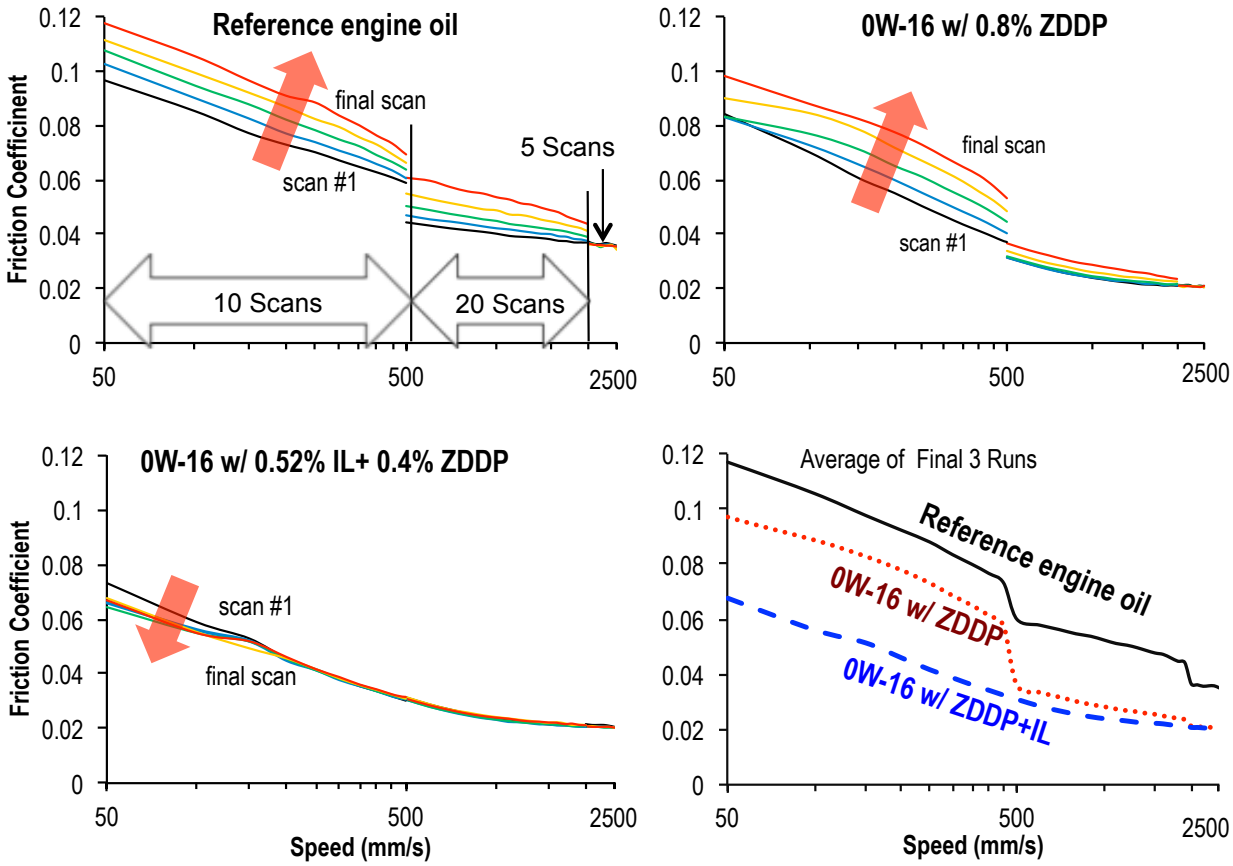

Figure 5.6 MTM representative Stribeck curves for ring-on-liner method. Only 5 scans in each speed range are shown for clarity. The summary represents the average of the final three scans for each lubricant. [75]

Table 5.6. Measured arithmetic average surface roughness of balls and discs for each set of MTM results. [75]

Lubricant	MTM Data Set 1 (Figure 5.5)		MTM Data Set 2 (Figure 5.6)	
	Disc, R_a (nm)	Ball, R_a (nm)	Disc, R_a (nm)	Ball, R_a (nm)
EF + 0.8% ZDDP	22.8 ± 5.4	22.3 ± 0.9	12.6 ± 2.4	24.2 ± 4.3
EF + 0.52% IL + 0.4% ZDDP	10.2 ± 4.1	21.4 ± 1.1	8.8 ± 3.8	20.7 ± 0.5

With very encouraging results for the IL-additized formulated oil in the previous boundary wear and friction tests and in both MTM Stribeck scan experiments, we moved forward with full-scale, multi-cylinder, fired engine fuel economy evaluation.

5.2.4 Sequence VIE fuel economy engine dynamometer test (FEI 1)

Sequence VIE fuel economy engine test FEI 1 results are shown in Table 5.7. In agreement with bench test friction measurements, EF + 0.52% IL + 0.4% ZDDP demonstrated improved fuel economy in all six stages of the Sequence VIE compared with the baseline by 2.12% and EF + 0.8% ZDDP by 0.25%, respectively. Stages 4, 5 and 6, which constitute 35.7% of the final weighted score, subject the test engine to increased levels of BL and ML regimes; under these conditions there is more pronounced benefit as a result of adding the IL (0.76%, 0.48% and 0.79% for Stages 4, 5 and 6 respectively) compared to ZDDP only. On the other hand, Stages 1, 2 and 3 show smaller IL-induced improvements because EHL and HL are the dominant lubrication regime. These test results indicate that an IL such as $[P_{8888}][DEHP]$ can function in tandem with ZDDP in an anti-wear context and reduce the friction between engine components in the Sequence VIE assessment thus improving fuel economy across a spectrum of engine operating conditions.

Table 5.7 ASTM D7589 Sequence VIE engine test fuel economy test results. [75]

	Stage 1	**Stage 2**	**Stage 3**	**Stage 4**	**Stage 5**	**Stage 6**	**Weighted FEI**
Lubrication Regime	**EHL/HL Dominant**			**More BL/ML**	**Some BL/ML**	**More BL/ML**	
EF + 0.8% ZDDP vs. baseline	2.36%	2.84%	1.66%	3.72%	5.98%	3.03%	1.87%
EF + 0.4% ZDDP + 0.52% IL vs. baseline	2.54%	2.91%	1.77%	4.48%	6.46%	3.81%	**2.12%**
IL-induced Improvement	0.17%	0.07%	0.11%	0.76%	0.48%	0.79%	**0.25%**

CHAPTER 6. Impact of a Phosphonium-Organophosphate Ionic Liquid on Exhaust and Three-Way Catalysts

6.1. Experimental details and materials

6.1.1 Engine/genset experimental setup

In order to evaluate the compatibility of anti-wear additives with three-way catalyst (TWC) technology, a 3.5 kW Westerbeke SBCG 60 Hz gasoline generator was purchased for the purpose of exposing the TWCs with the additives of interest: ZDDP, ionic liquid (IL), ZDDP plus ionic liquid (ZDDP+IL). Additionally, a no-additive (NA) case was also performed for a baseline. The genset is shown in Figure 6.1 with the stock catalyst removes and the TWCs of interest installed. The water-cooled engine has 2 cylinders, 0.35L, and operates at a constant 2200 rpm. It has electronic fuel injection that is feedback controlled using an air-to-fuel ratio (AFR) sensor that is in the exhaust; also known as a lambda or UEGO sensor. This ensures that the exhaust mixture that the TWCs are exposed to, are stoichiometric as it would be in practice. Additionally, the setup was instrumented with a port in the exhaust manifold that was used to introduce O_2 upstream of the AFR sensor. Thus, when a controlled quantity of O_2 was included in the exhaust the engine would inject additional fuel into the cylinder. This allowed control of the temperature of the catalyst by creating an exothermic reaction over the TWC. The effect of this additional O_2 on the gas inlet, TWC midbed, and gas exhaust temperatures can be observed in Figure 6.2. The target initial mid bed temperature for each evaluation was 700°C for this study.

Figure 6.1. Stoichiometric gasoline genset employed for exposing TWC to anti-wear additives.

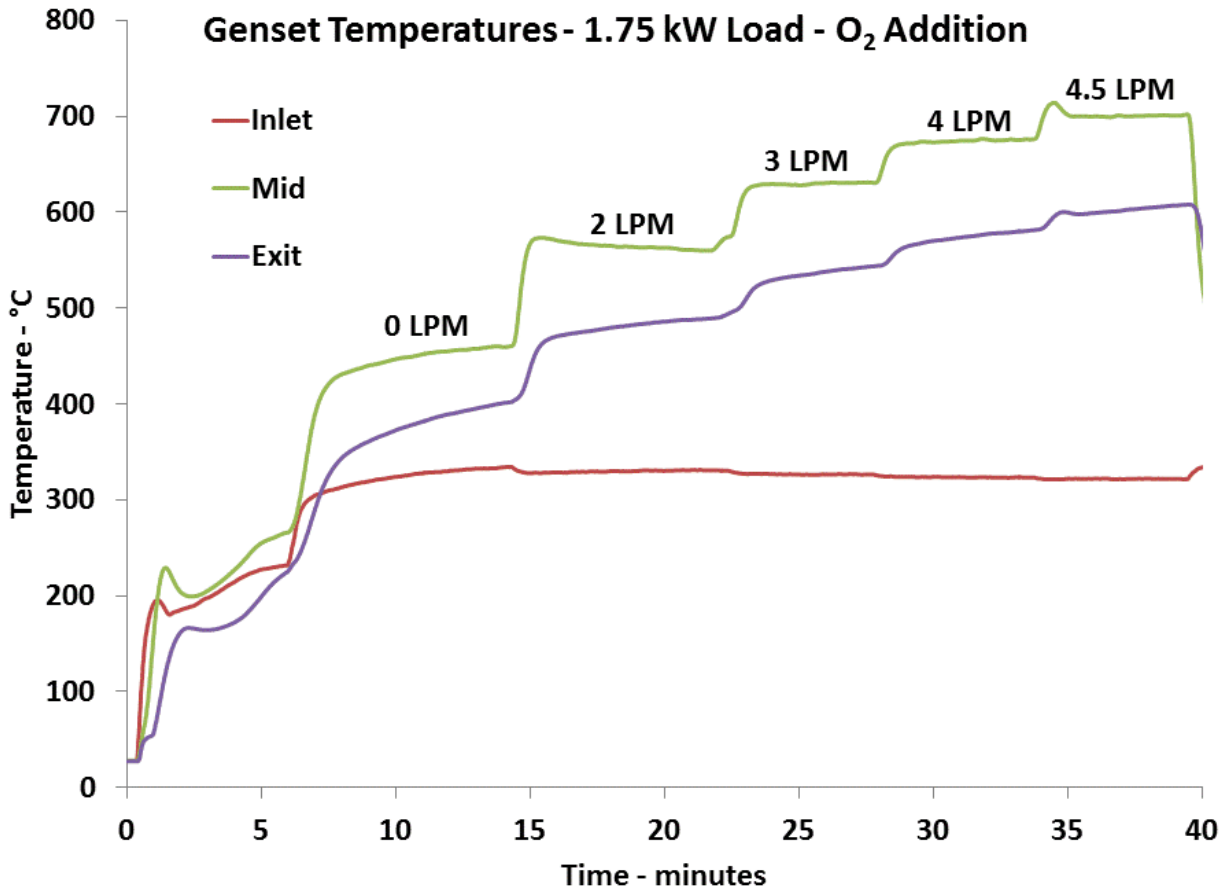

Figure 6.2. Impact of O_2 addition on the measured on the gas inlet, TWC midbed, and gas exit temperatures.

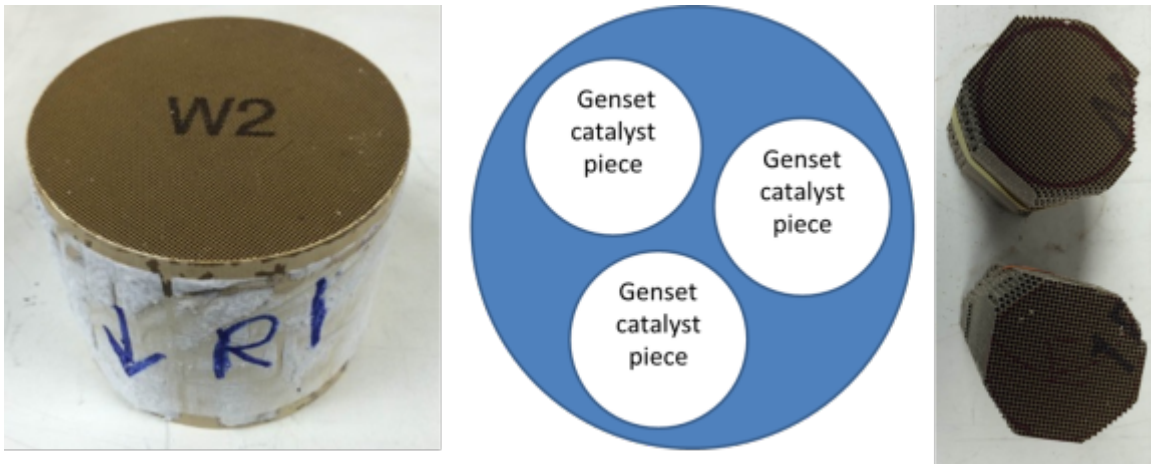

Figure 6.3. TWC downsized to accommodate smaller genset engine displacement.

The TWC chosen for this evaluation was obtained from a 2009MY Jeep Liberty that contained a front section with high precious metal content and a rear equally-sized low precious metal content. These full-size monoliths, 105mm OD x 85 mm in length, were reduced in size to such that the engine:catalyst volumetric ratios were maintained. Thus the genset TWCs were 42 mm OD x 85 mm in length. The TWCs are shown in Figure 6.3.

6.1.2 Exposure of anti-wear additives to three-way catalysts (TWC)

To determine the amount of anti-wear additive to expose the TWC, it was necessary to estimate the amount of oil consumed in a vehicle over the full-useful-life of the catalyst. A recent study by West et al. [SAE 2013-01-0884] indicated the oil consumption rate of a wide range of vehicles that are currently in use, thus we settled on one of the vehicles that was a "high normal" oil consumer, meaning that it was in the normal range, but higher than average. This will thus represent the worst case scenario for the anti-wear additive exposure. Table 6.1 lists the detailed steps of how this rate can be normalized to engine and catalyst size and the required calculations to determine the expected exposure of ZDDP to the TWC is 32g for ZDDP. Since the anti-wear additives are mixed based on volume and there is a different density for the IL, the dose for an IL-only lubricant is 40g and for ZDDP+IL is 16g ZDDP + 20g IL.

Table 6.1. Key parameters needed in calculating the necessary quantity of additive to introduce.

2.4	L-eng	High normal oil consumer engine size
145	mg/mile	Oil consumption rate [SAE 2013-01-0884]
60	mg/mile/L-eng	Normalized oil consumption
0.85	g/ml	Oil density
150000	miles	Catalyst lifetime
1.5	L-eng/L-cat	Engine/catalyst ratio
0.228	L-cat	Target catalyst volume in 0.35 L Westerbeke
16.4	L-oil/L-catalyst	Natural oil consumption in lifetime
1.00%		additive concentration
31.7	g-additive	Target ZDDP dose for full-useful life

To introduce this dose of additive to the TWCs the genset described in section 6.1.1 was employed with the additive directly mixed in the fuel. The engine was operated for approximately 25 hours until the needed quantity of fuel+additive was consumed and thus the required additive was introduced to the exhaust system.

6.1.3 Bench flow reactor evaluation of aged TWCs

Once the TWCs have been exposed to exhaust conditions, the front 25 mm is cut into 22 mm OD cores to be evaluated on a bench flow reactor; the catalyst cores and schematic of the bench reactor are shown in Figures 6.4 and 6.5, respectively. It should be noted that these evaluations are designed to accentuate the differences in the additives, thus we are only evaluating the front section that will have the largest concentration and thus largest impact. Three primary experimental evaluations were performed on the aged TWCs to determine the impact: determination of the stoichiometric point, light-off temperature ramps, and oxygen storage measurements. The experimental procedure for each is as follows:

- Determination of the stoichiometric point or oxygen concentration resulting in the highest conversion
    - 850 ppm C_3H_6, 100 ppm C_3H_8, 0.5% CO, 0.1% NO, 0.167% H_2, 0.40-0.80% O_2, 13% H_2O, 13% CO_2, and N_2 balance
    - Vary O_2 in increments of 0.05-0.02%
    - Hold temperature at 300°C
- Light-off temperature ramp under stoichiometric conditions
    - 850 ppm C_3H_6, 100 ppm C_3H_8, 0.5% CO, 0.1% NO, 0.167% H_2, 0.69% O_2, 13% H_2O, 13% CO_2, and N_2 balance
    - Temperature ramp: 100-600°C @ 5 °C/min
    - Natural cooling: 600-100°C
- Oxygen storage for determining impact on ceria
    - Use switching valve to cycle between 0.5% CO or 0.72% O_2 (N_2 balance)
    - 300-550°C in 50°C increments
    - 2 minutes lean followed by 2 minutes rich for four cycles (total 16 minutes)

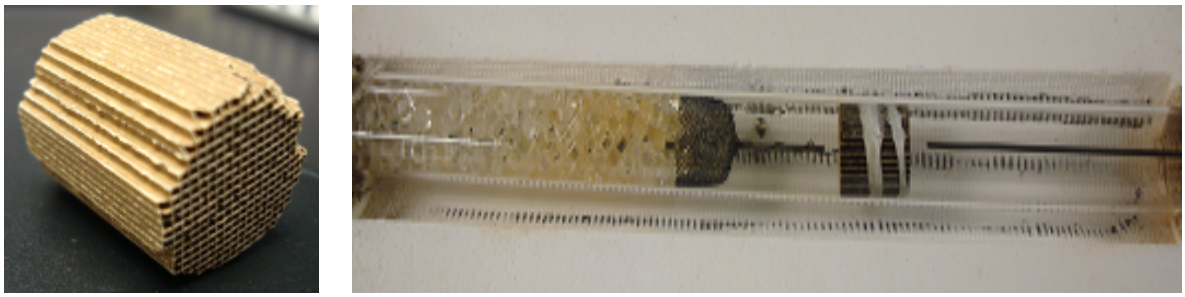

Figure 6.4. TWC cores removed for evaluation in the bench flow reactor.

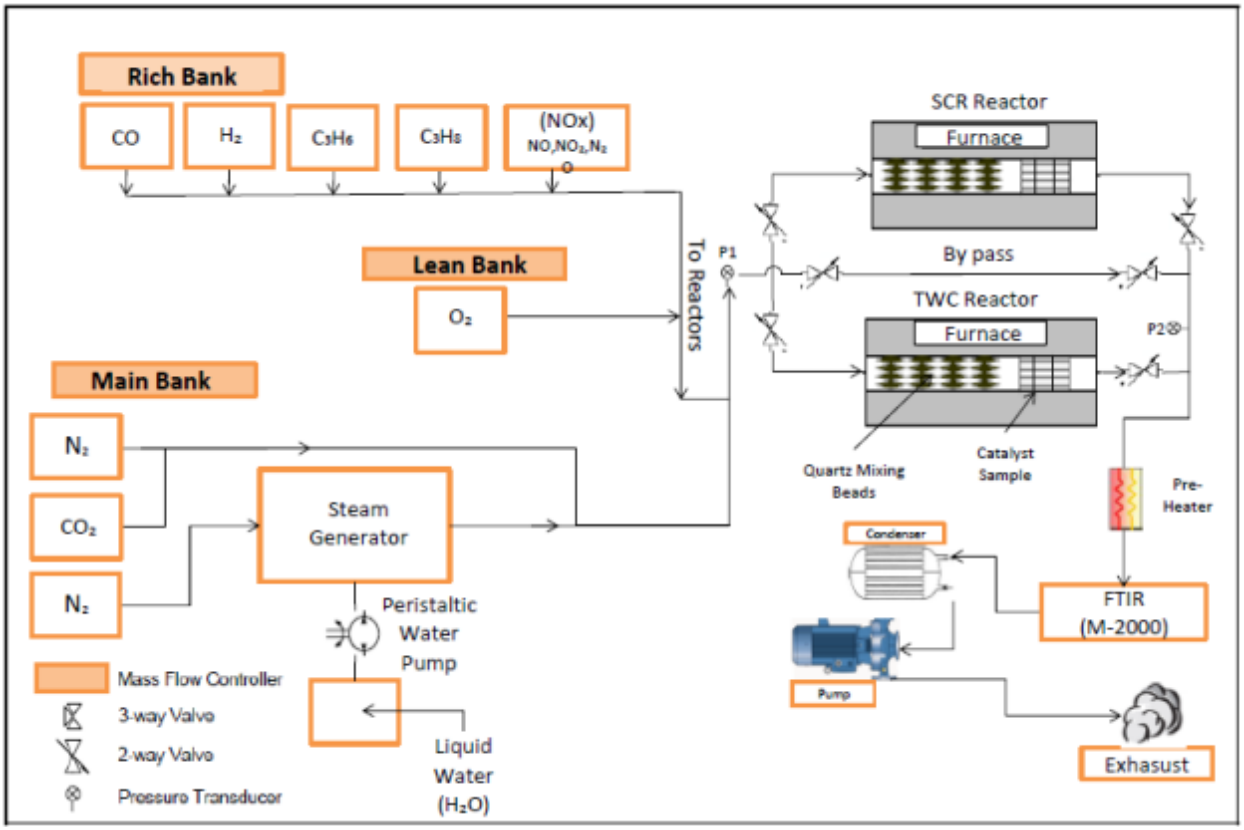

Figure 6.5. Schematic of bench flow reactor used to evaluate the aged TWCs.

6.2 Results

6.2.1 Temperatures during exposure of TWC to anti-wear additives

The aging routine described in the previous section was successfully completed using TWCs from a Jeep Liberty (MY2009) for each of the following cases: no additive (NA), ZDDP, IL, and ZDDP+IL. Additive introduction was performed using a stoichiometric gasoline genset

with the additive mixed with the fuel and the O_2 flow was established at the beginning of the run to achieve a midbed temperature of 700°C. after establishing this initial condition the O_2 flow was kept constant throughout the duration of the experiment. The temperature was measured during the exposure and is shown in Figure 6.6 for each of the runs. The decrease in the midbed temperature generally indicates that the activity is decreasing in the portion of the catalyst upstream of the thermocouple, thus the heat generated during the reduction of emission is moving towards the back of the catalyst. Thus the exit temperature is not largely affected just the local temperature where the thermocouple is located. This is our first indication of deactivation, but is very much qualitative in nature.

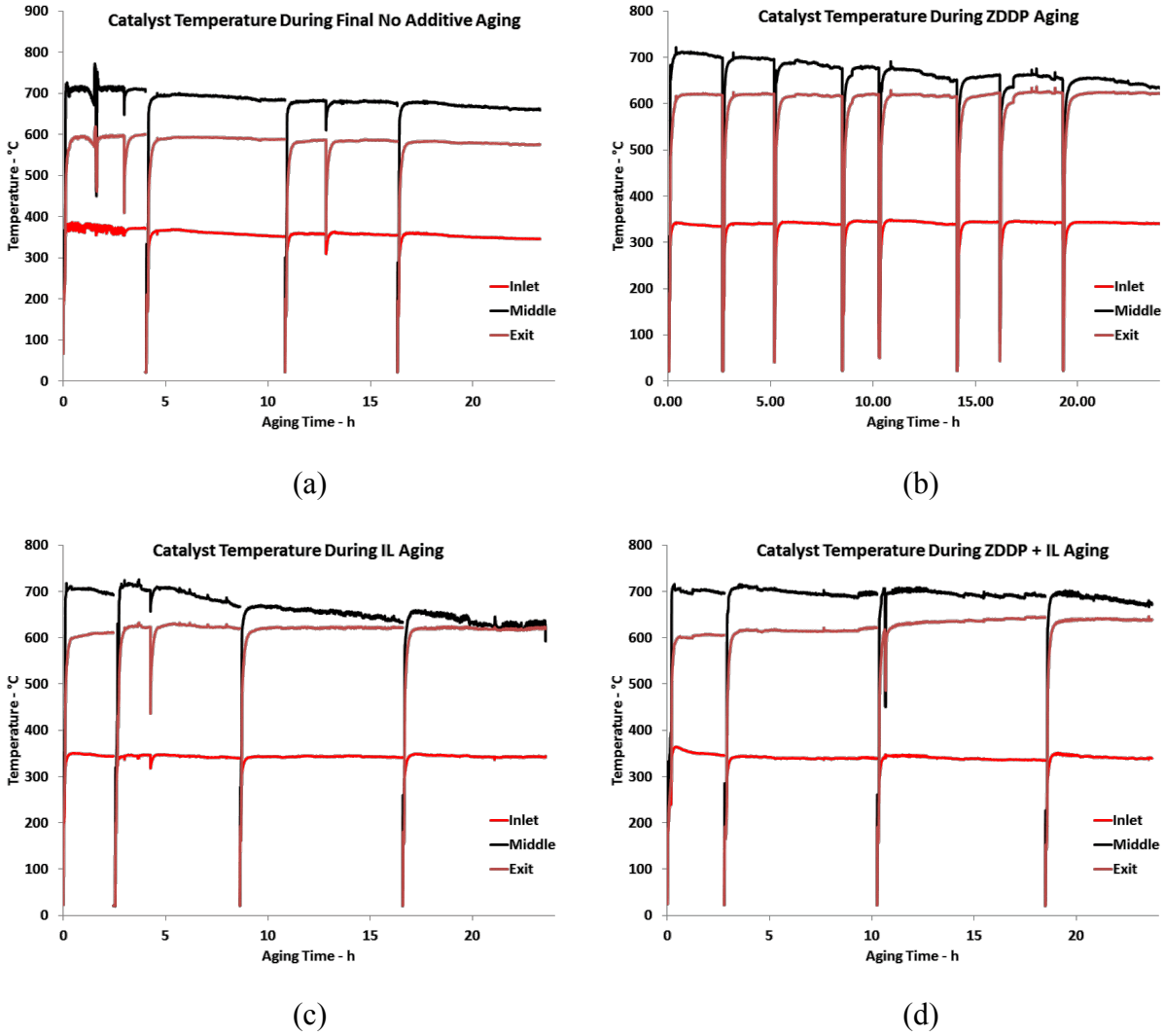

Figure 6.6. Exhaust temperatures during the aging of the TWCs on the gasoline genset for (a) no-additive, (b) ZDDP, (c) IL and (d) ZDDP+IL.

6.2.2 Evaluation of TWCs for light-off behavior in simulated exhaust conditions

Once the TWCs had been aged, efforts moved to the bench reactor evaluation. The first part of the evaluation was determining the exact concentration of O_2 to flow at for maximum conversion near stoichiometric operation. Figure 6.7 shows the strong influence of O_2 on the reactivity of the components in the exhaust. With this it was determined for the flowrates being used that 0.69% O_2 was the optimum concentration.

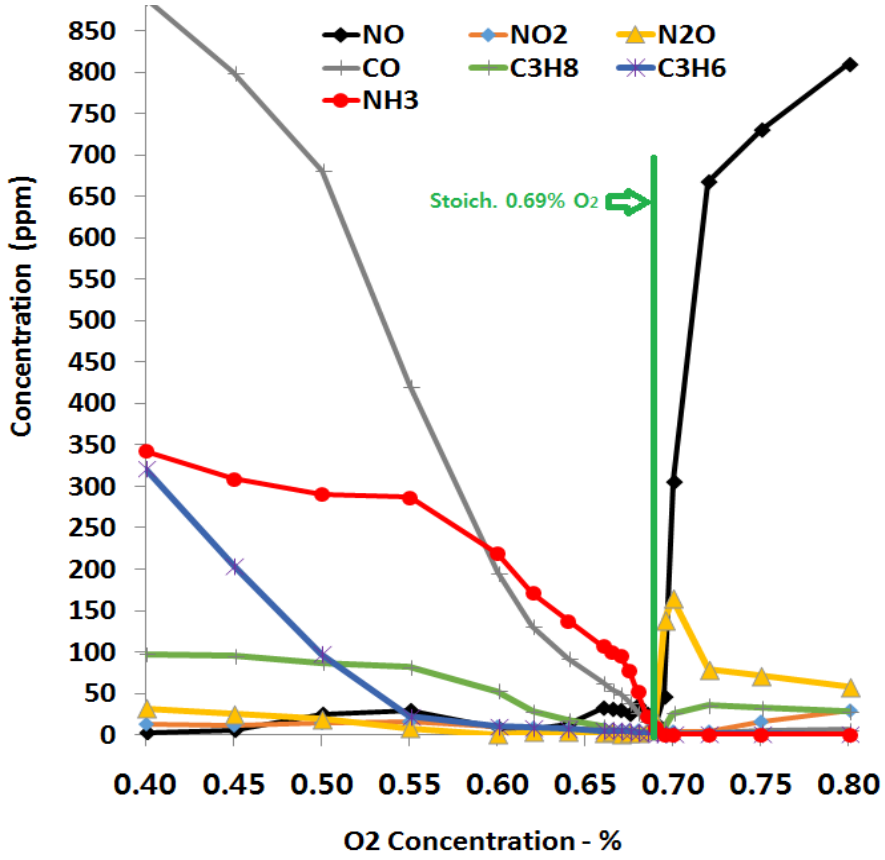

Figure 6.7. O_2 concentration sweep for the fresh TWC at 300°C.

Having established the optimum O_2 concentration the light-off temperature ramps were performed on tall of the samples. Figure 6.8 shows all of the criteria reactants that are being evaluated for each of the TWCs. The temperature of 50% (T50) and 90% (T90) conversion are shown in Figure 6.9. In general, the reactivity was similar for all of the TWCs, but a notable impact was observed for each additive. The impact on reactivity was typically less for IL-only, followed by ZDDP-only, and finally ZDDP+IL. The measured increase in T50 for the IL+ZDDP TWC, compared to the NA-TWC, was 8, 21, 30 and 61°C for NO, CO, C_3H_6 and C_3H_8, respectively. It should be noted that these evaluations are designed to accentuate the

differences in the additives, thus we are only evaluating the front section that will have the largest concentration, and should not be extrapolated to suggest that the overall TWC in a vehicle will have a 60°C delay in light off for C_3H_8.

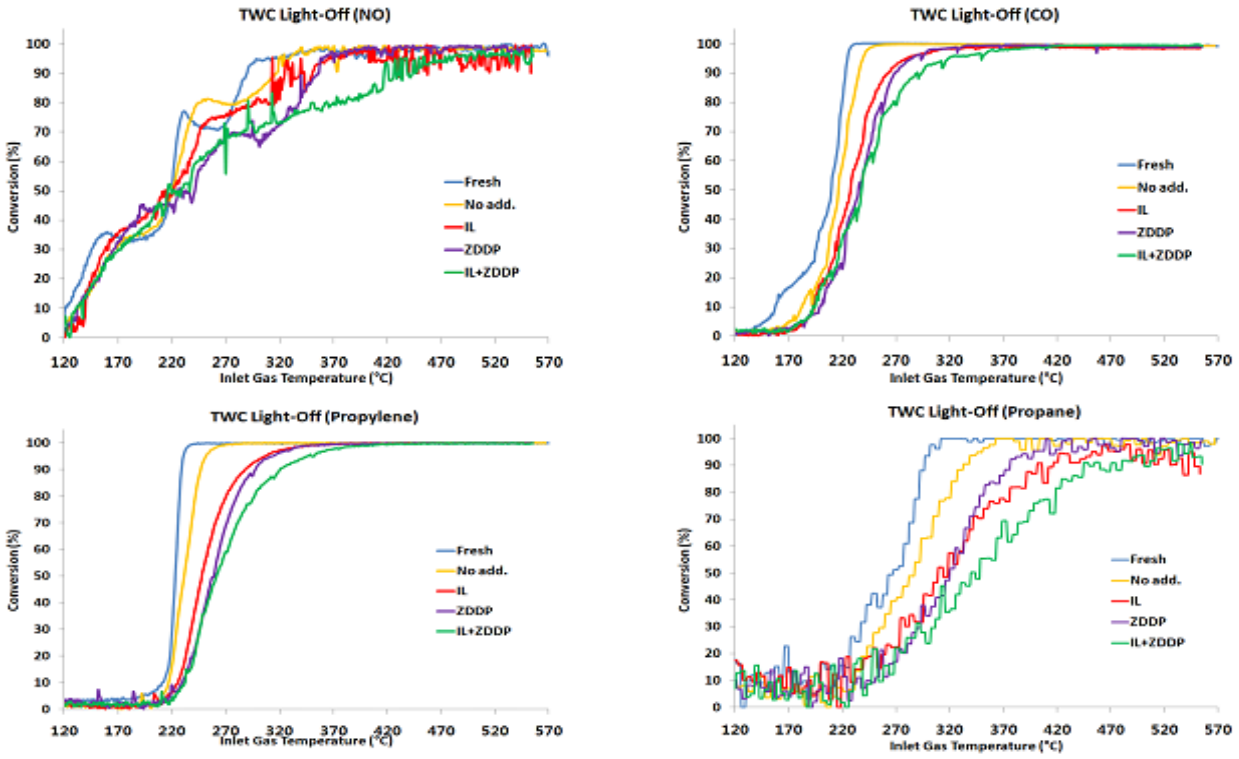

Figure 6.8. Light off curves for each TWC for the following reactants: NO, CO, C_3H_6 (propylene), and C_3H_8 (propane).

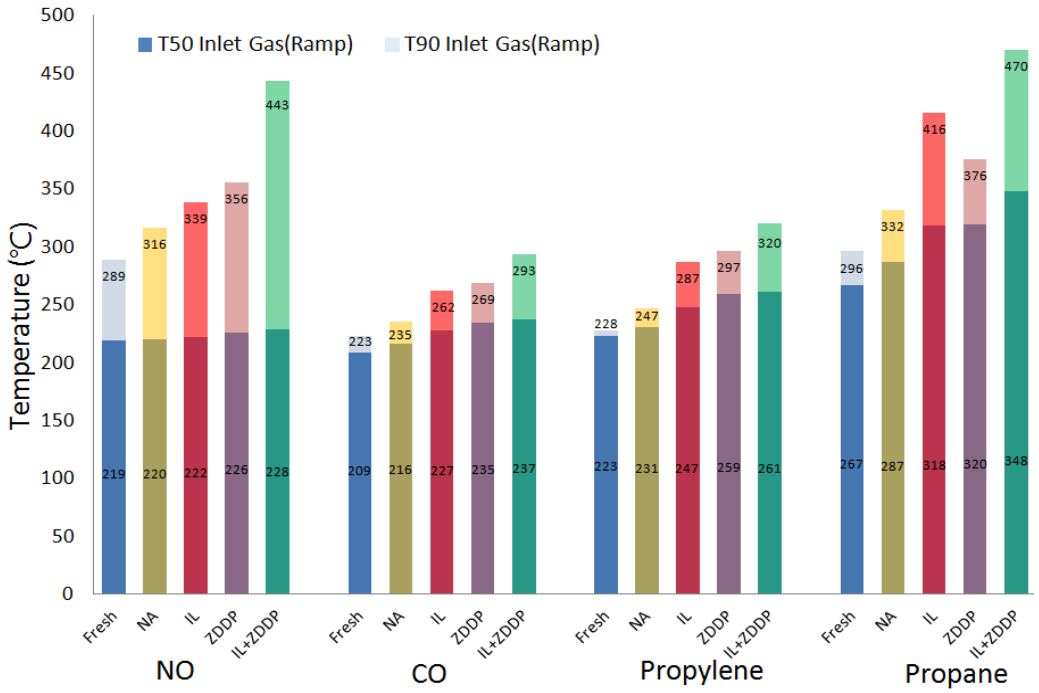

Figure 6.9. Impact of the anti-wear additives on the TWC T50 and T90 compared to the fresh and no-additive (NA) samples.

6.2.3 Evaluation of TWCs for oxygen storage capacity

Additionally, the impact of the anti-wear additives on a key function of the TWCs, oxygen storage, was measured. The phosphorous in these components can from cerium phosphate which can significantly impact its ability to store and release oxygen during the lean-rich dithering that occurs during typical stoichiometric operation. The results are shown in Figure 6.10. In these results it is clear that the ZDDP component has the largest impact on oxygen storage while IL by itself has much less interference. The combined IL+ZDDP is similar to IL at 300 and 350°C, but behaves more like ZDDP above 400°C. Similar to our initial studies with IL, these results indicate that ZDDP interacts more with the cerium phase than IL.

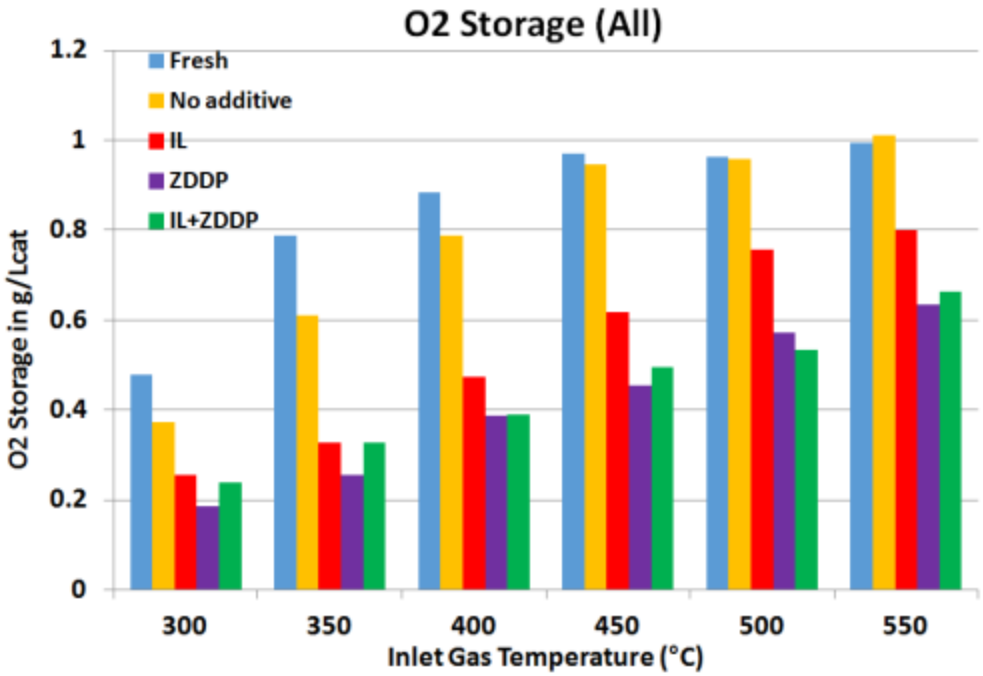

Figure 6.10. Measured oxygen storage functionality of each aged TWC between 300 and 550°C.

COMMERCIALIZATION POSSIBILITIES AND PLANS FOR FUTURE COLLABORATIONS

Three inventions were generated from this CRADA including two new groups of oil-miscible ionic liquids and a unique engine oil formulation. These IPs and the new discovery of unique synergistic effects between ILs and ZDDP are strongly supported by the full-scale engine dynamometer test results of the first prototype low-viscosity engine oil using the synergistic IL+ZDDP pair. A follow-on research project has recently been launched with an automotive OEM to further develop and optimize the IL chemistry and oil formulation as well as to expand the ionic liquid technology to other bearing components in the vehicle.

CONCLUSIONS

In this CRADA between ORNL and Shell, several groups of oil-miscible ILs were successfully developed as potential lubricant additives with anti-wear and friction reduction functionalities. Particularly, synergistic effects were discovered between phosphonium-organophosphate ILs and the conventional anti-wear additive ZDDP. Tribological bench test results showed > 30% friction reduction and 70% wear reduction for the synergistic IL+ZDDP pair compared with using ZDDP or IL alone. The IL+ZDDP tribofilm contains substantially higher contents of metal phosphates but less metal oxides and sulfur compounds. The concentrations of functional elements on the droplet surface of the oil containing IL+ZDDP are found to be one order magnitude higher than their nominal values and believed to be responsible for the superior performance. The compatibility between the IL and other additives were systematically explored to allow formulation of a prototype SAE 0W-16 engine oil using a synergistic IL+ZDDP combination as the anti-wear additive. This prototype oil demonstrated 2.12% fuel economy improvement (FEI) over the standard reference oil in Sequence VIE full-scale engine dynamometer tests. Among the 2.12% FEI, 1.87% is believed to be contributed by the lower oil viscosity while 0.25% is attributed to the reduced boundary friction by the IL. Based on accelerated small engine aging tests, the adverse impact of IL and IL+ZDDP on three-way catalyst seemed to be slightly less and more compared with ZDDP, respectively.

REFERENCES

1. Shiau, C.-S.N., Michalek, J.J.Hendrickson, C.T.: A structural analysis of vehicle design responses to corporate average fuel economy policy. Transp. Res. Part A Policy Prac. **43**(9–10), 814-828 (2009)
2. Dreyfus, M.K.Viscusi, W.K.: Rates of time preference and consumer valuations of automobile safety and fuel efficiency. Journal of Law and Economics **38**(1), 79-105 (1995)
3. Holmberg, K., Andersson, P. Erdemir, A.: Global energy consumption due to friction in passenger cars. Tribol. Int. **47**(0), 221-234 (2012)
4. Tung, S.C.McMillan, M.L.: Automotive tribology overview of current advances and challenges for the future. Tribol. Int. **37**(7), 517-536 (2004)
5. Ye, C., Liu, W., Chen, Y.Yu, L.: Room-temperature ionic liquids: A novel versatile lubricant. Chem. Commun.(21), 2244-2245 (2001)
6. Torimoto, T., Tsuda, T., Okazaki, K., Kuwabata, S.: New Frontiers in Materials Science Opened by Ionic Liquids. Adv. Mater. **22**, 1196-1221 (2010)
7. Mu, Z., Liu, W., Zhang, S.Zhou, F.: Functional room-temperature ionic liquids as lubricants for an aluminum-on-steel system. Chemistry Letters **33**(5), 524-525 (2004)
8. Phillips, B.S.Zabinski, J.S.: Ionic liquid lubrication effects on ceramics in a water environment. Tribol. Lett. **17**(3), 533-541 (2004)
9. Chen, Y.M., Zeng, Z.X., Yang, S.R.Zhang, J.Y.: The tribological performance of bcn films under ionic liquids lubrication. Diam. Relat. Mater. **18**(1), 20-26 (2009)
10. González, R., Hernández Battez, A., Blanco, D., Viesca, J.L.Fernández-González, A.: Lubrication of tin, crn and dlc pvd coatings with 1-butyl-1-methylpyrrolidinium tris(pentafluoroethyl)trifluorophosphate. Tribol. Lett. **40**(2), 269-277 (2010)
11. Bermúdez, M.-D., Jiménez, A.-E., Sanes, J.Carrión, F.-J.: Ionic liquids as advanced lubricant fluids. Molecules **14**(8), 2888-2908 (2009)
12. Minami, I.: Ionic liquids in tribology. Molecules. **14**(6), 2286-2305 (2009)
13. Palacio, M.Bhushan, B.: A review of ionic liquids for green molecular lubrication in nanotechnology. Tribol. Lett. **40**(2), 247-268 (2010)
14. Jiménez, A.E., Bermúdez, M.D., Iglesias, P., Carrión, F.J.Martínez-Nicolás, G.: 1-n-alkyl -3-methylimidazolium ionic liquids as neat lubricants and lubricant additives in steel–aluminium contacts. Wear **260**(7–8), 766-782 (2006)
15. Jiménez, A.-E.Bermúdez, M.-D.: Imidazolium ionic liquids as additives of the synthetic ester propylene glycol dioleate in aluminium–steel lubrication. Wear **265**(5), 787-798 (2008)
16. Yao, M., Liang, Y., Xia, Y.Zhou, F.: Bis-imidazolium ionic liquids as the high performance anti-wear additives in polyethylene glycol for steel–steel contacts. Acs appl. Mater. Interface **1** 467-471 (2009)
17. Cai, M., Liang, Y., Yao, M., Xia, Y., Zhou, F.Liu, W.: Imidazolium ionic liquids as antiwear and antioxidant additive in poly (ethylene glycol) for steel/steel contacts. ACS Appl. Mater. Interface. **2**(3), 870-876 (2010)
18. Liu, W., Ye, C., Gong, Q., Wang, H.Wang, P.: Tribological performance of room-temperature ionic liquids as lubricant. Tribol. Lett. **13**(2), 81-85 (2002)
19. Qu, J., Truhan, J., Dai, S., Luo, H.Blau, P.: Ionic liquids with ammonium cations as lubricants or additives. Tribol. Lett. **22**(3), 207-214 (2006)

20. Mistry, K., Fox, M.Priest, M.: Lubrication of an electroplated nickel matrix silicon carbide coated eutectic aluminium—silicon alloy automotive cylinder bore with an ionic liquid as a lubricant additive. Proc. Inst. Mech. Eng., Part J **223**(3), 563-569 (2009)
21. Qu, J., Blau, P.J., Dai, S., Luo, H.Meyer III, H.M.: Ionic liquids as novel lubricants and additives for diesel engine applications. Tribol. Lett. **35**(3), 181-189 (2009)
22. Qu, J., Truhan Jr, J.J., Dai, S., Luo, H.Blau, P.J., Lubricants or lubricant additives composed of ionic liquids containing ammonium cations. 2010, U.S. Patent #7,754,664, July 13, 2010.
23. Schneider, A., Brenner, J., Tomastik, C.Franek, F.: Capacity of selected ionic liquids as alternative ep/aw additive. Lubr. Sci. **22**(6□7), 215-223 (2010)
24. Libardi, A., Schmid, S.R., Sen, M.Schneider, W.: Evaluation of ionic fluids as lubricants in manufacturing. Journal of Manufacturing Processes **15**(4), 414-418 (2013)
25. Shah, F.U., Glavatskih, S., MacFarlane, D.R., Somers, A., Forsyth, M.Antzutkin, O.N.: Novel halogen-free chelated orthoborate–phosphonium ionic liquids: Synthesis and tribophysical properties. Phys. Chem. Chem. Phys. **13**(28), 12865-12873 (2011)
26. Somers, A., Howlett, P., Sun, J., MacFarlane, D.Forsyth, M.: Phosphonium ionic liquids as lubricants for aluminium-steel. Tribology Des 273-283 (2010)
27. Somers, A., Howlett, P., Sun, J., MacFarlane, D.Forsyth, M.: Transition in wear performance for ionic liquid lubricants under increasing load. Tribol. Lett. **40**(2), 279-284 (2010)
28. Minami, I., Inada, T., Sasaki, R.Nanao, H.: Tribo-chemistry of phosphonium-derived ionic liquids. Tribol. Lett. **40**(2), 225-235 (2010)
29. Forsyth, M., Kemp, T.F., Howlett, P.C., Sun, J.Smith, M.E.: A potential novel rapid screening nmr approach to boundary film formation at solid interfaces in contact with ionic liquids. J. Phys. Chem. C. **112**(36), 13801-13804 (2008)
30. Weng, L., Liu, X., Liang, Y.Xue, Q.: Effect of tetraalkylphosphonium based ionic liquids as lubricants on the tribological performance of a steel-on-steel system. Tribol. Lett. **26**(1), 11-17 (2007)
31. Liu, X., Zhou, F., Liang, Y.Liu, W.: Tribological performance of phosphonium based ionic liquids for an aluminum-on-steel system and opinions on lubrication mechanism. Wear **261**(10), 1174-1179 (2006)
32. Qu, J., Bansal, D.G., Yu, B., Howe, J.Y., Luo, H., Dai, S., Li, H., Blau, P.J., Bunting, B.G., Mordukhovich, G.Smolenski, D.J.: Antiwear performance and mechanism of an oil-miscible ionic liquid as a lubricant additive. ACS Appl. Mater. Interface. **4**(2), 997-1002 (2012)
33. Qu, J., Luo, H., Chi, M., Ma, C., Blau, P.J., Dai, S.Viola, M.B.: Comparison of an oil-miscible ionic liquid and zddp as a lubricant anti-wear additive. Tribol. Int. **71**(0), 88-97 (2014)
34. Yu, B., Bansal, D.G., Qu, J., Sun, X., Luo, H., Dai, S., Blau, P.J., Bunting, B.G., Mordukhovich, G.Smolenski, D.J.: Oil-miscible and non-corrosive phosphonium-based ionic liquids as candidate lubricant additives. Wear **289**(0), 58-64 (2012)
35. Zhou, Y., Dyck, J., Graham, T.W., Luo, H., Leonard, D.N.Qu, J.: Ionic liquids composed of phosphonium cations and organophosphate, carboxylate, and sulfonate anions as lubricant antiwear additives. Langmuir **30**(44), 13301-13311 (2014)

36. Otero, I.s., López, E.R., Reichelt, M., Villanueva, M., Salgado, J.Fernández, J.: Ionic liquids based on phosphonium cations as neat lubricants or lubricant additives for a steel/steel contact. ACS Appl. Mater. Interface. **6**(15), 13115-13128 (2014)
37. Somers, A.E., Khemchandani, B., Howlett, P.C., Sun, J., MacFarlane, D.R.Forsyth, M.: Ionic liquids as antiwear additives in base oils: Influence of structure on miscibility and antiwear performance for steel on aluminum. ACS Appl. Mater. Interface. **5**(22), 11544-11553 (2013)
38. Barnes, A.M., Bartle, K.D.Thibon, V.R.A.: A review of zinc dialkyldithiophosphates (zddps): Characterisation and role in the lubricating oil. Tribol. Int. **34**(6), 389-395 (2001)
39. Stojanovic, A., Keppler, B.K., Morgenbesser, C., Kogelnig, D.Krachler, R.: Quaternary ammonium and phosphonium ionic liquids in chemical and environmental engineering. INTECH Open Access Publisher (2011)
40. Yagci, M.B., Bolca, S., Heuts, J.P.A., Ming, W.de With, G.: Antimicrobial polyurethane coatings based on ionic liquid quaternary ammonium compounds. Progress in Organic Coatings **72**(3), 343-347 (2011)
41. Barabanova, G., Ivanov, V., Kossova, L.Akimova, N.: Use of esters of acids of phosphorus as lubricity additives for high-temperature synthetic lubricating oils (a review). Chemistry and Technology of Fuels and Oils **12**(5), 404-408 (1976)
42. Holweger, W.: Fundamentals of lubricants and lubrication. (2013)
43. Kondo, H.: Protic ionic liquids with ammonium salts as lubricants for magnetic thin film media. Tribol. Lett. **31**(3), 211-218 (2008)
44. Zhao, Q., Zhao, G., Zhang, M., Wang, X.Liu, W.: Tribological behavior of protic ionic liquids with dodecylamine salts of dialkyldithiocarbamate as additives in lithium complex grease. Tribol. Lett. **48**(2), 133-144 (2012)
45. Espinosa, T., Sanes, J., Jiménez, A.-E.Bermúdez, M.-D.: Protic ammonium carboxylate ionic liquid lubricants of ofhc copper. Wear **303**(1), 495-509 (2013)
46. Espinosa, T., Sanes, J., Jiménez, A.-E.Bermúdez, M.-D.: Surface interactions, corrosion processes and lubricating performance of protic and aprotic ionic liquids with ofhc copper. Applied Surface Science **273** 578-597 (2013)
47. Espinosa, T., Jiménez, M., Sanes, J., Jiménez, A.-E., Iglesias, M.Bermúdez, M.-D.: Ultra-low friction with a protic ionic liquid boundary film at the water-lubricated sapphire–stainless steel interface. Tribol. Lett. **53**(1), 1-9 (2014)
48. Westerholt, A., Weschta, M., Bösmann, A., Tremmel, S., Korth, Y., Wolf, M., Schlücker, E., Wehrum, N., Lennert, A.Uerdingen, M.: Halide-free synthesis and tribological performance of oil-miscible ammonium and phosphonium-based ionic liquids. ACS Sustainable Chemistry & Engineering **3**(5), 797-808 (2015)
49. Greaves, T.L.Drummond, C.J.: Protic ionic liquids: Properties and applications. Chemical reviews **108**(1), 206-237 (2008)
50. Greaves, T.L., Kennedy, D.F., Weerawardena, A., Tse, N.M., Kirby, N.Drummond, C.J.: Nanostructured protic ionic liquids retain nanoscale features in aqueous solution while precursor brønsted acids and bases exhibit different behavior. The Journal of Physical Chemistry B **115**(9), 2055-2066 (2011)
51. Pinkert, A., Ang, K.L., Marsh, K.N.Pang, S.: Density, viscosity and electrical conductivity of protic alkanolammonium ionic liquids. Phys. Chem. Chem. Phys. **13**(11), 5136-5143 (2011)

52. Rana, U.A., Vijayaraghavan, R., Walther, M., Sun, J., Torriero, A.A., Forsyth, M.MacFarlane, D.R.: Protic ionic liquids based on phosphonium cations: Comparison with ammonium analogues. Chem. Commun. **47**(42), 11612-11614 (2011)
53. Angell, C.A., Ansari, Y.Zhao, Z.: Ionic liquids: Past, present and future. Faraday discussions **154** 9-27 (2012)
54. Miran, M.S., Kinoshita, H., Yasuda, T., Susan, M.A.B.H.Watanabe, M.: Hydrogen bonds in protic ionic liquids and their correlation with physicochemical properties. Chem. Commun. **47**(47), 12676-12678 (2011)
55. Odi-Owei, S., Roylance, B.Xie, L.: An experimental study of initial scuffing and recovery in sliding wear using a four-ball machine. Wear **117**(3), 267-287 (1987)
56. Qu, J., Truhan, J.Blau, P.: Detecting the onset of localized scuffing in a pin-on-twin fuel-lubricated test for heavy-duty diesel fuel injectors. International Journal of Engine Research **6**(1), 1-9 (2005)
57. Qu, J., Chi, M., Meyer III, H.M., Blau, P.J., Dai, S.Luo, H.: Nanostructure and composition of tribo-boundary films formed in ionic liquid lubrication. Tribol. Lett. **43**(2), 205-211 (2011)
58. Qu, J.Luo, H., Ionic liquids containing symmetric quaternary phosphonium cations and phosphorus-containing anions, and their use as lubricant additives., U.S.P. Appplication, Editor. 2014. p. 14.
59. Sun, J., Howlett, P.C., MacFarlane, D.R., Lin, J.Forsyth, M.: Synthesis and physical property characterisation of phosphonium ionic liquids based on p (o) 2 (or) 2− and p (o) 2 (r) 2− anions with potential application for corrosion mitigation of magnesium alloys. Electrochimica acta **54**(2), 254-260 (2008)
60. Spikes, H.: The history and mechanisms of zddp. Tribol. Lett. **17**(3), 469-489 (2004)
61. Joslin, D.Oliver, W.: A new method for analyzing data from continuous depth-sensing microindentation tests. Journal of Materials Research **5**(01), 123-126 (1990)
62. Pearson, R.G.: Chemical hardness. Wiley-VCH (1997)
63. Rudnick, L.R.: Lubricant additives: Chemistry and applications. CRC Press (2009)
64. Zhang, F., Wu, W., Bian, X.Zeng, W.: Synergistic extraction and separation of lanthanum (iii) and cerium (iii) using a mixture of 2-ethylhexylphosphonic mono-2-ethylhexyl ester and di-2-ethylhexyl phosphoric acid in the presence of two complexing agents containing lactic acid and citric acid. Hydrometallurgy **149** 238-243 (2014)
65. Cholico-Gonzalez, D., Avila-Rodriguez, M., Cote, G.Chagnes, A.: Chemical properties of trihexyl (tetradecyl) phosphonium chloride and bis (2, 4, 4-trimethylpentyl) phosphinic acid mixtures: Interaction study by ft-ir and nmr spectroscopies. Journal of Molecular Liquids **187** 165-170 (2013)
66. John, S.T., Song, Y.Liu, Z.: Effects of temperature and pressure on zddp. Tribol. Lett. **28**(1), 45-49 (2007)
67. Sainz-Diaz, C., Klocker, H., Marr, R.Bart, H.-J.: New approach in the modelling of the extraction equilibrium of zinc with bis-(2-ethylhexyl) phosphoric acid. Hydrometallurgy **42**(1), 1-11 (1996)
68. Varlot, K., Martin, J., Grossiord, C., Vargiolu, R., Vacher, B.Inoue, K.: A dual-analysis approach in tribochemistry: Application to zddp/calcium borate additive interactions. Tribol. Lett. **6**(3-4), 181-189 (1999)

69. Zhang, J., Yamaguchi, E.Spikes, H.: The antagonism between succinimide dispersants and a secondary zinc dialkyl dithiophosphate. Tribology Transactions **57**(1), 57-65 (2014)
70. Unnikrishnan, R., Jain, M., Harinarayan, A.Mehta, A.: Additive–additive interaction: An xps study of the effect of zddp on the aw/ep characteristics of molybdenum based additives. Wear **252**(3), 240-249 (2002)
71. D7589-15, A., Standard test method for measurement of effects of automotive engine oils on fuel economy of passenger cars and light-duty trucks in sequence vid spark ignition engine. 2015, ASTM International: West Conshohocken, PA.
72. Nicholls, M.A., Do, T., Norton, P.R., Kasrai, M.Bancroft, G.M.: Review of the lubrication of metallic surfaces by zinc dialkyl-dithiophosphates. Tribol. Int. **38**(1), 15-39 (2005)
73. Barnhill, W.C., Qu, J., Luo, H.M., Meyer, H.M., Ma, C., Chi, M.F.Papke, B.L.: Phosphonium-organophosphate ionic liquids as lubricant additives: Effects of cation structure on physicochemical and tribological characteristics. ACS Appl. Mater. Interface. **6**(24), 22585-22593 (2014)
74. Barnhill, W.C., Qu, J., Luo, H.M., Meyer, H.M., Leonard, D.N., Landauer, A.K., Kheireddin, B., Gao, H., Papke, B.L., Dai, S.: Synergistic effects between phosphonium-alkylphosphate ionic liquids and ZDDP as lubricant additives, Adv. Mater. **27**, 4767-4774 (2015)
75. Barnhill, W.C., Gao, H., Kheireddin, B., Papke, B.L., Luo, H.M., West, B.H., Qu, J.: Tribological bench and engine dynamometer tests of a low viscosity SAE 0W-16 engine oil using a combination of ionic liquid and ZDDP as anti-wear additives, *Frontiers Mech. Eng.* 1 (2015) DOI: 10.3389/fmech.2015.00012.